NASA Technical Memorandum 86405

NASA-TM-86405 19860000549

Operating Characteristics of the Multiple Critical Venturi System and Secondary Calibration Nozzles Used for Weight-Flow Measurements in the Langley 16-Foot Transonic Tunnel

Bobby L. Berrier, Laurence D. Leavitt, and Linda S. Bangert

SEPTEMBER 1985

NASA

NASA Technical Memorandum 86405

Operating Characteristics of the Multiple Critical Venturi System and Secondary Calibration Nozzles Used for Weight-Flow Measurements in the Langley 16-Foot Transonic Tunnel

Bobby L. Berrier, Laurence D. Leavitt,
and Linda S. Bangert
Langley Research Center
Hampton, Virginia

National Aeronautics
and Space Administration

Scientific and Technical
Information Branch

1985

SUMMARY

An investigation has been conducted in the Langley 16-Foot Transonic Tunnel to determine and document the weight-flow measurement characteristics of a multiple critical venturi system and the nozzle discharge coefficient characteristics of a series of convergent calibration nozzles. The effects on model discharge coefficient of nozzle-throat area, model choke-plate open area, nozzle pressure ratio, jet total temperature, and number and combination of operating venturis were investigated. Tests were conducted at static conditions (tunnel wind off) at nozzle pressure ratios from 1.3 to 7.0. Results of this investigation indicate that the measurement uncertainty of the multiple critical venturi system is generally within 0.5 percent and that the discharge coefficients of the Langley 16-Foot Transonic Tunnel Stratford choke nozzles fall within the expected range of 0.9925 to 0.9975 if throat Reynolds number is slightly higher than 1×10^6 and if excessive total-pressure profile distortion is not present.

INTRODUCTION

Accurate measurement of air weight-flow rate being supplied to subscale wind tunnel models for jet exhaust simulation is critical to obtaining high-accuracy propulsion-model data. The demands for high-accuracy data from propulsion models increase proportionally with demands for aircraft with higher performance or lower fuel consumption or both. Weight-flow measurements are not only used to compute discharge coefficients but are also used to compute values of ideal isentropic gross thrust which are used in thrust ratios for determining nozzle efficiency.

With the introduction of a high-pressure air jet-simulation system in the Langley 16-Foot Transonic Tunnel, a turbine-type meter (refs. 1 and 2) was adopted for air weight-flow rate measurements. Because the calibration of electronic equipment associated with the turbine-meter frequency measurements "drifted" with time and also because turbine-meter calibration was a slight function of bearing wear, there was a gradual shift from use of a turbine-type meter to a calibration technique which uses sonic nozzles located at the exit of the model high-pressure plenum (refs. 3 to 5). Calibrations of these sonic nozzles against secondary standard nozzles with known performance were required to establish the relationship between upstream temperature and pressure measurements and weight-flow rate. Although this method for computing weight-flow rate proved to be very reliable and gave satisfactory results, calibrations before each model entry were required because the relationship between the upstream temperature and pressure measurements and the model air weight-flow rate was often a function of model design (e.g., upstream temperature and pressure measurement location, choke-plate open area, and nozzle-throat area). The secondary standard nozzles used in the Langley 16-Foot Transonic Tunnel for calibrating weight-flow rate measurements (and, as described in ref. 3, for obtaining balance tares resulting from airflow momentum and pressure) are Stratford choke (sonic) nozzles of the type described and analyzed in reference 6. In an effort to simplify and improve air weight-flow rate measurement, a multiple critical venturi system was installed in the high-pressure air supply system of the tunnel in late 1982. Design criteria, advantages, and operating characteristics of critical venturis can be found in references 7 and 8.

The objective of this paper is to determine and document the weight-flow measurement characteristics of the Langley 16-Foot Transonic Tunnel multiple critical venturi system and the nozzle discharge coefficient characteristics of a series of convergent calibration nozzles. The effects on model discharge coefficient of nozzle-throat area, model choke-plate open area, number and combination of operating venturis, nozzle pressure ratio, and jet total temperature are shown. This test was conducted at static conditions (tunnel wind off) and nozzle pressure ratio was varied from 1.3 to 7.0.

SYMBOLS

A_{choke} — total open area formed by holes in choke plate, in^2

A_{max} — maximum internal nozzle flow area, in^2

A_t — measured nozzle-throat area, in^2

A_x — measured throat area of individual venturi (x = 1, 2, 4, 8, 16.1, or 16.2), in^2

C^* — critical-flow factor (see eq. (3a) and ref. 9)

C_d — measured discharge coefficient of Stratford choke nozzle, w_p/w_i

$\bar{C}_d$ — average of Stratford-choke-nozzle discharge coefficients measured at choked flow conditions for a particular A_t and A_{choke} combination

$\bar{C}_{d,avg}$ — average of $\bar{C}_d$ for a particular value of A_t (includes $\bar{C}_d$ for all values of A_{choke} except screens)

$C_{d,x}$ — discharge coefficient of individual venturi (x = 1, 2, 4, 8, 16.1, or 16.2)

D_{max} — maximum internal diameter of model tail pipe (see fig. 2(a)), in.

D_t — throat diameter of Stratford choke nozzle (see fig. 2(a)), in.

D_2 — diameter of Stratford choke nozzle at throat plane including nozzle base (see fig. 2(a)), in.

g — acceleration due to gravity, 32.174 ft/sec^2

$K_0, K_1, \ldots, K_{15}$ — constants used to determine critical flow factor (see eq. (3))

$K_{R,1}, K_{R,2}, \ldots, K_{R,5}$ — rake correction factors for individual internal jet total-pressure probes (see fig. 2(b))

ΔK_R — total-pressure distortion parameter (maximum rake correction factor minus minimum rake correction factor times 100; percent deviation from no-distortion case ($K_{R,1}$ to $K_{R,5}$ = 1.0))

L_1 — length used for geometric definition of Stratford choke nozzle (see fig. 2(a)), in.

L_2 distance throat circular arc profile extends upstream of throat (see fig. 2(a)), in.

l length of Stratford choke nozzles (see fig. 2(a)), in.

M throat Mach number

MCV multiple critical venturi code (sum of the venturi numbers that are being used)

NPR nozzle pressure ratio, $p_{t,j}/p_a$

$(NPR)_c$ nozzle pressure ratio required for choked flow (1.8928 for air)

p_a ambient pressure, psi

p_{rake} jet total pressure measured by individual rake probe at Stratford-choke-nozzle throat, psi

$(p_{rake})_{int}$ value of jet total pressure obtained by integrating rake-measured values at Stratford-choke-nozzle throat, psi

$p_{t,j}$ average jet total pressure obtained from internal probes in instrumentation section (see fig. 2(a)), psi; value may or may not be corrected to $(p_{rake})_{int}$ depending on values of rake correction factors $(K_{R,1}, K_{R,2}, \ldots, K_{R,5})$ used

$p_{t,j,1}, p_{t,j,2}, \ldots, p_{t,j,5}$ jet total pressure measured with individual internal probes (see fig. 2), psi

p_{V1} upstream pressure in multiple critical venturi system (see fig. 3(a)), psi

p_{V2} downstream pressure in multiple critical venturi system (see fig. 3(a)), psi

R gas constant, 53.36 ft-lbf/lb-°R

R_d throat Reynolds number for Stratford choke nozzle (eq. (9))

$R_{d,v}$ venturi-throat Reynolds number (eq. (4)), per inch

R_1, R_2 radii of curvature for geometric definition of Stratford choke nozzles (see fig. 2(a)), in.

r radius from nozzle centerline to probe centerline (see fig. 5), in.

r_t throat radius of Stratford choke nozzle (see fig. 5), in.

$T_{t,j}$ jet total temperature, °R

T_V upstream multiple critical venturi air temperature, °R

w_i ideal total weight-flow rate (see eq. (6)), lb/sec

$w_{i,x}$ ideal weight-flow rate for any individual critical venturi (x = 1, 2, 4, 8, 16.1, or 16.2), lb/sec

w_p measured total weight-flow rate, lb/sec

X length used for geometric definition of Stratford choke nozzles (see fig. 2(a)), in.

x venturi number (1, 2, 4, 8, 16.1, or 16.2)

γ ratio of specific heats, 1.3997 for air

μ absolute viscosity of air based on venturi-throat static conditions, lb/sec-in

Subscript:

nom nominal

APPARATUS AND METHODS

Test Facility

This investigation was conducted in the Langley 16-Foot Transonic Tunnel (ref. 10). All tests were made with the tunnel test section top in a raised position such that the model exhaust was vented to the atmosphere. Jet exhaust flow was simulated with high-pressure air supplied and maintained at a constant stagnation temperature by a heat exchanger in the system.

Single-Engine Propulsion-Simulation System

A sketch and a photograph of the single-engine nacelle model on which various Stratford choke nozzles were mounted are presented in figure 1 with a typical nozzle configuration attached. The body shell forward of station 26.50 was removed for this investigation.

An external high-pressure air system provided a continuous flow of clean, dry air at a controlled temperature of about 530°R. Air was brought through the support-system strut by six tubes and collected in a high-pressure (up to 900 psi) plenum located on top of the strut. The air was then routed aft and discharged perpendicularly into the integral centerbody—low-pressure-plenum—tail-pipe section through eight multiholed sonic nozzles equally spaced around the aft end of the high-pressure plenum. This design minimizes any forces imposed by the transfer of axial momentum as the air passes from the nonmetric high-pressure plenum to the metric tail pipe. Two opposing flexible metal bellows were used as seals and served to compensate for axial forces caused by pressurization. From the centerbody—low-pressure-plenum—tail-pipe section, the air was passed through a choke plate and an instrumentation section and then through the nozzle attached at model station 42.00. Details of the choke plate, which was a test variable, and of the instrumentation section are given in figure 2. Five choke plates with varying open areas (2.7 percent to 75.9 percent) were tested. Four of the choke plates were actually perforated disks with the upstream end of each hole countersunk. The choke plate with the largest open area

(75.9 percent) consisted of wire screen material supported by an open metal latticework.

Stratford Choke Nozzles

Since gas-flow measuring devices cannot generally be calibrated by direct weighing of the flow per unit of time, secondary standard nozzles are employed to calibrate weight-flow rate measurements (and, as described in ref. 3, to obtain balance tares resulting from airflow momentum and pressure). The secondary standard nozzles used at the Langley 16-Foot Transonic Tunnel are choke (sonic) nozzles of the type described in reference 6. Choke nozzle design guidelines from reference 6 are as follows:

1. Choked flow. This eliminates the need for difficult measurement of the static pressure in the throat. It also eliminates the effect of small variations in static pressure across the throat since the change in mass flow with changes in static pressure is equal to zero at a Mach number of unity.

2. Continuously curving wall profile through the throat. If the wall profile curves continuously through the throat, the flow in a choked nozzle can accelerate continuously and can develop only a very thin boundary layer. The reduction of discharge coefficient resulting from the boundary layer is thus very small.

3. $D_{max}/D_t = 2$ to 3. This ratio is governed by practical circumstances but a ratio of two or three would seem reasonable.

4. $R_1/D_t = 2$. Although higher discharge coefficients could be obtained with lower values of this ratio, lower values of R_1/D_t also produce relatively large differences between discharge coefficient values for laminar and turbulent boundary layers. Thus, a moderate curvature for the throat is recommended to minimize this difference.

5. $L_2/D_t > 0.8$. Boundary-layer growth is roughly proportional to M^4. For $R_1/D_t = 2$, this value has become very small at a distance upstream of the throat of $L_2/D_t = 0.8$ and discharge coefficient would be virtually independent of the shape of the nozzle profile upstream of this point, provided the surface were smooth and the flow attached.

6. $R_d > 10^6$. The uncertainty in discharge coefficient resulting from transition is decreased for throat Reynolds numbers above this value.

Seven sizes of Stratford choke nozzles were constructed with throat areas ranging from 0.999 in^2 to 11.352 in^2. Table I presents the geometry of these nozzles with the design guidelines from reference 6. As shown in table I, except for D_{max}/D_t, which was limited by a fixed upstream duct area for all nozzles, the geometries of the seven secondary standard nozzles generally met the desired design criteria. Two exceptions are noted. Because of model restraints, L_2/D_t for the 8.501-in^2 and 11.352-in^2 throat area nozzles was less than the desired value. For the $A_t = 0.999$ in^2 nozzle, the throat Reynolds number did not meet or only marginally met the design criteria at low values of NPR because of the small throat diameter.

The $A_t = 1.933$ in^2 and $A_t = 5.711$ in^2 secondary standard nozzles (Stratford choke nozzles) were calibrated against several primary standard nozzles at the Colorado Engineering Experiment Station, Inc., in March of 1968. Primary standard nozzles have known discharge coefficients which have been verified by laboratories such as the National Bureau of Standards. The range of discharge coefficients measured for these nozzles agreed well with that predicted theoretically in reference 6.

Multiple Critical Venturi System

Sketches and a photograph of the Langley 16-Foot Transonic Tunnel multiple critical venturi system are presented in figure 3. This system provides for high accuracy of flow measurement, an extremely wide range of weight flow, small pressure losses, and a very low level of noise in the airstream and pipe structures.

This flow-measurement system is designed to accommodate up to 44 lb/sec of air at a maximum pressure level of 1500 psi. As shown in figure 3(a), the system inlet flow is distributed uniformly into a common plenum by a radial inlet diffuser and a large perforated plate. The perforated plate also acts as a heat exchanger to eliminate small fluctuations in flow temperature. A pressure-tight bulkhead contains six critical-flow venturis. (See fig. 3(c).) The venturis vary in size in binary increments of throat area so that each successively larger venturi will pass twice the flow of the preceding one. The sizes of venturis in this system are multiples of 1, 2, 4, 8, and 16, values which also represent their nominal weight flow at 1600 psi. There are two venturis (numbered 16.1 and 16.2) of the largest size to provide maximum weight-flow capability within the smallest possible pressure vessel. Each venturi has its own individual screw-on cap. With all caps installed, no flow may pass through the system as each cap has an O-ring seal to prevent leakage. Any or all of the caps may be removed through the access port (see fig. 3(a)) to meet flow requirements. The binary sizes of the 6 venturis permit 47 increments of flow area to be used at any pressure level from 20 psi to 1500 psi. This provides a weight-flow range from 0.014 lb/sec at 20 psi to 44 lb/sec at 1500 psi, as shown in figure 4. Also shown in figure 4 are the pressure and weight-flow ranges covered during the current investigation.

Each individual venturi is designed to minimize losses and to reduce the noise which can be generated by a critical venturi. (See ref. 7.) Each venturi has an inlet radius of 3.64 times the throat radius, a 5° half-angle conical diffuser which enlarges to at least 5.80 times the throat area, and a perforated cylindrical diffuser with a perforated area equal to 8.00 times the venturi throat area. The 5° half-angle conical diffuser permits the venturi to maintain critical flow with pressure losses as low as 7 percent. The perforated cylindrical diffuser prevents the generation of noise and resonance in the airstream and pipe structures by shock systems which form in the conical diffuser at high pressure ratios.

The Langley 16-Foot Transonic Tunnel multiple critical venturi system was calibrated in the Boeing Airflow Calibration Facility over a pressure range from approximately 36 psi to 920 psi. Calibration results are shown in table II as tabulated discharge coefficients. The airflow standard used for this calibration was another multiple critical venturi system which was calibrated in 1977 by Colorado Engineering Experiment Station, Inc. (CEESI) with their 300 ft^3 primary volumetric airflow standard. This calibration was certified by CEESI to have a measurement uncertainty within 0.07 percent over the airflow range from 0.1 lb/sec to 20.0 lb/sec. Transfer of this calibration to the Langley multiple critical venturi system was performed with an estimated precision of 0.03 percent over the entire calibration range. Since the certified calibration accuracy of the airflow standard used for calibration of the Langley system is within 0.07 percent, a calibration accuracy of 0.1 percent can be validly assumed to apply to the Langley 16-Foot Transonic Tunnel multiple critical venturi system.

Instrumentation

Jet total pressure was measured at a fixed station in the model instrumentation section (see fig. 2) with a five-probe rake and a one-probe rake. Because of a plugged tube, the fourth probe from the bottom on the five-probe rake was not used for the current investigation. (See fig. 2(b).) Jet total pressure $p_{t,j}$ was obtained by averaging the five probe values measured. In addition, the jet total-pressure distribution at the nozzle throat was determined for each configuration tested with a 13-probe rake shown by the sketch of figure 5. This rake was mounted rigidly on each nozzle configuration to avoid relative movement between the rake and the nozzle throat resulting from model loads and vibration. The number of probes used with each nozzle varied with nozzle-throat diameter. Jet total pressures from the internal rakes and from the external 13-probe rake were measured with an electronic scanning pressure device.

The multiple critical venturi system (see fig. 3) described previously was used to measure the weight flow of the high-pressure air being supplied to the nozzles. Three pressure measurements upstream of the venturis (p_{V1}) and one pressure measurement downstream of the venturis (p_{V2}) were made with individual pressure transducers at the locations shown in figure 3(a). A temperature measurement upstream of the venturis (T_V) was made with a platinum resistance thermometer at the location shown in figure 3(a). The outstanding characteristics of this type of temperature measurement device can be found in reference 1.

Data Reduction

All data were recorded on magnetic tape. Fifty frames of data taken at a rate of 10 frames per second were averaged for each data point; average values were used in computations. Two nozzle-pressure-ratio-sweep runs were conducted on each configuration investigated, one with the 13-probe rake installed and one with it removed. Runs with the 13-probe rake installed were used only to provide total-pressure distributions at the nozzle throat and to determine rake correction factors, which are discussed later, for each internal total-pressure probe. Data obtained during the run with the rake removed were used to compute nozzle discharge coefficients.

The basic performance parameter used for the presentation of results is nozzle discharge coefficient C_d. Nozzle discharge coefficient is the ratio of measured weight flow w_p to ideal weight flow w_i. This parameter reflects the ability of a nozzle to pass weight flow and is reduced by any momentum and vena contracta losses (ref. 11). An excellent discussion of discharge coefficient losses in a venturi (which is a special purpose nozzle) is contained in reference 7. The two major sources of discharge coefficient losses given in this reference are

1. Development of a boundary layer along the nozzle walls because of the real-gas viscous effects

2. Variation of weight flow per unit area in the radial direction because of the centrifugal forces which exist in the gas as a result of flow through a contracting section

The values of measured weight flow used to determine nozzle discharge coefficients presented in this paper were determined from the multiple critical venturi system by use of equation (1).

$$w_p = w_{i,1}(C_{d,1}) + w_{i,2}(C_{d,2}) + \dots + w_{i,16.2}(C_{d,16.2}) \tag{1}$$

Since the product of ideal weight flow and discharge coefficient equals actual weight flow, each term in equation (1) represents the weight flow through a particular venturi shown in figure 3(c). For any venturi not used (capped off), the appropriate term or terms are dropped from equation (1). The venturis which are operating can be determined from the value of a unique multiple critical venturi code number MCV. Its value is the sum of the venturi numbers (see fig. 3(c)) that are being used. For example, MCV = 22 indicates that venturi number 2, venturi number 4, and venturi number 16.1 are being used (2 + 4 + 16 = 22). Venturi number 16.1 is always used when only one of the largest size venturis is required. The ideal weight-flow terms in equation (1) are defined as

$$w_{i,x} = \frac{p_{V1} A_x C^* \sqrt{g}}{\sqrt{RT_V}} \tag{2}$$

where x is the venturi number. Values for each venturi throat area A_x are given in figure 3(c). The critical-flow factor used in equation (2) is defined as

$$C^* = A + B(p_{V1}) + C(p_{V1})^2 + D(p_{V1})^3 \tag{3a}$$

where

$$A = K_0 + K_1(T_V - 460) + K_2(T_V - 460)^2 + K_3(T_V - 460)^3 \tag{3b}$$

$$B = K_4 + K_5(T_V - 460) + K_6(T_V - 460)^2 + K_7(T_V - 460)^3 \tag{3c}$$

$$C = K_8 + K_9(T_V - 460) + K_{10}(T_V - 460)^2 + K_{11}(T_V - 460)^3 \tag{3d}$$

$$D = K_{12} + K_{13}(T_V - 460) + K_{14}(T_V - 460)^2 + K_{15}(T_V - 460)^3 \tag{3e}$$

where constants $K_0, K_1, \dots, K_{15}$ are provided in table III. Equation (3a) is limited to values of p_{V1} = 0 psia to 1500 psia and values of T_V = 460°R to 660°R. The venturi discharge coefficient terms $C_{d,x}$ in equation (1) are obtained from table II as a function of venturi throat Reynolds number per inch, which is defined as

$$R_{d,v} = \frac{p_{V1} C^* \sqrt{g}}{\mu \sqrt{RT_V}} \tag{4}$$

The viscosity term μ in equation (4) is obtained from the following approximation of Sutherland's formula:

$$\mu = (2.6812 \times 10^{-8})\frac{2.27(0.8333T_V)^{1.5}}{0.8333T_V + 198.6} \tag{5}$$

Ideal weight flow through each nozzle tested was determined from equations (6) depending on the value of nozzle pressure ratio NPR. If $NPR < (NPR)_c$:

$$w_i = p_{t,j}A_t\left(\frac{1}{NPR}\right)^{1/\gamma}\sqrt{\frac{2g\gamma}{(\gamma - 1)RT_{t,j}}\left[1 - \left(\frac{1}{NPR}\right)^{(\gamma-1)/\gamma}\right]} \tag{6a}$$

If $NPR > (NPR)_c$:

$$w_i = p_{t,j}A_t\sqrt{\frac{g\gamma}{RT_{t,j}}\left(\frac{2}{\gamma + 1}\right)^{(\gamma+1)/(\gamma-1)}} \tag{6b}$$

Nozzle discharge coefficients presented in this paper were then determined from measured nozzle weight-flow (eq. (1)) and nozzle ideal weight-flow (eq. (6)) values.

As discussed in the "Instrumentation" section, a 13-probe rake was used to measure jet total-pressure profiles at the throat of each configuration tested. Values of average (for internal probes 1 to 5; see fig. 2(b)) jet total pressure $p_{t,j}$, individual internal-probe total pressures, $p_{t,j,1}$ to $p_{t,j,5}$, radial position of each probe used on the 13-probe rake r/r_t, and individual throat jet total pressures (measured with 13-probe rake) p_{rake} are provided in table IV for each configuration and NPR tested. Typical exhaust total-pressure profiles measured at the nozzle throat are shown in figure 6 for several configurations. The values of wall static pressure shown in figure 6 were assumed to be equal to $0.5283p_{t,j}$ (for $M = 1.0$). The total-pressure profiles measured at the throat of each configuration were used to determine rake correction factors $K_{R,1},K_{R,2},\ldots,K_{R,5}$ for each individual internal total-pressure probe. The area under each total-pressure profile at the throat (typical examples shown in fig. 6) was obtained by using a compensating polar planimeter to provide an integrated value of jet total pressure at the throat $(p_{rake})_{int}$ for each $p_{t,j}$ set by the internal total-pressure probes. The integrated values of jet total pressure at the throat $(p_{rake})_{int}$ were then plotted against jet total pressure measured with each internal rake probe $p_{t,j,1},p_{t,j,2},\ldots,p_{t,j,5}$. A typical plot of this variation is presented in figure 7 for internal probe number 1 (see fig. 2(b)) on the configuration with $A_t = 0.999$ in^2 and $A_{choke} = 3.853$ in^2. The resulting slope of the line representing this variation is equal to the rake correction factor for the particular probe and configuration plotted. For the example given in figure 7, the result is the value of $K_{R,1}$ for the configuration with $A_t = 0.999$ in^2 and $A_{choke} = 3.853$ in^2. Values of rake correction factors obtained in this manner for all internal jet total-pressure probes in all configurations tested are provided in the table of figure 2(b). Two passes through the data reduction code were then conducted using equations (7) and (8) to compute average jet total pressure and nozzle pressure ratio, respectively.

$$p_{t,j} = \frac{\sum_{i=1}^{5} (p_{t,j,i})(K_{R,i})}{5} \tag{7}$$

$$NPR = \frac{p_{t,j}}{p_a} \tag{8}$$

The first data reduction pass used rake correction factors equal to 1.0 (uncorrected internal total-pressure probe data). The second data reduction pass used the rake correction factors determined with the procedure discussed above and provided in the table of figure 2(b). The resulting values of $p_{t,j}$ and NPR were used to determine nozzle ideal weight-flow rate w_i and nozzle discharge coefficient C_d for each data reduction pass. Of course, when the rake correction factors determined from measured total-pressure profiles at the throat are used, the jet total pressures measured with the internal rakes are corrected to the integrated rake values and most, if not all, of the effects of boundary-layer growth and streamline curvature are removed from the data. The resulting values of discharge coefficient should then be near unity.

As mentioned in the "Instrumentation" section, three measurements of the upstream venturi pressure p_{V1} were recorded simultaneously for each data point. Except for the case when a study of discharge coefficient sensitivity to small errors in measured p_{V1} was conducted, the value of p_{V1} used in equations (2), (3a), and (4) was the average of the three separate measurements.

Throat Reynolds number of the Stratford choke nozzles is defined as

$$R_d = (0.3192 \times 10^6)\left(\frac{D_t}{12}\right)(p_{t,j}) \tag{9}$$

The constant used in equation (9) represents Reynolds number per foot at a total pressure of 1 psia and was obtained from chart 25 of reference 12 for $M = 1.0$ and $T_{t,j} = 530°R$.

RESULTS AND DISCUSSION

Validation of Multiple Critical Venturi System

An initial study was conducted to determine the sensitivity of the multiple critical venturi system operation (determination of nozzle weight flow and discharge coefficient) to individual venturi measurements (p_{V1} and T_V). As described in the "Instrumentation" section, three separate measurements of p_{V1} were made. Two separate passes through the data reduction code were made for the $A_t = 3.992$ in^2 configuration, one for a single measurement of p_{V1} in equations (2), (3a), and (4) of the "Data Reduction" section and one for the average of the three p_{V1} measurements. Resulting discharge coefficients from these two data reduction passes are presented in figure 8 as a function of NPR. Although the differences between these two data sets are small, close examination indicates a slightly smaller data spread when the averaged venturi pressure is used, particularly at NPR < 2.0. The relative effect of a small error in T_V or in p_{V1} on measured weight-flow rate is shown in the following table for MCV = 22 (venturi number 2, venturi number 4, and venturi number 16.1 operating).

T_V, °R	p_{V1}, psi	w_p, lb/sec	Error, percent
560	200	2.7068	Baseline
561	200	2.7043	.09
560	210	2.8428	5.02
560	1000	13.7788	Baseline
561	1000	13.7643	.11
560	1010	13.9195	1.02

Two baseline venturi operating conditions were assumed for the calculations presented in the above table, one at low-weight-flow conditions (p_{V1} = 200 psi) and one at high-weight-flow conditions (p_{V1} = 1000 psi). A venturi operating temperature of 560°R was assumed at both baseline flow conditions. Weight-flow values at both conditions were computed with an assumed temperature measurement uncertainty of 1° and then with an assumed pressure measurement uncertainty of 1 percent of gage full-scale reading (for example, 10 psi for a 1000-psi gage reading). As illustrated by the data in this table, a 1° uncertainty in measurement of T_V would have very little effect on computed weight flow. However, as shown in the table, a 1-percent uncertainty in the measurement of p_{V1} would have a significant effect on the computed value of weight flow. The uncertainty in w_p was particularly large at low-weight-flow operating conditions since a large gage size is required to cover the full operating range of the multiple critical venturi system. For this reason, measured weight flows (and thus discharge coefficients) presented in the remainder of this paper were computed with an average value of p_{V1} from the three separate measurements. This procedure will help eliminate data scatter, particularly at low values of NPR. It also points out the importance of correctly sizing the pressure transducers used to measure the upstream venturi pressure.

As mentioned in the "Stratford Choke Nozzles" section, the Langley 16-Foot Transonic Tunnel Stratford choke nozzles with A_t = 1.933 in^2 and A_t = 5.711 in^2 have been previously calibrated against primary standard nozzles at the Colorado Engineering Experiment Station, Inc. (CEESI). Correct operation of the Langley 16-Foot Transonic Tunnel multiple critical venturi system was validated by comparing discharge coefficients of these two nozzles obtained from the venturi system with those obtained during the CEESI calibration (unpublished data). This comparison is presented in figure 9. The data points on figure 9 identified with flags were obtained at unchoked nozzle conditions (NPR < $(NPR)_c$). Thus, the exhaust velocity at the nozzle throat for these data points was not sonic and the equation for Reynolds number (eq. (9)) given in the "Data Reduction" section is not valid ($M \neq 1.0$). Reynolds numbers for these data points were computed with the appropriate constants from chart 25 of reference 13. As shown in figure 9, excellent agreement generally exists between the multiple critical venturi discharge coefficients and the CEESI calibration data, particularly for the A_t = 5.711 in^2 nozzle. Venturi-derived discharge coefficients generally agree within 0.5 percent with the calibration data at NPR > 1.5 for the A_t = 1.933 in^2 nozzle and at NPR > 1.75 for the A_t = 5.711 in^2 nozzle. The loss of data agreement at very low NPR (less than 1.75) may be a result of inaccuracies in the p_{V1} measurement. The data shown in figure 9 indicate that the Langley 16-Foot Transonic Tunnel multiple critical venturi system provides an accurate (within 0.005) measurement of nozzle discharge coefficients, particularly at NPR > 1.75. Substitution of a lower range pressure transducer for p_{V1} measurement during low-NPR operation should measurably improve the accuracy of discharge coefficients for NPR < 1.75.

Stratford-Choke-Nozzle Discharge Coefficients

Stratford-choke-nozzle discharge coefficients measured with the multiple critical venturi system are presented in figures 10 and 11 as a function of NPR for every combination of nozzle-throat area and choke-plate open area tested. Discharge coefficients shown in figure 10 were computed with jet total pressure $p_{t,j}$ corrected to the integrated value of total pressure at the throat by use of the rake correction factors discussed in the "Data Reduction" section. Discharge coefficients shown in figure 11 were computed with jet total pressure as measured with the internal rakes ($K_{R,1}$ to $K_{R,5}$ = 1.0). Also presented in figures 10 and 11 are the average discharge coefficients for choked flow conditions $\bar{C}_d$ (average of all C_d for NPR > 1.89) for each nozzle--choke-plate combination.

When jet total pressure is corrected to the integrated value at the throat (see fig. 10), discharge coefficients at NPR > 2.0 are approximately equal to unity. With only two exceptions (A_t = 0.999 in^2, A_{choke} = 1.750 in^2 and A_t = 5.711 in^2, A_{choke} = 3.853 in^2), values of average discharge coefficient $\bar{C}_d$ are within 0.005 of unity (demonstrated accuracy of multiple critical venturi system; see fig. 9). This result was expected since correcting internal jet total pressure to the value at the throat (assuming no total-pressure losses between the internal instrumentation location and the nozzle throat) would eliminate most of the loss sources described in reference 7. Two of the most notable total-pressure losses which would be eliminated are the boundary-layer growth along the nozzle walls and the distortion of the total-pressure profile resulting from upstream piping effects. The rake correction factors affect jet total pressure $p_{t,j}$ (see eq. (7)), nozzle pressure ratio NPR (see eq. (8)), and ideal weight-flow rate w_i (see eq. (6)) only; measured weight-flow rate w_p (see eqs. (1) to (5)) is not affected by the rake correction factors. Thus, the discharge coefficients shown in figures 10 and 11 are based on the same measured values of weight-flow rate.

Figure 11 presents Stratford-choke-nozzle discharge coefficients computed from uncorrected internal jet total pressures. Discharge coefficients shown in this figure include total-pressure losses from the internal total-pressure instrumentation location to the nozzle throat. Average nozzle discharge coefficients $\bar{C}_d$ shown in figure 11 are always less than unity and range in value from 0.978 to 0.996, depending on the configuration. Computed discharge coefficients given in reference 6 for nozzles conforming to the design guidelines from which the Langley 16-Foot Transonic Tunnel Stratford choke nozzles were designed ranged from 0.9925 to 0.9975. The values of $\bar{C}_d$ measured during the present test which fall below the range of computed discharge coefficients given in reference 6 ($\bar{C}_d$ < 0.9925) probably result from nonconformance to prescribed design guidelines for some of the current test nozzles. These effects are discussed later along with the effects of nozzle-throat area and choke-plate open area on measured discharge coefficient.

As shown in figures 10 and 11, nozzle discharge coefficient is nearly independent of NPR once choke flow conditions are reached at the nozzle throat (NPR > 1.89).

However, several of the nozzles with smaller throat areas ($A_t \leq 3.002$ in^2) did show a slight increasing trend of C_d with NPR. Since the small-throat-area nozzles have throat Reynolds numbers of approximately 1×10^6 at low NPR (see table I), this variation in C_d with NPR may be a result of transition (and movement thereof) from a laminar to a turbulent wall boundary layer.

The effect of MCV (number and combination of venturis operating) on measured discharge coefficient is shown in the (d) and (f) parts of figures 10 and 11. If the multiple critical venturi system operates as designed, the number and combination of venturis operating should have no effect on measured discharge coefficient. As shown in these figures, the data agreement for all MCV values tested is excellent, and it can be concluded that the number and combination of venturis operating does not have an effect on measured discharge coefficient.

To investigate the effect of venturi temperature (and thus jet total temperature), the $A_t = 5.711$ in^2 configuration with $A_{choke} = 3.853$ in^2 was tested at $(T_{t,j})_{nom} = 530°R$ and 550°R. Again, if the multiple critical venturi system is operating properly, venturi temperature should have no effect on measured discharge coefficient. These data are shown in figures 10(e) and 11(e), and excellent agreement of discharge coefficients for the two different venturi temperatures is exhibited; measured discharge coefficient is independent of venturi temperature.

Figure 12 presents a summary plot showing the effect of Stratford-choke-nozzle-throat area A_t on average nozzle discharge coefficient $\bar{C}_d$ for all choke-plate open areas A_{choke} tested. Average discharge coefficients are those values listed on figures 10 and 11 and do not include unchoked (NPR < 1.89) nozzle data. The data points identified with flags in figure 12 were obtained on a configuration with A_{choke} greater than A_t. This condition would indicate that the flow through the choke plate is not choked and that the choke plate is serving as a flow straightening device only. Whether or not the choke-plate flow is choked or unchoked should have no effect on discharge coefficient. As shown in figure 12, average discharge coefficients tend to peak for nozzle throat areas between 2.0 in^2 and 6.0 in^2. A more descriptive conclusion is that for the Stratford choke nozzles of the current test, average discharge coefficient decreases for nozzle-throat areas less than 2.0 in^2 or greater than 6.0 in^2. As mentioned previously, the range of experimental average discharge coefficients (0.978 to 0.996 for uncorrected internal total pressures) from the current investigation exceeds the range of computed discharge coefficients (0.9925 to 0.9975) given in reference 6. From figure 12, the average discharge coefficients for nozzles of the current test with 1.933 in$^2 \leq A_t \leq 5.711$ in^2 generally fall within the computed discharge coefficient range of reference 6. It is hypothesized that discharge coefficients for the Stratford choke nozzles with $A_t = 0.999$ in^2, 8.501 in^2, and 11.352 in^2 are reduced because of nonconformance to the design criteria of reference 6. Comparison of the current Stratford-choke-nozzle geometries with the design guidelines of reference 6 is shown in table I. Table I indicates that although Stratford recommends that nozzle operation be limited to nozzle-throat Reynolds numbers greater than 1×10^6, the $A_t = 0.999$ in^2 nozzle of the current test does not reach this value until an NPR between 2.0 and 3.0 is reached. Thus, the $A_t = 0.999$ in^2 nozzle is operating near the extreme end of this design guideline. Another factor which could affect discharge coefficient values of small-throat-area nozzles is that the nozzle wall boundary-layer thickness constitutes a large percentage of the throat area. However, if wall boundary-layer thickness were a problem, it should be eliminated by correcting the internal total pressure to the integrated value of total pressure at the throat. As indicated by the right side of figure 12 (corrected $p_{t,j}$), this is not the case, and the decrease in discharge coefficient for the lower values of A_t appears to be caused by some other factor (probably operating at a Reynolds number which is too low, as discussed earlier).

As shown in table I, the recommended value of L_2/D_t was not obtained with the $A_t = 8.501\ in^2$ and $11.352\ in^2$ nozzles of the current test. The reason for this deviation from prescribed guidelines is that the maximum internal tail-pipe-model diameter D_{max} was fixed at a constant value. Both of these nozzles show substantial decreases in discharge coefficient (for $K_{R,1}$ to $K_{R,5} = 1.0$) to values below the lower bound of computed discharge coefficients from reference 6. One factor which could affect discharge coefficient for the large-throat-area nozzles is upstream convergence. Since D_{max} of the current model was fixed, the amount of convergence leading into the throat decreases with increasing throat area. For the nozzles with larger throat areas, particularly for the $A_t = 11.352\ in^2$ nozzle, throat convergence was small. Results from reference 13 indicate that flow distortion (distortion of total-pressure profile at the throat) increases significantly with decreasing nozzle contraction ratio A_{max}/A_t. The effect of nozzle contraction ratio (hence, of throat area) and of choke-plate open area on a total-pressure distortion parameter ΔK_R derived from the rake correction factors is presented in figure 13. The total-pressure distortion parameter shown in figure 13 is an indicator of distortion at the internal total-pressure instrumentation location. As shown in figure 13, ΔK_R increases rapidly as contraction ratio is decreased (by increasing A_t) to values less than 3.5. The $A_t = 8.501\ in^2$ and $11.352\ in^2$ nozzles have contraction ratios of 2.37 and 1.77, respectively. Figure 13 also indicates that total-pressure distortion is reduced by increasing choke-plate open area.

The amount of flow distortion in the large-throat-area nozzles discussed above could have a significant effect on the measurement of $p_{t,j}$ and, thus, on discharge coefficient. Correcting internal rake total-pressure measurements to the integrated value of jet total pressure at the nozzle throat should eliminate flow distortion effects on discharge coefficient. As shown in the right side of figure 12, applying the rake correction factors to the discharge coefficient computation either eliminates or greatly reduces the decrease in $\bar{C}_d$ exhibited by the $A_t = 8.501\ in^2$ and $A_t = 11.352\ in^2$ nozzles when uncorrected total-pressure measurements are used to compute $\bar{C}_d$ (left side of fig. 12). This result indicates that most of the decrease in $\bar{C}_d$ measured for the large-throat-area nozzles is caused by flow distortion in the total-pressure profiles.

The effect of choke-plate (flow straightener) open area A_{choke} on average discharge coefficient is presented in figure 14. Choke-plate open area should have no effect on nozzle discharge coefficient unless a large amount of flow distortion is introduced by the choke plate itself. From the results shown in figure 13, the choke plates with the smallest open areas produce the largest amounts of flow distortion, particularly for large-throat-area nozzles. As shown in figure 14, choke-plate open area generally has little effect on average discharge coefficient except for the two nozzles with the largest throat areas tested. The variation in $\bar{C}_d$ with A_{choke} for $K_{R,1}$ to $K_{R,5} = 1.0$ is less than 1.5 percent for all nozzles tested and is generally less than 0.5 percent for nozzles with $A_t < 8.501\ in^2$. Total-pressure profile distortion is obviously affecting the discharge coefficient data spread for the two nozzles with the largest throat areas. Correcting measured total pressures with the rake correction factors (right side of fig. 14) reduces the variation of $\bar{C}_d$ with A_{choke} from 0.9 to 1.5 percent to 0.6 to 0.8 percent for these two nozzles. The only consistent trend shown in figure 14 is that the $A_{choke} = 15.286\ in^2$ choke plate always provides the highest value of average discharge coefficient when $K_{R,1}$ to $K_{R,5} = 1.0$. The variation in $\bar{C}_d$ with A_{choke} for all other choke plates tested is generally less than 0.3 percent.

A summary plot of the discharge coefficients for the Langley 16-Foot Transonic Tunnel Stratford choke nozzles is presented in figure 15. The discharge coefficient parameter $\bar{C}_{d,avg}$ shown in this figure is the average of all average discharge coefficients $\bar{C}_d$ obtained at each nozzle-throat area (see figs. 12 and 14), with one exception. Since most nozzle test procedures typically dictate a choke-plate flow straightener (as opposed to screens) and since the screen configurations ($A_{choke} = 15.286$ in^2) consistently produced higher discharge coefficients than the other choke-plate configurations, data for the screen configurations are omitted from $\bar{C}_{d,avg}$. In addition, since discharge coefficients obtained for unchoked flow conditions (NPR < 1.89) were omitted from the computation of average discharge coefficient $\bar{C}_d$, these data are also not included in $\bar{C}_{d,avg}$. Thus the data of figure 15 are for choked flow Stratford choke nozzles with choke-plate flow straighteners only. Discharge coefficients for unchoked flow conditions can be obtained from figures 10 and 11. Discharge coefficients for Stratford choke nozzles with screens as flow straighteners can be obtained from figures 12 and 14.

When internal total-pressure rakes are corrected to the integrated value of total pressure at the throat, $\bar{C}_{d,avg}$ is generally within 0.5 percent of unity (fig. 15). When internal total-pressure rakes are not corrected (typical), measured discharge coefficients for 1.933 in^2 < A_t < 5.711 in^2 generally fall within the computed range of discharge coefficient given in reference 6 for these types of nozzles. Measured discharge coefficient for the $A_t = 0.999$ in^2 nozzle falls below the computed value (ref. 6), probably because nozzle-throat Reynolds number falls below the limit recommended in reference 6. Discharge coefficients for the $A_t = 8.501$ in^2 and 11.352 in^2 nozzles fall below the computed value because of total-pressure profile distortion caused by low nozzle contraction ratios A_{max}/A_t.

CONCLUSIONS

An investigation has been conducted in the Langley 16-Foot Transonic Tunnel to determine and document the weight-flow measurement characteristics of a multiple critical venturi system and the nozzle discharge coefficient characteristics of a series of convergent calibration nozzles. The effects on model discharge coefficient of nozzle-throat area, model choke-plate open area, nozzle pressure ratio, jet total temperature, and number and combination of operating venturis were investigated. Tests were conducted at static conditions (tunnel wind off) at nozzle pressure ratios from 1.3 to 7.0. Results of this investigation indicate the following conclusions:

1. The Langley 16-Foot Transonic Tunnel multiple critical venturi system measures nozzle discharge coefficient to an uncertainty of 0.5 percent for nozzle pressure ratios equal to or above 1.75.

2. The measurement which was determined to have the largest effect on the multiple critical venturi system accuracy is the upstream venturi pressure. It is highly recommended that the average of multiple upstream venturi pressure measurements be used to compute weight flow from the venturi system. In addition, the pressure transducers used to measure the upstream venturi pressure should be carefully sized to cover the required pressure range only.

3. Discharge coefficients measured with the multiple critical venturi system are independent of the number or combination of venturis used. Discharge coefficients are also independent of small variations in venturi temperature.

4. Discharge coefficients measured for the Langley 16-Foot Transonic Tunnel Stratford choke nozzles fall within the expected range of 0.9925 to 0.9975 when nozzle-throat area is between 1.933 in^2 and 5.711 in^2.

5. A low nozzle-throat Reynolds number causes the discharge coefficient of the 0.999-in^2 throat area Stratford choke nozzle to be below the expected value.

6. Total-pressure profile distortion as a result of low contraction ratios is believed to cause the relatively low discharge coefficient levels of 0.986 and 0.979, respectively, for the 8.501-in^2 and the 11.352-in^2 throat area Stratford choke nozzles.

NASA Langley Research Center
Hampton, VA 23665-5225
May 16, 1985

REFERENCES

1. Beckwith, T. G.; and Buck, N. Lewis: Mechanical Measurements. Addison-Wesley Pub. Co., Inc., c.1961.

2. Berrier, Bobby L.: Effect of Nonlifting Empennage Surfaces on Single-Engine Afterbody/Nozzle Drag at Mach Numbers From 0.5 to 2.2. NASA TN D-8326, 1977.

3. Capone, Francis J.: Static Performance of Five Twin-Engine Nonaxisymmetric Nozzles With Vectoring and Reversing Capability. NASA TP-1224, 1978.

4. Capone, Francis J.; and Berrier, Bobby L.: Investigation of Axisymmetric and Nonaxisymmetric Nozzles Installed on a 0.10-Scale F-18 Prototype Airplane Model. NASA TP-1638, 1980.

5. Re, Richard J.; and Berrier, Bobby L.: Static Internal Performance of Single Expansion-Ramp Nozzles With Thrust Vectoring and Reversing. NASA TP-1962, 1982.

6. Stratford, B. S.: The Calculation of the Discharge Coefficient of Profiled Choked Nozzles and the Optimum Profile for Absolute Air Flow Measurement. J. R. Aeronaut. Soc., vol. 68, no. 640, Apr. 1964, pp. 237-245.

7. Smith, Robert E., Jr.; and Matz, Roy J.: A Theoretical Method of Determining Discharge Coefficients for Venturis Operating at Critical Flow Conditions. Trans. ASME, Ser. D: J. Basic Eng., vol. 84, no. 4, Dec. 1962, pp. 434-446.

8. Arnberg, B. T.: Review of Critical Flowmeters for Gas Flow Measurements. Trans. ASME, Ser. D: J. Basic Eng., vol. 84, no. 4, Dec. 1962, pp. 447-460.

9. Johnson, Robert C.: Real-Gas Effects in Critical-Flow-Through Nozzles and Tabulated Thermodynamic Properties. NASA TN D-2565, 1965.

10. Peddrew, Kathryn H., compiler: A User's Guide to the Langley 16-Foot Transonic Tunnel. NASA TM-83186, 1981.

11. Shapiro, Ascher H.: The Dynamics and Thermodynamics of Compressible Fluid Flow. Volume I. Ronald Press Co., c.1953.

12. Ames Research Staff: Equations, Tables, and Charts for Compressible Flow. NACA Rep. 1135, 1953. (Supersedes NACA TN 1428.)

13. Salters, Leland B., Jr.; and Chamales, Nicholas C.: Studies of Flow Distortion in the Tailpipes of Hydrogen Peroxide Gas Generators Used for Jet-Engine Simulation. NASA TM X-1671, 1968.

TABLE I.- TEST NOZZLE GEOMETRY AND REFERENCE 6 DESIGN GUIDELINES

Design feature	Reference 6 guidelines	Test nozzle geometry for A_t, in^2, of -						
		0.999	1.933	3.002	3.992	5.711	8.501	11.352
Choked flow	Yes	Yes	Yes	Yes	Yes	Yes	Yes	Yes
Continuously curving throat wall profile	Yes	Yes	Yes	Yes	Yes	Yes	Yes	Yes
D_{max}/D_t	2 to 3	4.49	3.23	2.59	2.25	1.88	1.54	1.33
R_1/D_t	2	2	2	2	2	2	2	2
L_2/D_t	>.80	.80	1.03	.80	.91	.83	.69	.61
R_d at NPR = 2	$>1 \times 10^6$	8.8×10^5	1.2×10^6	1.5×10^6	1.8×10^6	2.1×10^6	2.6×10^6	3.0×10^6
R_d at NPR = 3	$>1 \times 10^6$	1.3×10^6	1.8×10^6	2.3×10^6	2.7×10^6	3.2×10^6	3.9×10^6	4.5×10^6
R_d at NPR = 5	$>1 \times 10^6$	2.2×10^6	3.1×10^6	3.8×10^6	4.4×10^6	5.3×10^6	6.4×10^6	7.4×10^6
R_d at NPR = 7	$>1 \times 10^6$	3.1×10^6	4.3×10^6	5.4×10^6	6.2×10^6	7.4×10^6	9.0×10^6	1.0×10^7

TABLE II.- INDIVIDUAL CALIBRATED-VENTURI DISCHARGE COEFFICIENTS

$R_{d,v}$, per inch	Discharge coefficients for venturi number -					
	1	2	4	8	16.1	16.2
0.6×10^6	0.9838	0.9857	0.9886	0.9892	0.9922	0.9921
.9	.9856	.9880	.9910	.9912	.9932	.9930
1.4	.9875	.9902	.9931	.9930	.9940	.9938
2.1	.9890	.9920	.9943	.9939	.9941	.9938
3.2	.9902	.9931	.9947	.9939	.9934	.9932
4.8	.9901	.9934	.9939	.9932	.9930	.9928
7.3	.9893	.9930	.9933	.9931	.9930	.9927
11.0	.9903	.9938	.9933	.9934	.9931	.9927
17.0	.9912	.9938	.9935	.9932	.9931	.9928
26.0	.9916	.9939	.9936	.9933	.9932	.9928
40.0	.9918	.9939	.9937	.9934	.9933	.9929

TABLE III.- CONSTANTS FOR CRITICAL-FLOW FACTOR EQUATION

[From unpublished multiple critical venturi data, Boeing Commercial Airplane Group]

Constant	Value of constant	Constant	Value of constant
K_0	0.68493	K_8	3.8268×10^{-9}
K_1	-6.7865×10^{-7}	K_9	-7.3594×10^{-11}
K_2	-4.9249×10^{-9}	K_{10}	4.9408×10^{-13}
K_3	-1.0056×10^{-11}	K_{11}	-1.1853×10^{-15}
K_4	3.0262×10^{-5}	K_{12}	-1.4721×10^{-12}
K_5	-1.9236×10^{-7}	K_{13}	1.7692×10^{-14}
K_6	5.4687×10^{-10}	K_{14}	-1.1238×10^{-16}
K_7	-6.5437×10^{-13}	K_{15}	2.8935×10^{-19}

TABLE IV.- VALUES OF TOTAL PRESSURE MEASURED IN THE INSTRUMENTATION SECTION AND AT THE NOZZLE EXIT

[All pressure measurements in psi.]

(a) A_t = 0.999 in^2; A_{choke} = 1.750 in^2

NPR	$p_{t,j}$	$p_{t,j,1}$	$p_{t,j,2}$	$p_{t,j,3}$	$p_{t,j,4}$	$p_{t,j,5}$
1.308	19.361	19.371	19.367	19.349	19.392	19.327
1.540	22.791	22.797	22.799	22.771	22.827	22.761
1.486	21.983	21.998	21.985	21.976	22.009	21.949
1.749	25.887	25.878	25.864	25.856	25.950	25.884
2.011	29.750	29.732	29.745	29.737	29.797	29.739
2.496	36.936	36.924	36.925	36.922	36.990	36.922
3.004	44.443	44.386	44.393	44.393	44.556	44.487
4.980	73.680	73.563	73.573	73.586	73.895	73.785
5.011	74.125	73.991	74.036	74.032	74.333	74.232
7.011	103.706	103.507	103.577	103.567	104.008	103.872

NPR	$p_{t,j}$	p_{rake} at r/r_t of -					
		-.87	-.53	-.18	.18	.51	.92
1.308	19.361	19.328	19.367	19.356	19.373	19.329	19.358
1.540	22.791	22.737	22.777	22.774	22.787	22.748	22.774
1.486	21.983	21.948	21.985	21.984	22.002	21.958	21.983
1.749	25.887	25.871	25.919	25.908	25.926	25.894	25.908
2.011	29.750	29.730	29.760	29.764	29.782	29.737	29.766
2.496	36.936	36.908	36.945	36.948	36.974	36.933	36.947
3.004	44.443	44.457	44.496	44.504	44.528	44.486	44.505
4.980	73.680	73.727	73.792	73.803	73.843	73.794	73.802
5.011	74.125	74.175	74.250	74.241	74.285	74.231	74.245
7.011	103.706	103.781	103.875	103.870	103.924	103.881	103.875

TABLE IV.- Continued

(b) $A_t = 0.999\ in^2$; $A_{choke} = 3.853\ in^2$

NPR	$p_{t,j}$	$p_{t,j,1}$	$p_{t,j,2}$	$p_{t,j,3}$	$p_{t,j,4}$	$p_{t,j,5}$
1.297	19.281	19.289	19.283	19.281	19.302	19.252
1.416	21.058	21.049	21.045	21.046	21.100	21.050
1.531	22.765	22.769	22.768	22.771	22.777	22.740
1.746	25.955	25.969	25.955	25.951	25.966	25.932
1.993	29.626	29.637	29.631	29.631	29.635	29.597
2.502	37.194	37.203	37.191	37.194	37.207	37.173
2.997	44.551	44.545	44.550	44.558	44.567	44.535
5.005	74.405	74.389	74.415	74.413	74.417	74.393
7.030	104.501	104.434	104.529	104.507	104.535	104.502

NPR	$p_{t,j}$	p_{rake} at r/r_t of -					
		-.89	-.56	-.18	.19	.58	.90
1.297	19.281	19.258	19.288	19.272	19.296	19.249	19.288
1.416	21.058	21.324	21.343	21.328	21.347	21.320	21.364
1.531	22.765	22.759	22.793	22.785	22.792	22.764	22.797
1.746	25.955	25.919	25.950	25.946	25.958	25.925	25.959
1.993	29.626	29.579	29.617	29.611	29.634	29.591	29.615
2.502	37.194	37.138	37.181	37.177	37.196	37.156	37.185
2.997	44.551	44.489	44.545	44.543	44.583	44.532	44.555
5.005	74.405	74.322	74.392	74.397	74.434	74.386	74.385
7.030	104.501	104.374	104.476	104.490	104.543	104.479	104.466

(c) $A_t = 0.999\ in^2$; $A_{choke} = 15.286\ in^2$

NPR	$p_{t,j}$	$p_{t,j,1}$	$p_{t,j,2}$	$p_{t,j,3}$	$p_{t,j,4}$	$p_{t,j,5}$
1.302	19.149	19.141	19.173	19.149	19.163	19.119
1.513	22.253	22.262	22.280	22.248	22.258	22.218
1.756	25.828	25.838	25.848	25.832	25.831	25.791
2.009	29.552	29.548	29.580	29.552	29.556	29.526
2.516	37.003	36.996	37.032	37.006	37.008	36.972
2.988	43.950	43.940	43.970	43.951	43.960	43.931
5.024	73.890	73.859	73.917	73.894	73.904	73.876
7.009	103.096	103.013	103.137	103.131	103.114	103.082

NPR	$p_{t,j}$	p_{rake} at r/r_t of -				
		-.91	-.47	.06	.56	.92
1.302	19.149	19.120	19.120	19.153	19.101	19.146
1.513	22.253	22.224	22.225	22.250	22.207	22.252
1.756	25.828	25.811	25.808	25.843	25.790	25.828
2.009	29.552	29.534	29.542	29.575	29.523	29.564
2.516	37.003	36.978	36.986	37.013	36.964	36.998
2.988	43.950	43.940	43.943	43.972	43.929	43.951
5.024	73.890	73.854	73.878	73.912	73.867	73.866
7.009	103.096	103.056	103.106	103.132	103.082	103.052

TABLE IV.- Continued

(d) A_t = 1.933 in^2; A_{choke} = 1.750 in^2

NPR	$p_{t,j}$	$p_{t,j,1}$	$p_{t,j,2}$	$p_{t,j,3}$	$p_{t,j,4}$	$p_{t,j,5}$
1.311	19.389	19.428	19.406	19.373	19.405	19.332
1.496	22.147	22.188	22.146	22.108	22.241	22.050
1.750	25.880	25.934	25.877	25.828	26.004	25.757
2.496	36.901	36.979	36.897	36.827	37.072	36.730
2.000	29.568	29.601	29.581	29.521	29.660	29.477
2.500	36.963	37.019	36.965	36.908	37.058	36.866
2.992	44.243	44.267	44.243	44.204	44.297	44.202
4.993	73.813	73.886	73.750	73.653	74.161	73.613
7.006	103.588	103.527	103.439	103.344	104.025	103.603

NPR	$p_{t,j}$	p_{rake} at r/r_t of -					
		-.94	-.62	-.33	.10	.54	.88
1.311	19.389	19.389	19.408	19.421	19.428	19.394	19.417
1.498	22.147	22.142	22.175	22.172	22.194	22.145	22.176
1.750	25.880	25.869	25.897	25.904	25.925	25.878	25.913
2.496	36.901	36.908	36.930	36.944	36.972	36.917	36.952
2.000	29.568	29.557	29.579	29.570	29.602	29.544	29.570
2.500	36.963	36.935	36.957	36.958	36.985	36.931	36.952
2.992	44.243	44.208	44.215	44.214	44.249	44.184	44.201
4.993	73.813	73.898	73.915	73.923	73.959	73.899	73.922
7.006	103.588	103.732	103.740	103.741	103.799	103.691	103.717

(e) A_t = 1.933 in^2; A_{choke} = 3.853 in^2

NPR	$p_{t,j}$	$p_{t,j,1}$	$p_{t,j,2}$	$p_{t,j,3}$	$p_{t,j,4}$	$p_{t,j,5}$
1.301	19.306	19.333	19.309	19.294	19.320	19.276
1.530	22.713	22.747	22.715	22.703	22.715	22.685
1.754	26.036	26.068	26.039	26.019	26.042	26.013
2.000	29.685	29.724	29.677	29.672	29.684	29.666
2.507	37.208	37.251	37.198	37.196	37.218	37.177
2.997	44.475	44.515	44.464	44.466	44.471	44.461
3.009	44.665	44.702	44.654	44.655	44.662	44.650
5.021	74.512	74.560	74.490	74.502	74.505	74.503
6.981	103.602	103.612	103.577	103.603	103.597	103.623
6.988	103.711	103.719	103.686	103.711	103.707	103.732

NPR	$p_{t,j}$	p_{rake} at r/r_t of -						
		-.90	-.62	-.35	-.07	.26	.54	.89
1.301	19.306	19.280	19.299	19.301	19.313	19.285	19.299	19.305
1.530	22.713	22.650	22.671	22.678	22.699	22.663	22.687	22.667
1.754	26.036	25.994	26.017	26.015	26.031	26.001	26.023	26.003
2.000	29.685	29.642	29.658	29.667	29.694	29.653	29.666	29.634
2.507	37.208	37.149	37.170	37.179	37.203	37.163	37.170	37.142
2.997	44.475	44.421	44.441	44.451	44.481	44.444	44.447	44.411
3.009	44.665	44.592	44.616	44.628	44.660	44.621	44.622	44.586
5.021	74.512	74.413	74.452	74.460	74.502	74.480	74.460	74.387
6.981	103.602	103.488	103.525	103.561	103.603	103.589	103.563	103.456
6.988	103.711	103.594	103.633	103.657	103.714	103.698	103.657	103.564

TABLE IV.- Continued

(f) A_t = 1.933 in^2; A_{choke} = 15.286 in^2

NPR	$p_{t,j}$	$p_{t,j,1}$	$p_{t,j,2}$	$p_{t,j,3}$	$p_{t,j,4}$	$p_{t,j,5}$
1.339	19.706	19.705	19.735	19.704	19.718	19.668
1.497	22.035	22.039	22.068	22.037	22.036	21.994
1.772	26.077	26.081	26.112	26.081	26.073	26.038
1.982	29.163	29.163	29.193	29.169	29.155	29.136
2.491	36.665	36.637	36.713	36.680	36.661	36.632
3.005	44.236	44.221	44.276	44.261	44.213	44.212
5.037	74.135	74.128	74.181	74.164	74.097	74.103
7.011	103.187	103.168	103.246	103.225	103.137	103.158

NPR	$p_{t,j}$	p_{rake} at r/r_t of -						
		-.94	-.71	-.40	.02	.34	.67	.96
1.339	19.706	19.651	19.692	19.685	19.710	19.667	19.710	19.704
1.497	22.035	21.995	22.029	22.014	22.050	22.011	22.040	22.048
1.772	26.077	26.012	26.058	26.060	26.083	26.044	26.085	26.067
1.982	29.163	29.108	29.148	29.140	29.168	29.137	29.179	29.149
2.491	36.665	36.617	36.658	36.651	36.688	36.648	36.681	36.654
3.005	44.236	44.167	44.210	44.208	44.240	44.200	44.237	44.203
5.037	74.135	74.054	74.110	74.111	74.135	74.101	74.135	74.079
7.011	103.187	103.096	103.185	103.166	103.185	103.170	103.191	103.126

(g) A_t = 3.002 in^2; A_{choke} = 1.750 in^2

NPR	$p_{t,j}$	$p_{t,j,1}$	$p_{t,j,2}$	$p_{t,j,3}$	$p_{t,j,4}$	$p_{t,j,5}$
1.305	19.293	19.333	19.293	19.266	19.296	19.274
1.496	22.111	22.172	22.114	22.082	22.103	22.085
1.747	25.819	25.918	25.804	25.788	25.810	25.776
1.998	29.539	29.638	29.521	29.508	29.532	29.494
2.495	36.880	37.015	36.863	36.828	36.871	36.824
3.019	44.634	44.797	44.616	44.582	44.612	44.564
4.980	73.610	73.880	73.565	73.527	73.584	73.495
5.004	73.968	74.214	73.932	73.892	73.941	73.961
6.007	88.798	89.114	88.751	88.694	88.762	88.670

NPR	$p_{t,j}$	p_{rake} at r/r_t of -						
		-.95	-.65	-.34	.02	.33	.63	.94
1.305	19.293	19.242	19.272	19.251	19.263	19.220	19.250	19.240
1.496	22.111	22.072	22.092	22.057	22.082	22.040	22.049	22.064
1.747	25.819	25.785	25.784	25.761	25.797	25.745	25.771	25.772
1.998	29.539	29.498	29.504	29.494	29.499	29.465	29.467	29.481
2.495	36.880	36.847	36.838	36.814	36.838	36.798	36.807	36.809
3.019	44.634	44.607	44.591	44.562	44.595	44.555	44.537	44.543
4.980	73.610	73.628	73.535	73.498	73.546	73.509	73.467	73.433
5.004	73.968	73.984	73.884	73.854	73.905	73.864	73.829	73.782
6.007	88.798	88.818	88.696	88.665	88.725	88.682	88.627	88.440

TABLE IV.- Continued

(h) $A_t = 3.002\ in^2$; $A_{choke} = 3.853\ in^2$

NPR	$p_{t,j}$	$p_{t,j,1}$	$p_{t,j,2}$	$p_{t,j,3}$	$p_{t,j,4}$	$p_{t,j,5}$
1.288	19.102	19.144	19.099	19.085	19.115	19.067
1.498	22.219	22.264	22.205	22.211	22.223	22.191
1.754	26.016	26.077	26.003	25.997	26.014	25.991
1.995	29.588	29.652	29.557	29.569	29.587	29.576
2.503	37.121	37.204	37.075	37.104	37.107	37.113
3.004	44.543	44.627	44.502	44.521	44.523	44.545
4.997	74.097	74.232	74.018	74.062	74.050	74.121
6.979	103.483	103.639	103.376	103.436	103.414	103.551

NPR	$p_{t,j}$	p_{rake} at r/r_t of -							
		-.94	-.75	-.56	-.25	.10	.44	.67	.92
1.288	19.102	19.097	19.043	19.059	19.071	19.101	19.055	19.076	19.070
1.498	22.219	22.178	22.151	22.176	22.190	22.213	22.175	22.183	22.178
1.754	26.016	25.969	25.944	25.964	25.979	26.014	25.963	25.973	25.956
1.995	29.588	29.543	29.514	29.525	29.550	29.596	29.547	29.536	29.521
2.503	37.121	37.060	37.036	37.050	37.078	37.121	37.072	37.052	37.042
3.004	44.543	44.470	44.455	44.469	44.501	44.552	44.503	44.462	44.446
4.997	74.097	73.971	73.943	73.983	74.029	74.100	74.044	73.975	73.937
6.979	103.483	103.290	103.279	103.330	103.390	103.463	103.427	103.316	103.243

(i) $A_t = 3.002\ in^2$; $A_{choke} = 15.286\ in^2$

NPR	$p_{t,j}$	$p_{t,j,1}$	$p_{t,j,2}$	$p_{t,j,3}$	$p_{t,j,4}$	$p_{t,j,5}$
1.310	19.293	19.285	19.316	19.305	19.290	19.270
1.517	22.338	22.340	22.368	22.338	22.330	22.313
1.757	25.869	25.876	25.882	25.883	25.849	25.857
1.994	29.353	29.359	29.370	29.375	29.327	29.334
2.501	36.827	36.834	36.848	36.845	36.792	36.816
3.009	44.304	44.311	44.329	44.330	44.248	44.301
3.504	51.580	51.590	51.609	51.614	51.504	51.585
5.021	73.919	73.922	73.953	73.962	73.820	73.937
6.988	102.879	102.875	102.936	102.931	102.739	102.914

NPR	$p_{t,j}$	p_{rake} at r/r_t of -								
		-.96	-.80	-.58	-.33	0.0	.26	.51	.73	.93
1.310	19.293	19.266	19.227	19.265	19.267	19.286	19.252	19.292	19.305	19.286
1.517	22.338	22.280	22.256	22.288	22.292	22.313	22.290	22.332	22.332	22.314
1.757	25.869	25.811	25.798	25.834	25.835	25.850	25.833	25.880	25.882	25.855
1.994	29.353	29.289	29.276	29.314	29.312	29.333	29.321	29.362	29.365	29.329
2.501	36.827	36.750	36.745	36.785	36.785	36.811	36.791	36.837	36.831	36.805
3.009	44.304	44.214	44.216	44.243	44.262	44.280	44.275	44.299	44.312	44.270
3.504	51.580	51.475	51.478	51.515	51.524	51.546	51.544	51.589	51.569	51.522
5.021	73.919	73.788	73.799	73.833	73.850	73.881	73.894	73.938	73.919	73.794
6.988	102.879	102.682	102.732	102.767	102.769	102.859	102.861	102.903	102.886	100.269

TABLE IV.- Continued

(j) A_t = 3.992 in^2; A_{choke} = 1.750 in^2

NPR	$p_{t,j}$	$p_{t,j,1}$	$p_{t,j,2}$	$p_{t,j,3}$	$p_{t,j,4}$	$p_{t,j,5}$
1.289	19.049	19.137	19.041	19.020	19.065	18.982
1.496	22.103	22.215	22.080	22.064	22.104	22.052
1.753	25.904	26.042	25.866	25.863	25.907	25.841
2.018	29.811	29.962	29.761	29.757	29.808	29.765
2.510	37.092	37.287	37.037	37.022	37.081	37.033
3.001	44.339	44.561	44.261	44.263	44.319	44.290
3.992	58.986	59.297	58.893	58.875	58.960	58.904
4.505	66.562	66.905	66.450	66.449	66.542	66.465

NPR	$p_{t,j}$	p_{rake} at r/r_t of -								
		-.96	-.68	-.41	-.17	.01	.23	.48	.71	.94
1.289	19.049	19.046	18.967	18.997	18.991	19.019	18.972	19.006	18.992	19.004
1.496	22.103	22.102	22.008	22.046	22.041	22.060	22.024	22.046	22.045	22.058
1.753	25.904	25.908	25.787	25.821	25.815	25.846	25.812	25.836	25.808	25.839
2.018	29.811	29.823	29.685	29.717	29.712	29.742	29.709	29.720	29.706	29.742
2.510	37.092	37.083	36.930	36.973	36.965	37.001	36.974	36.981	36.943	37.000
3.001	44.339	44.357	44.177	44.217	44.208	44.250	44.228	44.217	44.183	44.235
3.992	58.986	58.980	58.756	58.803	58.803	58.857	58.824	58.800	58.742	58.838
4.505	66.562	66.559	66.327	66.374	66.360	66.423	66.399	66.362	66.303	66.396

(k) A_t = 3.992 in^2; A_{choke} = 3.853 in^2

NPR	$p_{t,j}$	$p_{t,j,1}$	$p_{t,j,2}$	$p_{t,j,3}$	$p_{t,j,4}$	$p_{t,j,5}$
1.314	19.389	19.443	19.462	19.276	19.474	19.293
1.501	22.141	22.202	22.202	22.024	22.227	22.052
1.743	25.712	25.788	25.757	25.594	25.785	25.638
1.991	29.371	29.455	29.408	29.245	29.440	29.305
2.499	36.871	36.980	36.887	36.739	36.931	36.816
3.010	44.401	44.521	44.396	44.263	44.442	44.384
5.006	73.842	74.035	73.779	73.689	73.829	73.879
7.012	103.408	103.695	103.283	103.243	103.343	103.475

NPR	$p_{t,j}$	p_{rake} at r/r_t of -								
		-.96	-.83	-.64	-.36	-.05	.26	.53	.74	.96
1.314	19.389	19.346	19.190	19.252	19.263	19.418	19.313	19.341	19.394	19.219
1.501	22.141	22.088	21.968	22.006	22.028	22.184	22.078	22.099	22.139	21.963
1.743	25.712	25.648	25.523	25.552	25.597	25.749	25.648	25.648	25.674	25.489
1.991	29.371	29.291	29.171	29.207	29.249	29.398	29.314	29.305	29.318	29.136
2.499	36.871	36.782	36.640	36.691	36.733	36.891	36.811	36.793	36.782	36.582
3.010	44.401	44.289	44.163	44.204	44.249	44.429	44.351	44.311	44.290	44.086
5.006	73.842	73.622	73.530	73.570	73.634	73.854	73.798	73.685	73.613	73.310
7.012	103.408	102.924	103.026	103.040	103.115	103.402	103.350	103.180	103.081	102.182

TABLE IV.- Continued

(l) A_t = 3.992 in^2; A_{choke} = 5.779 in^2

NPR	$p_{t,j}$	$p_{t,j,1}$	$p_{t,j,2}$	$p_{t,j,3}$	$p_{t,j,4}$	$p_{t,j,5}$
1.301	19.173	19.213	19.173	19.168	19.158	19.152
1.500	22.115	22.173	22.116	22.107	22.090	22.086
1.751	25.805	25.881	25.793	25.801	25.772	25.778
2.007	29.583	29.669	29.566	29.590	29.538	29.553
2.452	36.135	36.234	36.109	36.144	36.076	36.115
2.499	36.827	36.928	36.801	36.831	36.772	36.805
3.001	44.229	44.336	44.202	44.237	44.161	44.208
5.013	73.858	74.030	73.818	73.859	73.739	73.847
6.993	103.038	103.278	102.985	103.035	102.857	103.036

NPR	$p_{t,j}$	p_{rake} at r/r_t of -								
		-.96	-.71	-.42	-.20	-.01	.22	.45	.69	.92
1.301	19.173	19.131	19.112	19.155	19.143	19.150	19.123	19.167	19.176	19.152
1.500	22.115	22.076	22.047	22.082	22.069	22.081	22.064	22.112	22.109	22.099
1.751	25.805	25.757	25.734	25.775	25.758	25.784	25.755	25.808	25.792	25.788
2.007	29.583	29.521	29.500	29.548	29.531	29.542	29.528	29.571	29.556	29.571
2.452	36.135	36.068	36.032	36.076	36.058	36.085	36.069	36.121	36.096	36.103
2.499	36.827	36.750	36.730	36.775	36.753	36.774	36.764	36.805	36.793	36.804
3.001	44.229	44.146	44.121	44.164	44.144	44.175	44.165	44.214	44.194	44.202
5.013	73.858	73.744	73.707	73.755	73.720	73.780	73.786	73.828	73.795	73.786
6.993	103.038	102.906	102.854	102.892	102.863	102.926	102.946	102.988	102.959	102.926

(m) A_t = 3.992 in^2; A_{choke} = 15.286 in^2

NPR	$p_{t,j}$	$p_{t,j,1}$	$p_{t,j,2}$	$p_{t,j,3}$	$p_{t,j,4}$	$p_{t,j,5}$
1.344	19.804	19.834	19.853	19.825	19.791	19.719
1.513	22.298	22.327	22.351	22.331	22.286	22.195
1.760	25.938	25.981	26.003	25.984	25.914	25.808
2.008	29.592	29.636	29.669	29.637	29.570	29.448
2.491	36.710	36.775	36.798	36.769	36.681	36.527
2.986	43.996	44.064	44.092	44.079	43.961	43.783
5.023	74.012	74.135	74.182	74.164	73.936	73.642
7.014	103.333	103.482	103.564	103.568	103.236	102.815

NPR	$p_{t,j}$	p_{rake} at r/r_t of -								
		-.96	-.76	-.50	-.28	-.04	.20	.41	.71	.96
1.344	19.804	19.771	19.738	19.759	19.773	19.794	19.754	19.805	19.801	19.777
1.513	22.298	22.270	22.240	22.272	22.280	22.299	22.275	22.310	22.307	22.280
1.760	25.938	25.917	25.886	25.928	25.919	25.946	25.913	25.966	25.966	25.928
2.008	29.592	29.563	29.547	29.571	29.573	29.595	29.566	29.623	29.626	29.577
2.491	36.710	36.691	36.672	36.708	36.705	36.717	36.695	36.751	36.759	36.702
2.986	43.996	43.980	43.958	43.994	43.991	44.008	43.991	44.053	44.070	43.992
5.023	74.012	73.909	73.967	74.008	73.991	74.028	74.026	74.097	74.105	74.002
7.014	103.333	102.647	103.326	103.348	103.297	103.369	103.388	103.465	103.486	103.276

TABLE IV.- Continued

(n) A_t = 5.711 in^2; A_{choke} = 3.853 in^2

NPR	$p_{t,j}$	$p_{t,j,1}$	$p_{t,j,2}$	$p_{t,j,3}$	$p_{t,j,4}$	$p_{t,j,5}$
1.299	19.362	19.440	19.299	19.321	19.332	19.421
1.506	22.436	22.546	22.350	22.380	22.358	22.545
1.754	26.129	26.281	25.998	26.059	26.011	26.293
2.002	29.833	29.989	29.688	29.752	29.707	30.028
2.503	37.298	37.502	37.098	37.208	37.117	37.566
2.993	44.586	44.832	44.348	44.491	44.368	44.891
5.007	74.598	74.987	74.198	74.438	74.233	75.133
5.998	89.364	89.817	88.699	89.176	88.931	89.997

NPR	$p_{t,j}$	p_{rake} at r/r_t of -					
		-.98	-.84	-.70	-.48	-.25	-.04
1.299	19.362	19.231	19.267	19.217	19.258	19.292	19.326
1.506	22.436	22.235	22.293	22.259	22.306	22.356	22.395
1.754	26.129	25.853	25.947	25.894	25.973	26.021	26.070
2.002	29.833	29.526	29.643	29.595	29.681	29.741	29.768
2.503	37.298	36.738	37.064	37.024	37.111	37.185	37.254
2.993	44.586	43.586	44.310	44.284	44.367	44.469	44.545
5.007	74.598	70.044	74.135	74.107	74.259	74.414	74.535
5.998	89.364	79.925	88.817	88.766	88.952	89.140	89.284

NPR	$p_{t,j}$	p_{rake} at r/r_t of -				
		.21	.41	.64	.85	.96
1.299	19.362	19.365	19.334	19.294	19.272	19.182
1.506	22.435	22.369	22.401	22.335	22.300	22.210
1.754	26.129	26.060	26.085	25.993	25.947	25.872
2.002	29.833	29.794	29.809	29.691	29.650	29.562
2.503	37.298	37.262	37.271	37.131	37.057	36.983
2.993	44.586	44.556	44.561	44.399	44.320	44.232
5.007	74.598	74.591	74.566	74.270	74.149	74.072
5.998	89.364	89.372	89.323	88.962	88.636	88.743

TABLE IV.- Continued

(o) $A_t = 5.711\ in^2$; $A_{choke} = 5.779\ in^2$

NPR	$p_{t,j}$	$p_{t,j,1}$	$p_{t,j,2}$	$p_{t,j,3}$	$p_{t,j,4}$	$p_{t,j,5}$
1.290	18.992	19.070	18.982	18.999	18.952	18.956
1.480	21.764	21.909	21.763	21.788	21.719	21.744
1.495	22.014	22.136	21.993	22.017	21.950	21.974
1.749	25.753	25.910	25.738	25.750	25.659	25.709
1.998	29.418	29.605	29.389	29.417	29.315	29.363
2.487	36.608	36.834	36.570	36.603	36.466	36.565
2.995	44.085	44.352	44.039	44.087	43.908	44.039
4.998	73.565	74.022	73.469	73.575	73.253	73.507
6.967	102.537	103.170	102.427	102.543	102.102	102.445

NPR	$p_{t,j}$	p_{rake} at r/r_t of -					
		-.96	-.78	-.58	-.34	-.15	.01
1.290	18.992	18.950	18.944	18.926	18.930	18.925	18.938
1.480	21.764	21.739	21.725	21.731	21.737	21.730	21.732
1.495	22.014	21.942	21.929	21.928	21.938	21.935	21.938
1.749	25.753	25.655	25.651	25.655	25.672	25.653	25.655
1.998	29.418	29.301	29.292	29.316	29.325	29.304	29.318
2.487	36.608	36.472	36.467	36.482	36.486	36.474	36.481
2.995	44.085	43.934	43.930	43.953	43.944	43.921	43.938
4.998	73.565	73.352	73.348	73.368	73.341	73.307	73.335
6.967	102.537	102.255	102.261	102.257	102.231	102.177	102.200

NPR	$p_{t,j}$	p_{rake} at r/r_t of -				
		.19	.39	.60	.79	.97
1.290	18.992	18.910	18.965	18.976	18.978	18.864
1.480	21.764	21.714	21.778	21.788	21.776	21.650
1.495	22.014	21.919	21.978	21.976	21.964	21.852
1.749	25.753	25.636	25.715	25.713	25.705	25.581
1.998	29.416	29.299	29.372	29.383	29.366	29.230
2.487	36.608	36.466	36.552	36.553	36.543	36.408
2.995	44.085	43.922	44.015	44.022	43.993	43.859
4.998	73.565	73.332	73.443	73.436	73.416	73.124
6.967	102.537	102.251	102.359	102.371	102.349	99.745

TABLE IV.- Continued

(p) $A_t = 5.711\ in^2$; $A_{choke} = 7.549\ in^2$

NPR	$p_{t,j}$	$p_{t,j,1}$	$p_{t,j,2}$	$p_{t,j,3}$	$p_{t,j,4}$	$p_{t,j,5}$
1.293	19.076	19.141	19.092	19.090	19.022	19.037
1.506	22.218	22.238	22.240	22.257	22.130	22.175
1.779	26.241	26.343	26.257	26.301	26.125	26.180
1.748	25.782	25.876	25.809	25.829	25.662	25.733
1.996	29.433	29.531	29.460	29.496	29.290	29.387
2.479	36.548	36.671	36.574	36.629	36.372	36.492
2.997	44.193	44.347	44.220	44.291	43.979	44.128
4.991	73.588	73.858	73.606	73.759	73.226	73.490
5.015	73.948	74.205	73.987	74.123	73.582	73.842
7.009	103.357	103.727	103.399	103.588	102.843	103.227

NPR	$p_{t,j}$	p_{rake} at r/r_t of -					
		-.95	-.82	-.63	-.41	-.23	-.03
1.293	19.076	19.037	19.039	19.026	19.048	19.021	19.032
1.506	22.218	22.166	22.176	22.174	22.178	22.154	22.155
1.779	26.241	26.139	26.160	26.151	26.168	26.146	26.132
1.748	25.782	25.690	25.723	25.717	25.724	25.696	25.692
1.996	29.433	29.337	29.367	29.365	29.379	29.348	29.326
2.479	36.548	36.429	36.490	36.480	36.488	36.436	36.419
2.997	44.193	44.042	44.107	44.122	44.122	44.078	44.040
4.991	73.588	73.310	73.430	73.483	73.476	73.386	73.328
5.015	73.948	73.679	73.786	73.826	73.839	73.742	73.687
7.009	103.357	102.939	103.137	103.198	103.189	103.068	102.991

NPR	$p_{t,j}$	p_{rake} at r/r_t of -				
		.18	.36	.56	.75	.96
1.293	19.076	19.015	19.059	19.066	19.063	18.961
1.506	22.218	22.149	22.179	22.186	22.200	22.098
1.779	26.241	26.128	26.171	26.177	26.200	26.083
1.748	25.782	25.679	25.729	25.735	25.756	25.639
1.996	29.433	29.331	29.385	29.393	29.419	29.288
2.479	36.548	36.433	36.472	36.482	36.520	36.400
2.997	44.193	44.055	44.110	44.125	44.162	44.040
4.991	73.588	73.371	73.431	73.460	73.536	73.434
5.015	73.948	73.712	73.793	73.809	73.887	73.785
7.009	103.357	103.014	103.127	103.192	103.257	103.134

TABLE IV.- Continued

(q) A_t = 5.711 in^2; A_{choke} = 15.286 in^2

NPR	$p_{t,j}$	$p_{t,j,1}$	$p_{t,j,2}$	$p_{t,j,3}$	$p_{t,j,4}$	$p_{t,j,5}$
1.316	19.408	19.438	19.454	19.421	19.343	19.382
1.497	22.079	22.105	22.127	22.116	22.001	22.047
1.751	25.829	25.680	25.865	25.863	25.737	25.781
1.999	29.477	29.523	29.535	29.530	29.364	29.434
2.523	37.208	37.277	37.235	37.269	37.047	37.162
3.008	44.369	44.447	44.455	44.445	44.176	44.324
4.996	73.691	73.796	73.827	73.830	73.371	73.632
7.022	103.570	103.712	103.775	103.778	103.103	103.480

NPR	$p_{t,j}$	p_{rake} at r/r_t of -					
		-.97	-.81	-.62	-.40	-.21	-.02
1.316	19.408	19.364	19.380	19.351	19.359	19.351	19.367
1.497	22.079	22.003	22.053	22.024	22.033	22.021	22.022
1.751	25.829	25.730	25.790	25.778	25.783	25.756	25.780
1.999	29.477	29.376	29.445	29.426	29.425	29.396	29.414
2.523	37.208	37.052	37.154	37.120	37.127	37.101	37.114
3.008	44.369	44.201	44.319	44.288	44.279	44.251	44.266
4.996	73.691	73.404	73.630	73.598	73.568	73.491	73.512
7.022	103.570	103.112	103.524	103.463	103.384	103.273	103.295

NPR	$p_{t,j}$	p_{rake} at r/r_t of -				
		.19	.37	.58	.76	.96
1.316	19.408	19.339	19.391	19.423	19.395	19.235
1.497	22.079	22.019	22.057	22.102	22.077	21.951
1.751	25.829	25.758	25.822	25.853	25.832	25.694
1.999	29.477	29.410	29.479	29.511	29.494	29.344
2.523	37.208	37.112	37.184	37.230	37.197	37.050
3.008	44.369	44.271	44.354	44.404	44.380	44.219
4.996	73.691	73.553	73.663	73.717	73.729	73.484
7.022	103.570	103.372	103.515	103.602	103.642	102.990

TABLE IV.- Continued

(r) A_t = 8.501 in^2; A_{choke} = 3.853 in^2

NPR	$p_{t,j}$	$p_{t,j,1}$	$p_{t,j,2}$	$p_{t,j,3}$	$p_{t,j,4}$	$p_{t,j,5}$
1.274	19.008	19.182	18.867	18.892	18.986	19.111
1.506	22.466	22.796	22.163	22.354	22.555	22.463
1.759	26.244	26.650	25.825	26.099	26.398	26.248
2.003	29.883	30.346	29.407	29.710	30.052	29.899
1.993	29.723	30.199	29.257	29.535	29.888	29.737
2.492	37.168	37.726	36.586	36.947	37.391	37.189
2.998	44.716	45.375	44.011	44.457	44.968	44.767
4.256	63.490	64.399	62.473	63.130	63.820	63.630

NPR	$p_{t,j}$	p_{rake} at r/r_t of -					
		-.96	-.82	-.68	-.56	-.39	-.20
1.274	19.008	18.750	18.861	18.860	18.859	18.931	18.966
1.506	22.466	22.234	22.384	22.406	22.399	22.448	22.466
1.759	26.244	25.957	26.124	26.184	26.163	26.194	26.225
2.003	29.883	29.575	29.743	29.812	29.796	29.820	29.863
1.993	29.723	29.416	29.594	29.648	29.638	29.658	29.713
2.492	37.168	36.812	37.011	37.084	37.078	37.085	37.155
2.998	44.716	44.304	44.526	44.630	44.639	44.622	44.698
4.256	63.490	63.065	63.343	63.442	63.436	63.346	63.420

NPR	$p_{t,j}$	p_{rake} at r/r_t of -						
		-.03	.17	.33	.53	.71	.84	.97
1.274	19.008	19.010	19.000	19.032	18.988	18.918	18.812	18.808
1.506	22.466	22.530	22.542	22.581	22.577	22.443	22.337	22.365
1.759	26.244	26.340	26.357	26.412	26.380	26.211	26.079	26.118
2.003	29.883	30.013	30.036	30.082	30.051	29.845	29.700	29.760
1.993	29.723	29.848	29.873	29.921	29.890	29.670	29.539	29.608
2.492	37.168	37.337	37.383	37.424	37.382	37.116	36.972	37.046
2.998	44.716	44.914	44.990	45.035	44.971	44.661	44.489	44.599
4.256	63.490	63.770	63.909	63.950	63.840	63.405	63.213	63.320

TABLE IV.- Continued

(s) A_t = 8.501 in^2; A_{choke} = 5.779 in^2

NPR	$p_{t,j}$	$p_{t,j,1}$	$p_{t,j,2}$	$p_{t,j,3}$	$p_{t,j,4}$	$p_{t,j,5}$
1.304	19.164	19.380	19.146	19.140	19.047	19.105
1.501	22.060	22.422	22.037	22.010	21.870	21.960
1.751	25.740	26.224	25.728	25.676	25.472	25.600
2.000	29.399	29.987	29.393	29.316	29.074	29.227
2.503	36.760	37.515	36.765	36.664	36.391	36.563
3.003	44.136	45.020	44.114	43.986	43.685	43.875
4.999	73.463	74.925	73.396	73.276	72.672	73.042
5.991	88.036	89.809	87.958	87.828	87.074	87.521
5.969	87.702	89.448	87.618	87.504	86.732	87.209

NPR	$p_{t,j}$	p_{rake} at r/r_t of -					
		-.96	-.79	-.65	-.48	-.29	-.13
1.304	19.164	18.933	19.045	19.046	19.043	19.039	19.022
1.501	22.060	21.806	21.874	21.910	21.901	21.874	21.842
1.751	25.740	25.399	25.479	25.512	25.511	25.488	25.453
2.000	29.399	29.019	29.072	29.127	29.134	29.103	29.065
2.503	36.780	36.326	36.382	36.455	36.460	36.400	36.374
3.003	44.136	43.595	43.606	43.730	43.760	43.685	43.646
4.999	73.463	72.768	72.667	72.807	72.868	72.714	72.655
5.991	88.036	87.259	87.125	87.253	87.323	87.148	87.083
5.969	87.702	86.943	86.798	86.925	86.993	86.811	86.740

NPR	$p_{t,j}$	p_{rake} at r/r_t of -						
		0.0	.15	.32	.49	.66	.80	.95
1.304	19.164	19.033	19.006	19.082	19.104	19.082	18.986	18.957
1.501	22.060	21.855	21.826	21.924	21.958	21.922	21.813	21.770
1.751	25.740	25.462	25.423	25.543	25.575	25.530	25.449	25.358
2.000	29.399	29.083	29.034	29.175	29.207	29.152	29.056	28.961
2.503	36.780	36.385	36.340	36.507	36.540	36.494	36.413	36.279
3.003	44.136	43.675	43.622	43.813	43.862	43.785	43.730	43.558
4.999	73.463	72.698	72.676	72.920	73.007	72.945	72.966	72.639
5.991	88.038	87.100	87.102	87.389	87.463	87.459	87.503	86.984
5.969	87.702	86.782	86.774	87.053	87.160	87.121	87.179	86.665

TABLE IV.- Continued

(t) $A_t = 8.501\ in^2$; $A_{choke} = 7.549\ in^2$

NPR	$p_{t,j}$	$p_{t,j,1}$	$p_{t,j,2}$	$p_{t,j,3}$	$p_{t,j,4}$	$p_{t,j,5}$
1.299	19.148	19.263	19.183	19.199	19.018	19.077
1.500	22.116	22.263	22.167	22.191	21.921	22.039
1.747	25.750	25.932	25.804	25.843	25.493	25.679
2.003	29.531	29.735	29.577	29.657	29.230	29.454
2.505	36.935	37.209	36.962	37.086	36.571	36.845
2.998	44.204	44.526	44.228	44.382	43.768	44.116
5.003	73.778	74.363	73.795	74.082	73.031	73.616
5.440	80.209	80.853	80.217	80.541	79.391	80.045

NPR	$p_{t,j}$	p_{rake} at r/r_t of -					
		-.95	-.79	-.66	-.49	-.31	-.17
1.299	19.148	19.016	19.110	19.106	19.077	19.074	19.039
1.500	22.116	21.945	22.062	22.064	22.012	22.016	21.967
1.747	25.750	25.524	25.653	25.678	25.619	25.618	25.550
2.003	29.531	29.302	29.436	29.456	29.398	29.381	29.324
2.505	36.935	36.674	36.801	36.836	36.787	36.760	36.673
2.998	44.204	43.889	44.032	44.083	44.033	43.992	43.904
5.003	73.776	73.249	73.468	73.574	73.506	73.415	73.260
5.440	80.209	79.598	79.869	79.972	79.920	79.804	79.653

NPR	$p_{t,j}$	p_{rake} at r/r_t of -						
		.01	.17	.32	.50	.64	.76	.95
1.299	19.148	19.027	19.035	19.104	19.100	19.112	19.046	19.066
1.500	22.116	21.961	21.964	22.035	22.021	22.048	22.009	21.989
1.747	25.750	25.540	25.560	25.636	25.625	25.658	25.618	25.592
2.003	29.531	29.300	29.334	29.413	29.391	29.431	29.390	29.388
2.505	36.935	36.644	36.694	36.779	36.765	36.817	36.788	36.789
2.998	44.204	43.868	43.933	44.027	43.995	44.070	44.039	44.054
5.003	73.776	73.198	73.338	73.459	73.430	73.530	73.567	73.579
5.440	80.209	79.583	79.729	79.847	79.828	79.946	79.966	79.980

TABLE IV.- Continued

(u) A_t = 8.501 in^2; A_{choke} = 15.286 in^2

NPR	$p_{t,j}$	$p_{t,j,1}$	$p_{t,j,2}$	$p_{t,j,3}$	$p_{t,j,4}$	$p_{t,j,5}$
1.306	19.224	19.234	19.255	19.253	19.131	19.225
1.500	22.073	22.054	22.077	22.096	21.965	22.173
1.756	25.844	25.815	25.850	25.868	25.700	25.987
2.009	29.556	29.523	29.555	29.601	29.382	29.720
2.497	36.737	36.702	36.736	36.786	36.517	36.945
3.010	44.284	44.245	44.286	44.337	44.013	44.538
5.003	73.597	73.500	73.586	73.705	73.137	74.055
5.420	79.729	79.628	79.719	79.851	79.206	80.237

NPR	$p_{t,j}$	p_{rake} at r/r_t of -					
		-.96	-.81	-.65	-.51	-.34	-.18
1.306	19.224	19.113	19.209	19.211	19.169	19.136	19.144
1.500	22.073	21.919	22.050	22.047	22.027	22.034	22.004
1.756	25.844	25.630	25.777	25.798	25.767	25.768	25.738
2.009	29.556	29.301	29.463	29.481	29.454	29.462	29.445
2.497	36.737	36.447	36.621	36.657	36.633	36.637	36.603
3.010	44.284	43.939	44.122	44.190	44.170	44.149	44.107
5.003	73.597	73.066	73.358	73.451	73.411	73.379	73.316
5.420	79.729	79.147	79.471	79.572	79.545	79.500	79.417

NPR	$p_{t,j}$	p_{rake} at r/r_t of -						
		-.02	.16	.34	.50	.66	.81	.96
1.306	19.224	19.174	19.138	19.222	19.251	19.236	19.150	19.137
1.500	22.073	22.035	22.011	22.086	22.103	22.088	21.977	21.922
1.756	25.844	25.777	25.757	25.834	25.853	25.815	25.719	25.635
2.009	29.556	29.465	29.463	29.529	29.537	29.516	29.409	29.306
2.497	36.737	36.625	36.631	36.720	36.734	36.692	36.574	36.457
3.010	44.284	44.147	44.156	44.247	44.268	44.236	44.106	43.957
5.003	73.597	73.358	73.437	73.563	73.568	73.522	73.370	73.047
5.420	79.729	79.466	79.569	79.721	79.708	79.654	79.498	79.127

TABLE IV.- Continued

(v) A_t = 11.352 in^2; A_{choke} = 3.853 in^2

NPR	$p_{t,j}$	$p_{t,j,1}$	$p_{t,j,2}$	$p_{t,j,3}$	$p_{t,j,4}$	$p_{t,j,5}$
1.296	19.335	19.819	18.883	19.091	19.531	19.348
1.523	22.721	23.432	21.881	22.217	22.884	23.189
1.751	26.120	27.233	25.164	25.585	26.251	26.367
1.994	29.754	31.075	28.692	29.157	29.879	29.965
2.498	37.261	38.895	35.954	36.544	37.412	37.501
2.995	44.686	46.625	43.165	43.853	44.895	44.891
3.037	45.313	47.267	43.776	44.473	45.523	45.528

NPR	$p_{t,j}$	p_{rake} at r/r_t of -					
		-.97	-.82	-.63	-.47	-.30	-.15
1.296	19.335	19.057	19.278	19.258	19.209	19.220	19.301
1.523	22.721	22.144	22.447	22.368	22.303	22.364	22.475
1.751	26.120	25.511	25.820	25.668	25.569	25.682	25.828
1.994	29.754	29.116	29.425	29.229	29.125	29.242	29.412
2.498	37.261	36.541	36.870	36.624	36.489	36.632	36.858
2.995	44.686	43.902	44.263	43.953	43.788	43.957	44.239
3.037	45.313	44.525	44.876	44.553	44.408	44.575	44.853

NPR	$p_{t,j}$	p_{rake} at r/r_t of -						
		-.01	.16	.36	.52	.70	.86	.97
1.296	19.335	19.439	19.447	19.463	19.427	19.248	19.133	19.139
1.523	22.721	22.645	22.662	22.691	22.628	22.381	22.283	22.229
1.751	26.120	26.003	26.013	26.054	26.017	25.717	25.690	25.541
1.994	29.754	29.596	29.623	29.671	29.635	29.310	29.298	29.117
2.498	37.261	37.074	37.132	37.188	37.142	36.727	36.747	36.533
2.995	44.686	44.502	44.562	44.612	44.572	44.081	44.144	43.909
3.037	45.313	45.109	45.189	45.242	45.202	44.701	44.764	44.533

TABLE IV.- Continued

(w) $A_t = 11.352\ in^2$; $A_{choke} = 5.779\ in^2$

NPR	$p_{t,j}$	$p_{t,j,1}$	$p_{t,j,2}$	$p_{t,j,3}$	$p_{t,j,4}$	$p_{t,j,5}$
1.304	19.238	19.784	19.290	19.156	18.946	19.016
1.496	22.081	22.878	22.111	21.998	21.631	21.789
1.749	25.808	26.920	25.814	25.664	25.168	25.454
1.999	29.507	30.803	29.518	29.356	28.775	29.080
2.501	36.903	38.518	36.929	36.730	35.979	36.361
2.997	44.228	46.157	44.261	44.039	43.120	43.563
3.996	58.963	61.539	58.986	58.719	57.487	58.083
4.067	60.013	62.622	60.048	59.758	58.513	59.126

NPR	$p_{t,j}$	p_{rake} at r/r_t of -					
		-.98	-.82	-.63	-.47	-.30	-.15
1.304	19.238	18.849	18.966	19.020	18.984	18.955	18.929
1.496	22.081	21.645	21.824	21.870	21.828	21.749	21.708
1.749	25.808	25.264	25.496	25.566	25.502	25.362	25.305
1.999	29.507	28.896	29.143	29.235	29.176	28.989	28.930
2.501	36.903	36.202	36.465	36.575	36.487	36.257	36.169
2.997	44.228	43.403	43.723	43.835	43.733	43.460	43.345
3.996	58.963	57.976	58.331	58.443	58.325	57.940	57.791
4.067	60.013	58.941	59.368	59.494	59.367	58.962	58.815

NPR	$p_{t,j}$	p_{rake} at r/r_t of -						
		-.01	.17	.33	.52	.67	.82	.98
1.304	19.238	18.932	18.910	19.031	19.054	19.007	18.856	18.686
1.496	22.081	21.698	21.660	21.817	21.880	21.900	21.872	21.622
1.749	25.808	25.273	25.240	25.421	25.551	25.576	25.575	25.294
1.999	29.507	28.899	28.849	29.052	29.197	29.252	29.251	28.910
2.501	36.903	36.145	36.097	36.342	36.530	36.593	36.620	36.186
2.997	44.228	43.313	43.267	43.538	43.772	43.857	43.923	43.381
3.996	58.963	57.755	57.712	58.056	58.373	58.489	58.591	57.792
4.067	60.013	58.776	58.735	59.088	59.420	59.528	59.643	58.818

TABLE IV.- Continued

(x) A_t = 11.352 in^2; A_{choke} = 7.549 in^2

NPR	$p_{t,j}$	$p_{t,j,1}$	$p_{t,j,2}$	$p_{t,j,3}$	$p_{t,j,4}$	$p_{t,j,5}$
1.302	19.199	19.368	19.303	19.302	18.922	19.098
1.503	22.164	22.450	22.247	22.334	21.743	22.046
1.749	25.784	26.199	25.829	26.000	25.246	25.644
2.006	29.583	30.082	29.616	29.828	28.956	29.433
2.503	36.906	37.531	36.933	37.203	36.133	36.727
2.997	44.185	44.942	44.199	44.541	43.275	43.970
4.162	61.359	62.434	61.347	61.843	60.092	61.079

NPR	$p_{t,j}$	p_{rake} at r/r_t of -					
		-.97	-.82	-.69	-.52	-.32	-.16
1.302	19.199	18.879	19.093	19.119	19.061	19.032	18.998
1.503	22.164	21.715	22.004	22.036	21.971	21.934	21.886
1.749	25.784	25.188	25.568	25.609	25.540	25.482	25.416
2.006	29.583	28.900	29.323	29.386	29.294	29.232	29.165
2.503	36.906	36.087	36.579	36.671	36.553	36.477	36.379
2.997	44.185	43.210	43.782	43.890	43.761	43.656	43.542
4.162	61.359	60.063	60.831	60.958	60.781	60.611	60.449

NPR	$p_{t,j}$	p_{rake} at r/r_t of -						
		0.0	.17	.33	.52	.67	.81	.97
1.302	19.199	18.971	18.992	19.043	19.047	19.074	19.029	18.922
1.503	22.164	21.833	21.880	21.935	21.927	21.995	21.978	21.830
1.749	25.784	25.344	25.423	25.470	25.464	25.564	25.574	25.431
2.006	29.583	29.062	29.171	29.220	29.190	29.308	29.345	29.199
2.503	36.906	36.267	36.410	36.453	36.415	36.570	36.634	36.460
2.997	44.185	43.407	43.596	43.635	43.590	43.782	43.885	43.682
4.162	61.359	60.280	60.569	60.605	60.540	60.808	60.971	60.674

TABLE IV.- Concluded

(y) A_t = 11.352 in^2; A_{choke} = 15.286 in^2

NPR	$p_{t,j}$	$p_{t,j,1}$	$p_{t,j,2}$	$p_{t,j,3}$	$p_{t,j,4}$	$p_{t,j,5}$
1.299	19.115	19.111	19.130	19.146	19.035	19.154
1.495	21.999	21.990	22.005	22.029	21.870	22.102
1.757	25.853	25.842	25.844	25.896	25.686	25.998
2.023	29.776	29.749	29.765	29.831	29.572	29.962
2.495	36.718	36.686	36.700	36.787	36.461	36.957
2.516	37.029	36.993	37.012	37.097	36.775	37.269
3.001	44.164	44.133	44.139	44.258	43.833	44.456
3.808	56.035	55.980	56.010	56.157	55.598	56.428
4.117	60.584	60.510	60.561	60.732	60.111	61.007

NPR	$p_{t,j}$	p_{rake} at r/r_t of -					
		-.96	-.83	-.65	-.48	-.32	-.17
1.299	19.115	18.905	19.071	19.079	19.067	19.070	19.043
1.495	21.999	21.714	21.939	21.982	21.977	21.958	21.918
1.757	25.853	25.491	25.772	25.827	25.836	25.814	25.761
2.023	29.776	29.387	29.675	29.754	29.761	29.723	29.673
2.495	36.718	36.267	36.600	36.697	36.716	36.670	36.600
2.516	37.029	36.572	36.913	37.010	37.032	36.980	36.913
3.001	44.164	43.626	44.018	44.132	44.161	44.102	44.021
3.808	56.035	55.353	55.814	55.980	56.010	55.932	55.831
4.117	60.584	59.864	60.366	60.540	60.585	60.489	60.380

NPR	$p_{t,j}$	p_{rake} at r/r_t of -						
		-.01	.18	.34	.51	.68	.83	.96
1.299	19.115	19.072	19.062	19.125	19.155	19.104	18.989	18.878
1.495	21.999	21.934	21.936	22.016	22.048	21.983	21.844	21.662
1.757	25.853	25.774	25.778	25.871	25.905	25.832	25.668	25.417
2.023	29.776	29.671	29.688	29.794	29.816	29.749	29.574	29.297
2.495	36.718	36.599	36.639	36.757	36.784	36.696	36.498	36.157
2.516	37.029	36.902	36.939	37.065	37.092	36.993	36.821	36.462
3.001	44.164	44.013	44.068	44.204	44.238	44.132	43.922	43.504
3.808	56.035	55.819	55.891	56.062	56.081	55.980	55.743	55.193
4.117	60.584	60.359	60.461	60.632	60.657	60.539	60.287	59.688

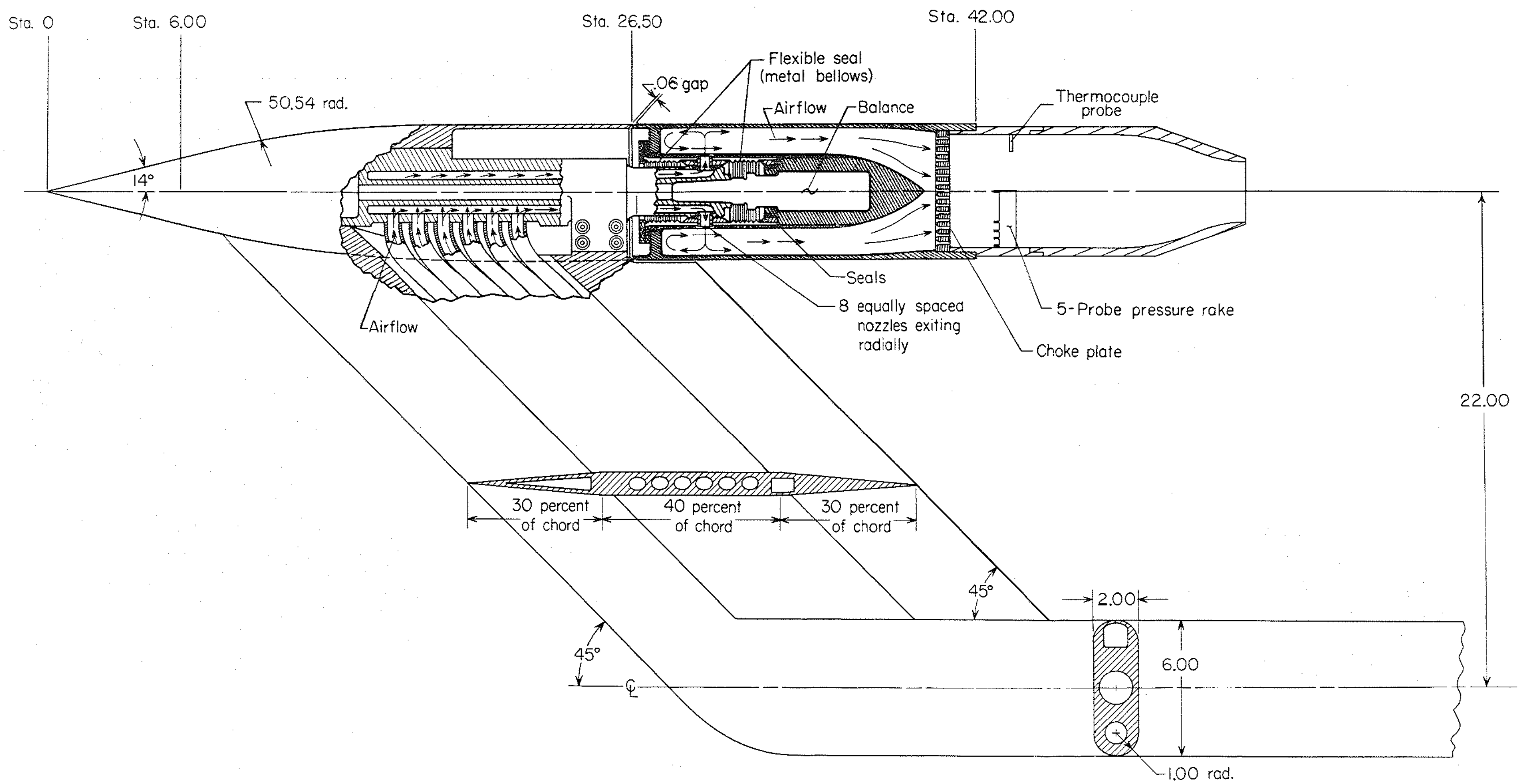

(a) Sketch of model and propulsion-simulation system.

Figure 1.- Air-powered single-engine propulsion-simulation system with a typical nozzle installed. Dimensions are in inches unless otherwise noted.

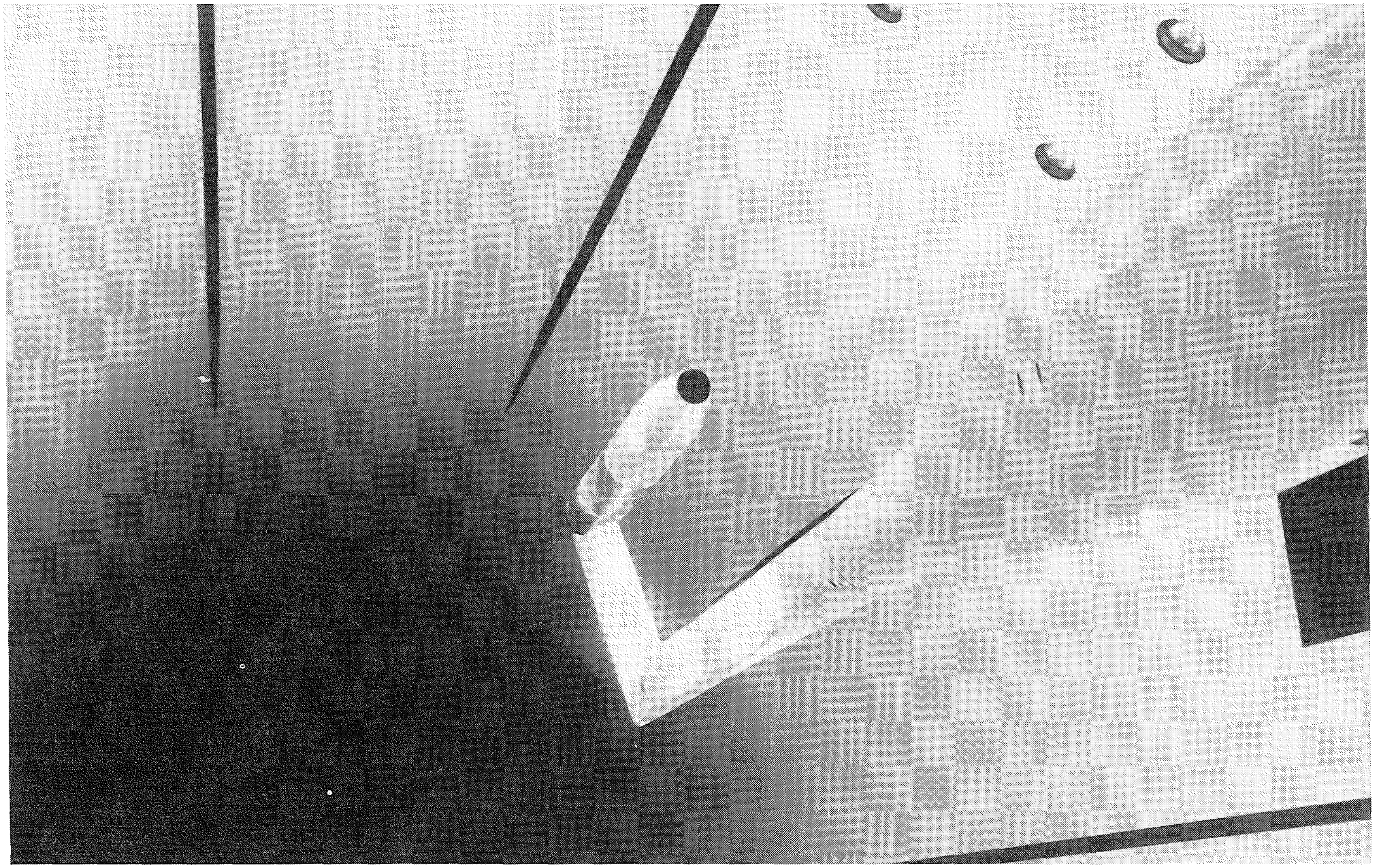

L-73-5555

(b) Photograph of model and propulsion-simulation system installed in Langley 16-Foot Transonic Tunnel.

Figure 1.- Concluded.

STRATFORD CHOKE NOZZLES								
MEASURED THROAT AREA (IN.^{2})	DESIGN GEOMETRY							
	R_1, IN.	R_2, IN.	X, IN.	D_t, IN.	D_2, IN.	L_1, IN.	l, IN.	L_2, IN.
0.999	2.257	21.314	9.428	1.128	1.378	5.500	11.88	0.903
1.933	3.140	9.000	6.274	1.569	1.820	4.000	9.00	1.623
3.002	3.909	14.715	7.450	1.955	2.204	4.500	9.00	1.564
3.992	4.510	8.320	5.837	2.255	2.505	4.000	9.00	2.052
5.711	5.400	7.700	5.432	2.700	2.950	4.000	9.00	2.239
8.501	6.580	7.868	4.985	3.290	3.540	4.000	9.00	2.270
11.352	7.600	5.900	4.086	3.800	4.050	3.500	9.00	2.300

CHOKE PLATES		
OPEN AREA (IN^2)	PERCENT DUCT AREA	HOLE DIA., IN.
1.750	2.7	0.098
3.853	19.1	0.147
5.779	28.0	0.180
7.549	37.1	0.206
15.286	75.9	

NOTE: 15.286-IN^2 CHOKE PLATE IS ACTUALLY WIRE SCREEN MATERIAL SUPPORTED BY AN OPEN METAL LATTICEWORK

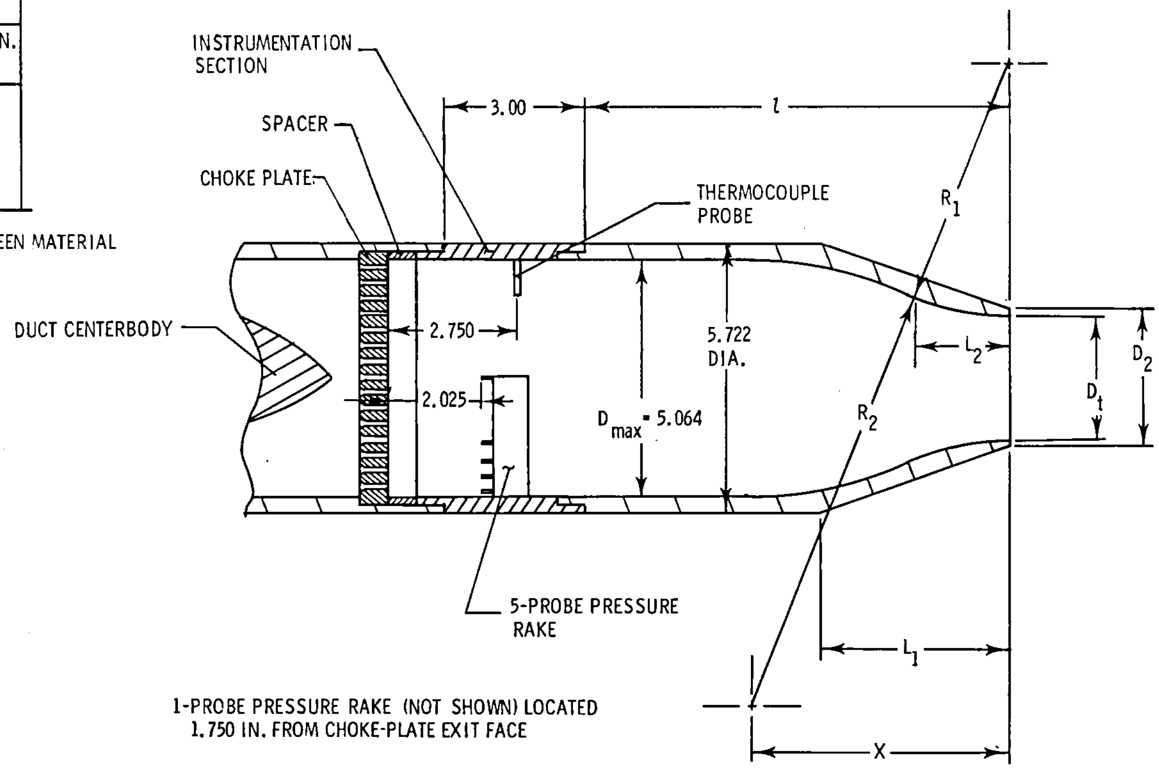

1-PROBE PRESSURE RAKE (NOT SHOWN) LOCATED 1.750 IN. FROM CHOKE-PLATE EXIT FACE

(a) Nozzle and choke-plate geometry.

Figure 2.- Nozzle and instrumentation section sketches.

SUMMARY OF RAKE CONSTANTS						
A_t (in^2)	A_{choke} (in^2)	$K_{R,1}$	$K_{R,2}$	$K_{R,3}$	$K_{R,4}$	$K_{R,5}$
.999	1.750	.9984	.9978	.9978	.9936	.9950
↓	3.853	.9955	.9948	.9950	.9951	.9949
↓	15.286	.9970	.9959	.9961	.9962	.9965
1.933	1.750	.9967	.9962	.9976	.9920	.9988
↓	3.853	.9938	.9944	.9942	.9942	.9941
↓	15.286	.9959	.9950	.9954	.9961	.9962
3.002	1.750	.9880	.9920	.9926	.9919	.9929
↓	3.853	.9909	.9936	.9930	.9932	.9920
↓	15.286	.9909	.9904	.9904	.9918	.9907
3.992	1.750	.9840	.9909	.9910	.9896	.9907
↓	3.853	.9881	.9919	.9926	.9913	.9903
↓	5.779	.9923	.9963	.9955	.9972	.9956
↓	15.286	.9948	.9940	.9941	.9974	1.0004
5.711	3.853	.9802	.9905	.9880	.9901	.9784
↓	5.779	.9839	.9915	.9901	.9948	.9908
↓	7.549	.9901	.9932	.9914	.9986	.9949
↓	15.286	.9923	.9918	.9918	.9981	.9946
8.501	3.853	.9760	1.0061	.9960	.9850	.9888
↓	5.779	.9684	.9857	.9880	.9957	.9907
↓	7.549	.9830	.9905	.9871	1.0009	.9931
↓	15.286	.9904	.9899	.9879	.9955	.9830
11.352	3.853	.9425	1.0177	1.0016	.9778	.9759
↓	5.779	.9393	.9803	.9844	1.0050	.9947
↓	7.549	.9630	.9802	.9717	1.0001	.9842
↓	15.286	.9902	.9895	.9859	.9967	.9824

NOTE: $K_{R,1}$ represents rake constant for probe number 1.

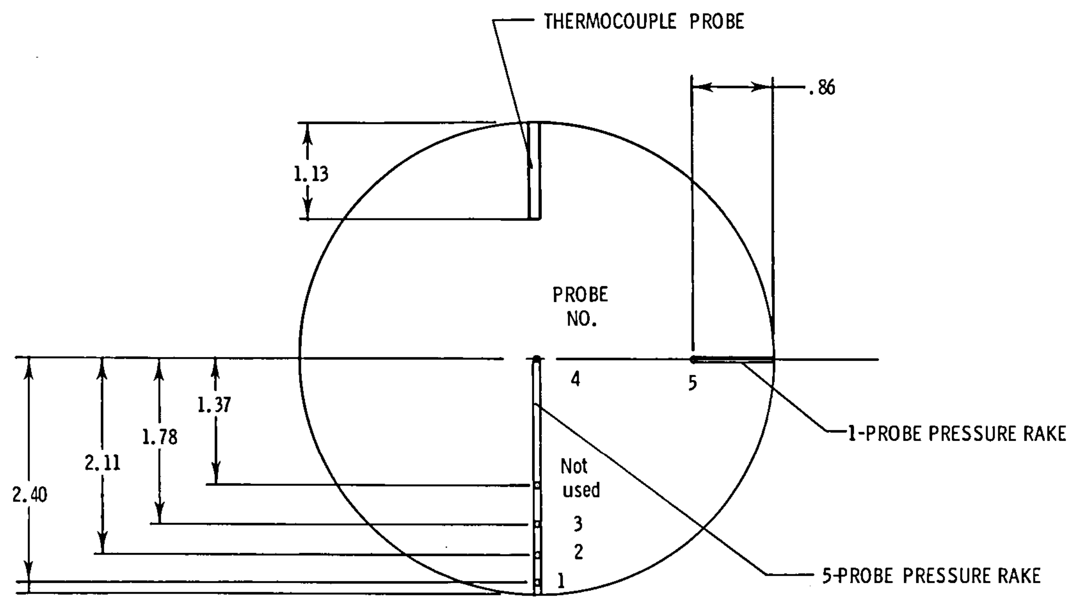

(b) Total-pressure-probe orientation and summary of rake correction factors.

Figure 2.- Concluded.

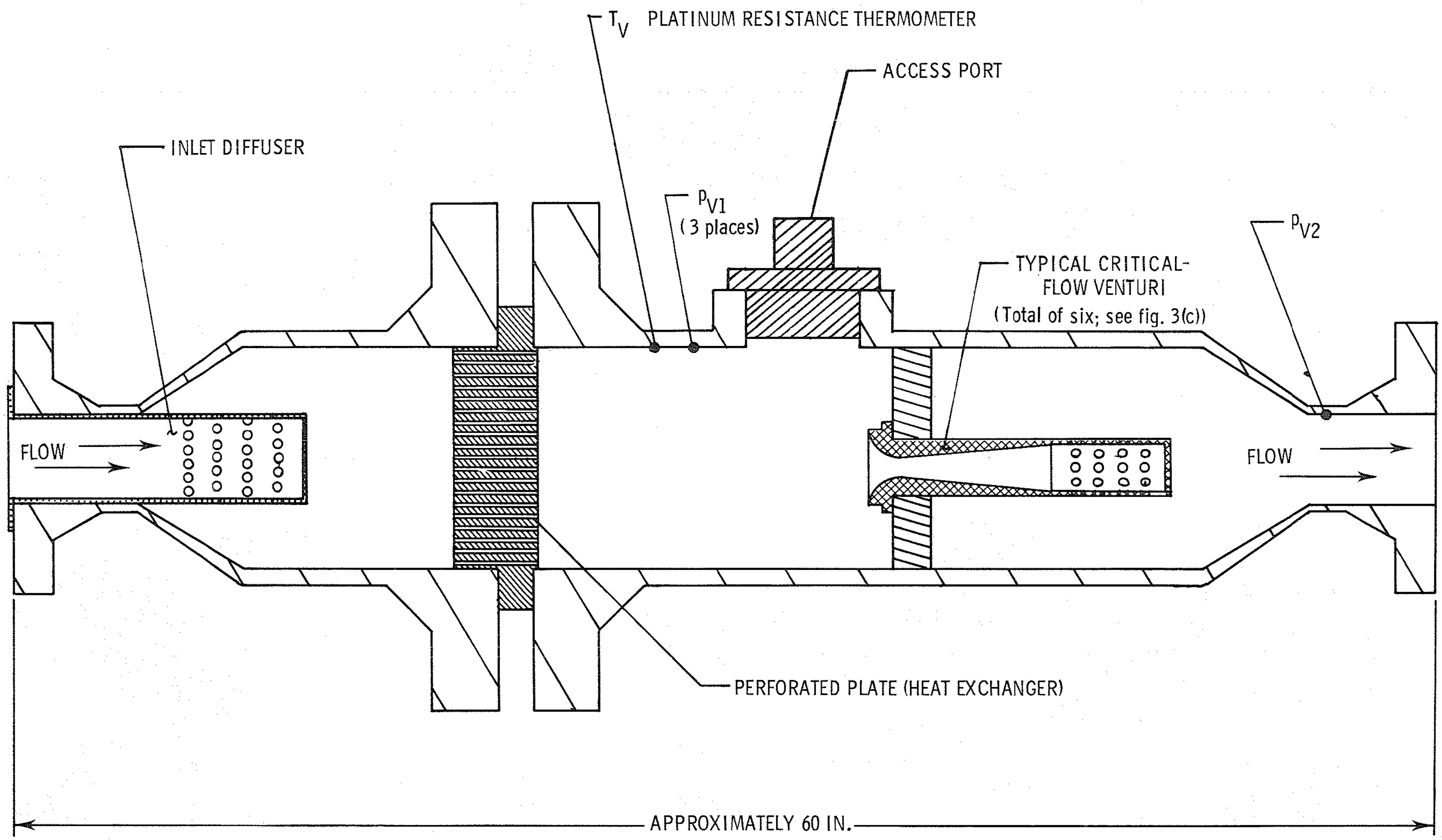

(a) Sketch of multiple critical venturi system.

Figure 3.- Geometry of multiple critical venturi system.

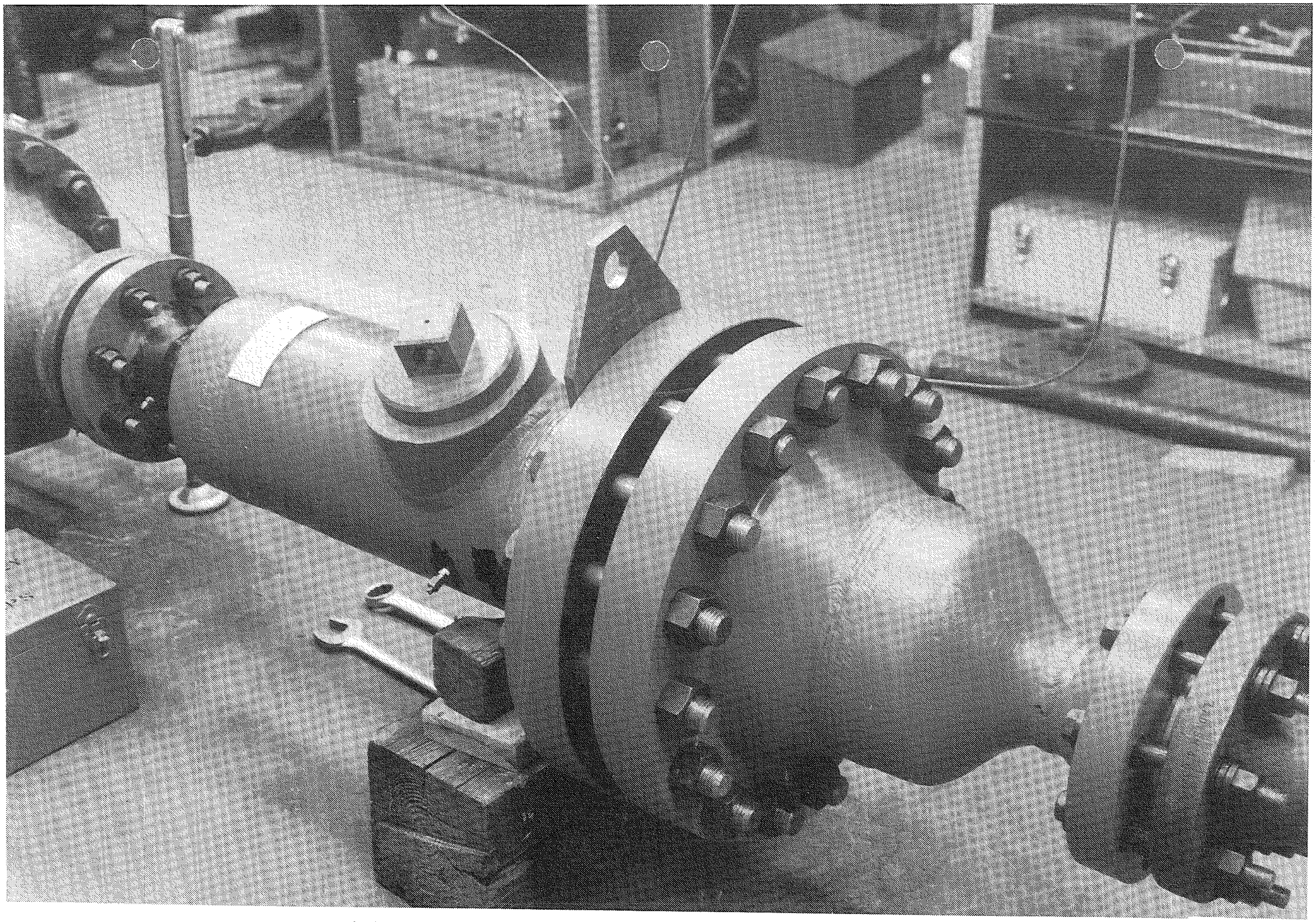

(b) Photograph of multiple critical venturi system. L-85-110

Figure 3.- Continued.

VENTURI GEOMETRY		
VENTURI NO.	THROAT DIA., IN.	THROAT AREA, IN^2
1	0.1877	0.0277
2	0.2639	0.0547
4	0.3741	0.1099
8	0.5281	0.2190
16.1	0.7475	0.4388
16.2	0.7478	0.4392

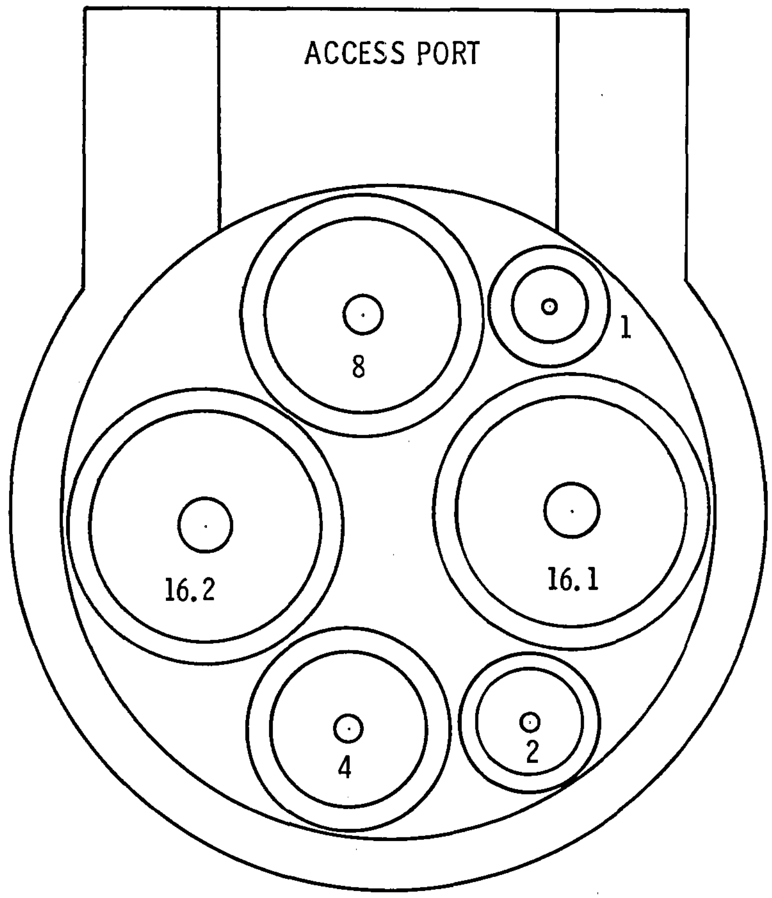

(c) Individual venturi geometry and orientation.

Figure 3.- Concluded.

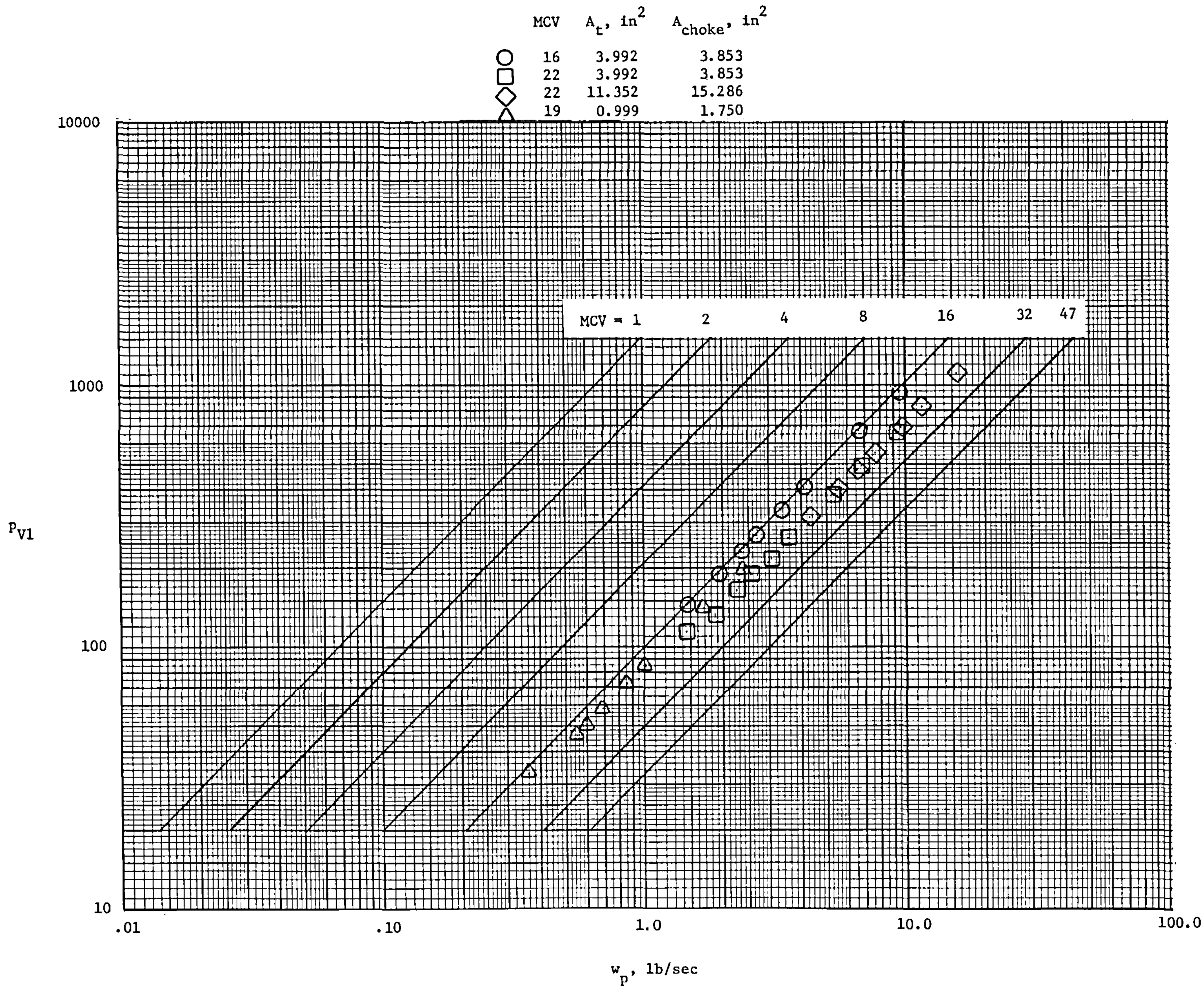

Figure 4.- Multiple critical venturi operating envelope.

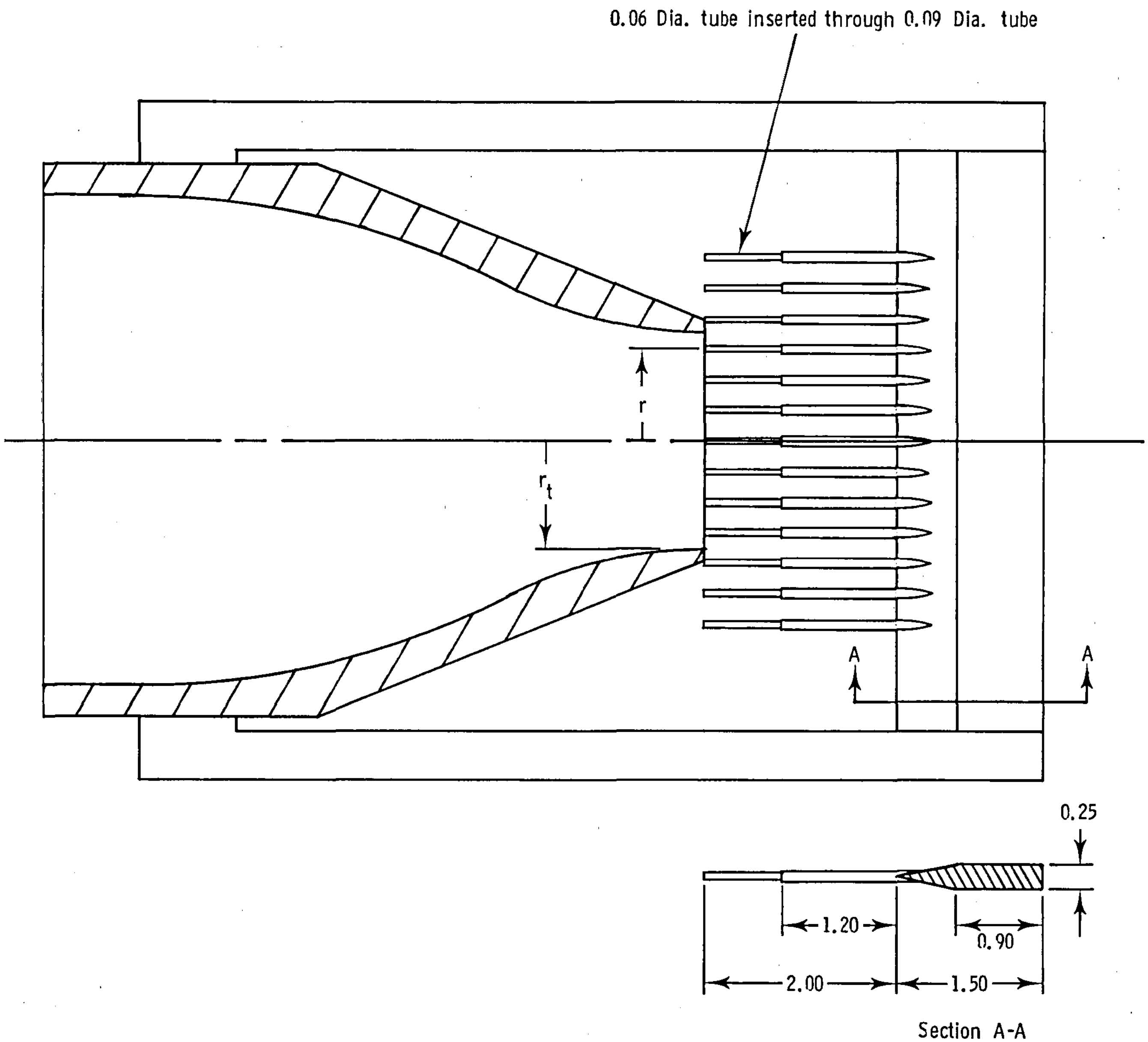

Figure 5.- Sketch of jet total-pressure rake mounted at throat of typical Stratford choke nozzle.

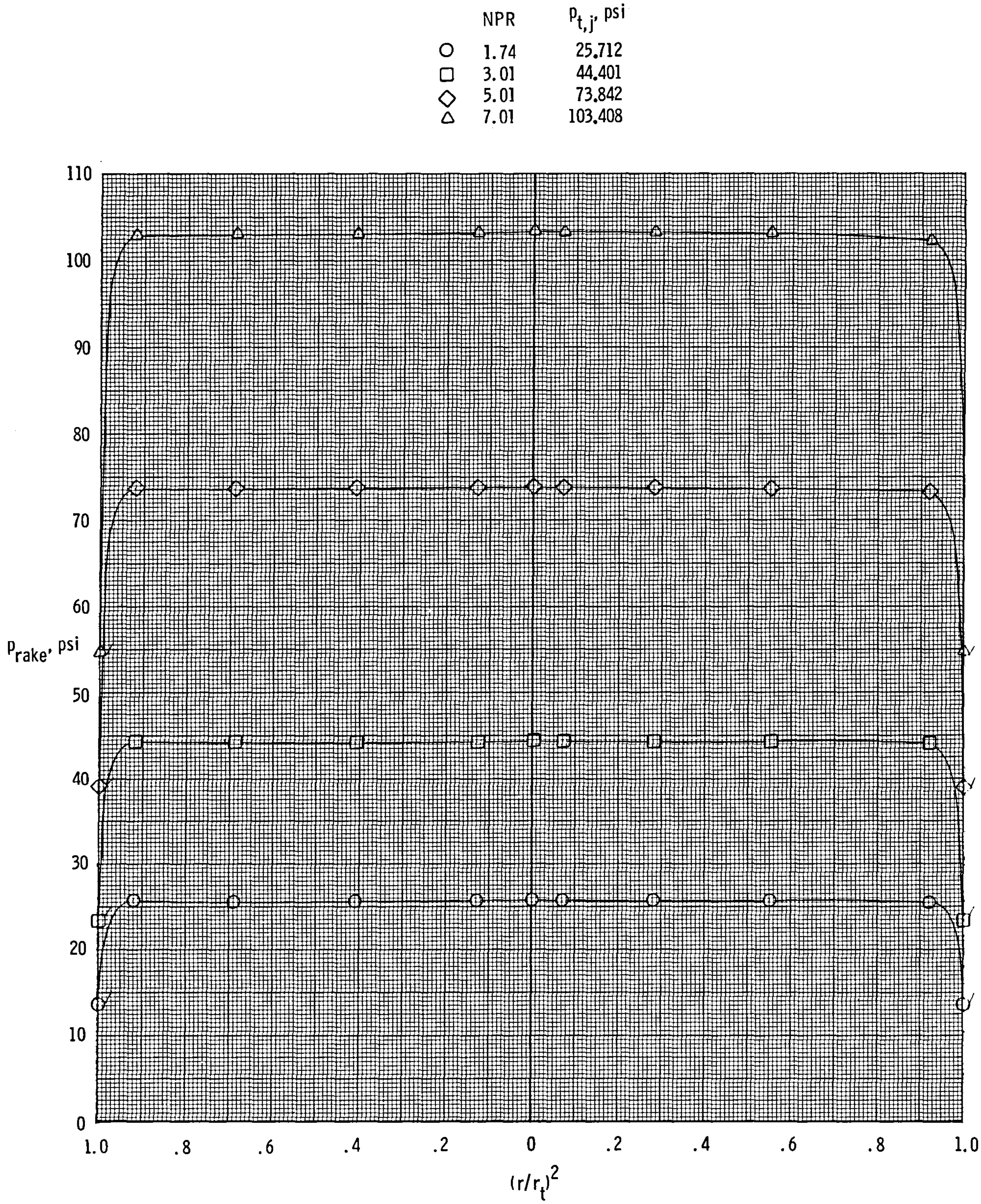

(a) $A_t = 3.992$ in^2; $A_{choke} = 3.853$ in^2.

Figure 6.- Typical exhaust total-pressure profiles measured with rake located at nozzle throat. Flagged symbols indicate wall static pressure.

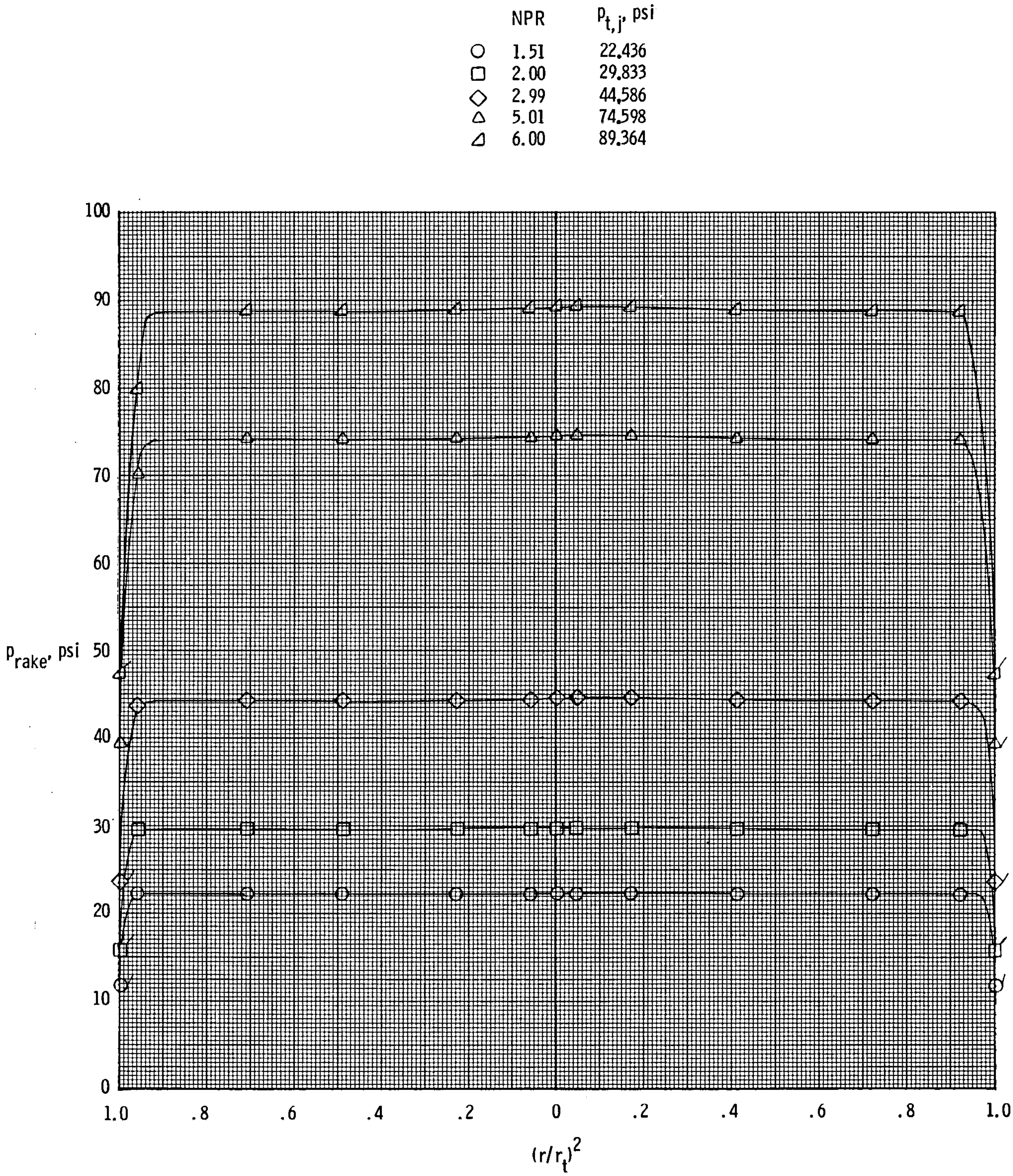

(b) $A_t = 5.711 \text{ in}^2$; $A_{choke} = 3.853 \text{ in}^2$.

Figure 6.- Continued.

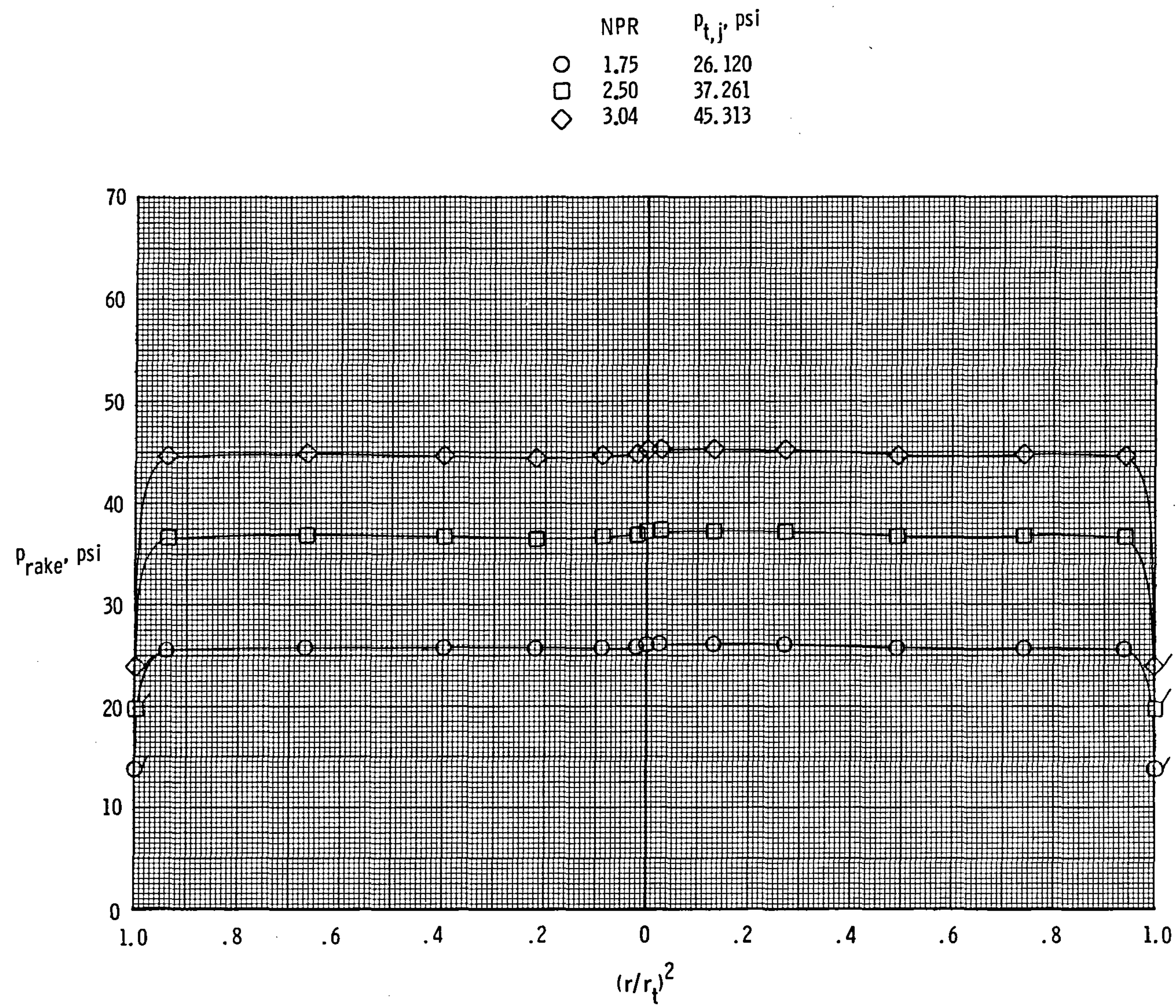

(c) $A_t = 11.352$ in^2; $A_{choke} = 3.853$ in^2.

Figure 6.- Concluded.

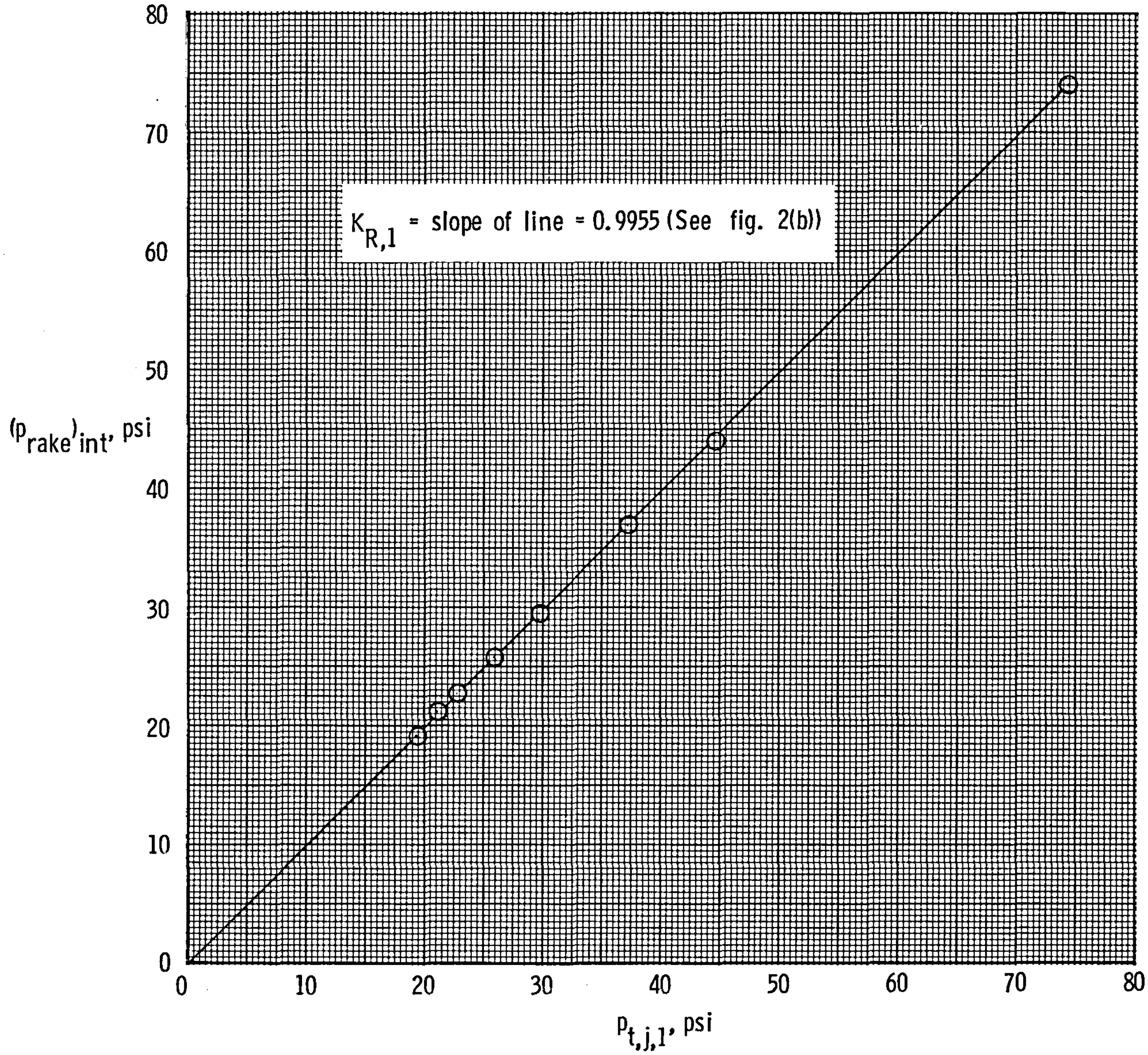

Figure 7.- Typical variation of total pressure obtained by integrating exhaust total-pressure profiles measured with rake (see fig. 6) as a function of jet total pressure measured with an individual probe (see fig. 2(b)) located in the instrumentation section. A_t = 0.999 in^2; A_{choke} = 3.853 in^2.

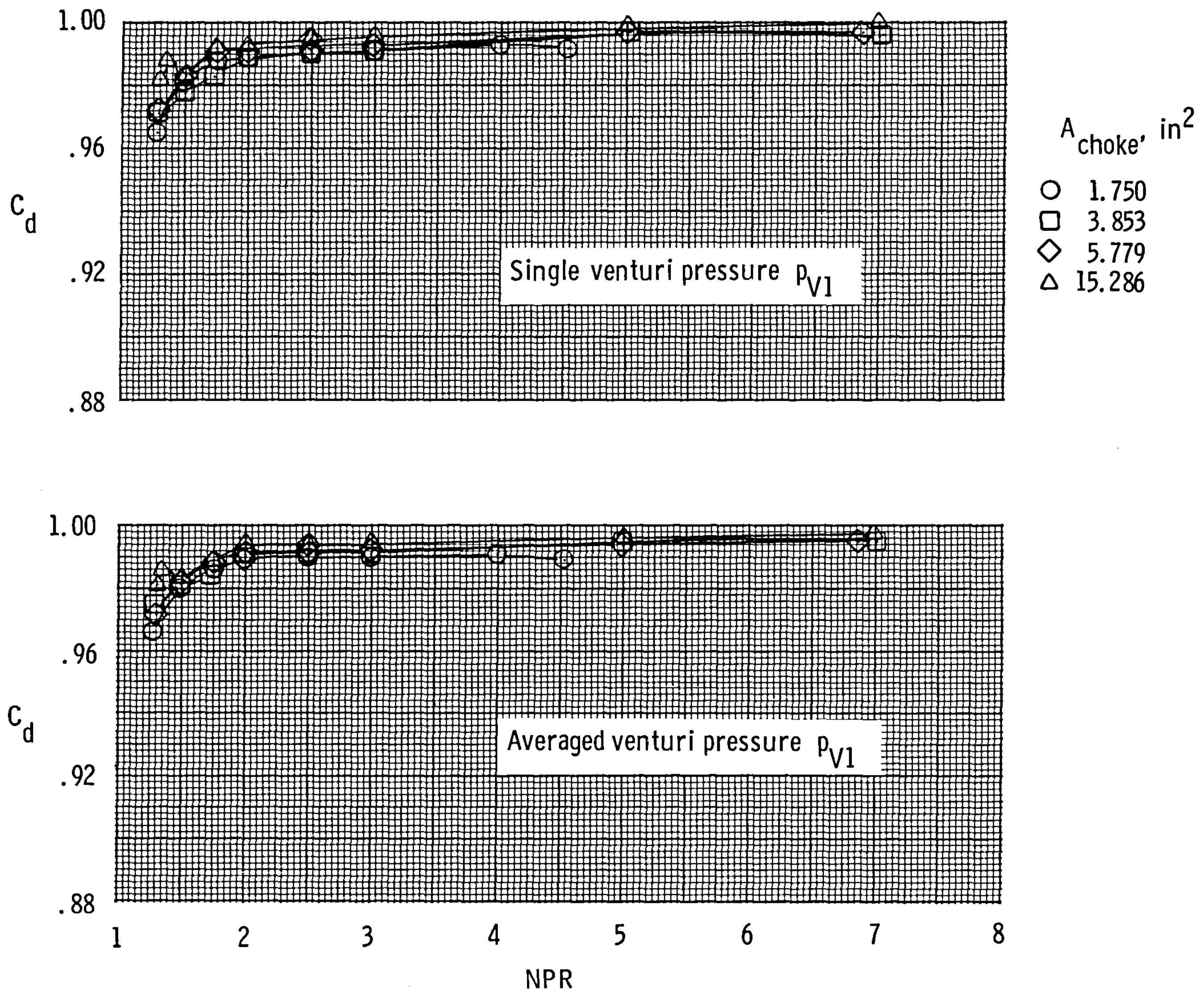

Figure 8.- Comparison of nozzle discharge coefficient calculations for single and averaged p_{V1} measurements. A_t = 3.992 in^2; $K_{R,1}$ to $K_{R,5}$ = 1.0; $(T_{t,j})_{nom}$ = 530°R; MCV = 22.

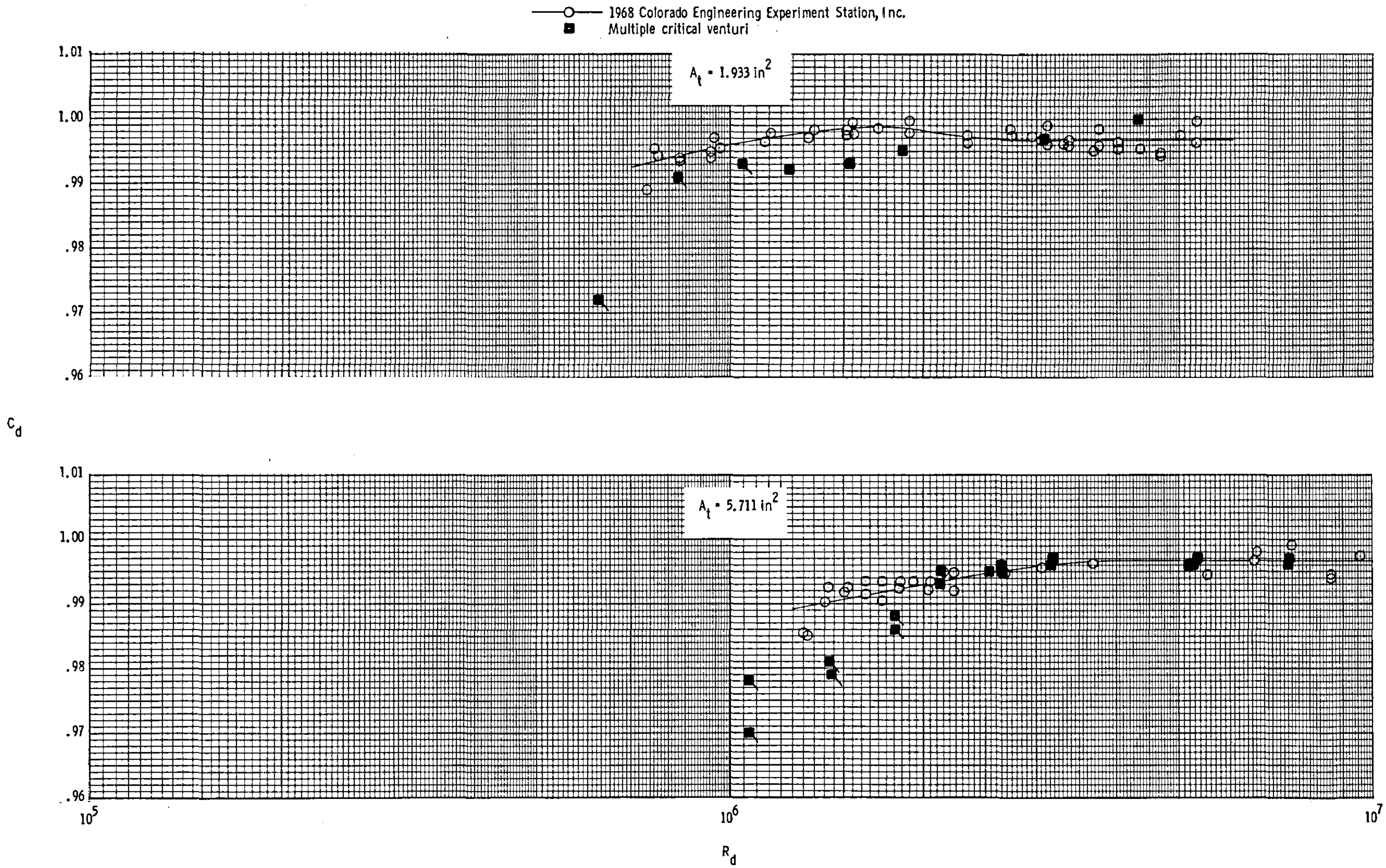

Figure 9.- Comparison of discharge coefficients obtained from multiple critical venturis with discharge coefficients obtained from standard-nozzle calibration in 1968 at Colorado Engineering Experiment Station, Inc. Flagged symbols indicate NPR < $(NPR)_c$. $K_{R,1}$ to $K_{R,5}$ = 1.0; A_{choke} = 15.286 in^2 (screens).

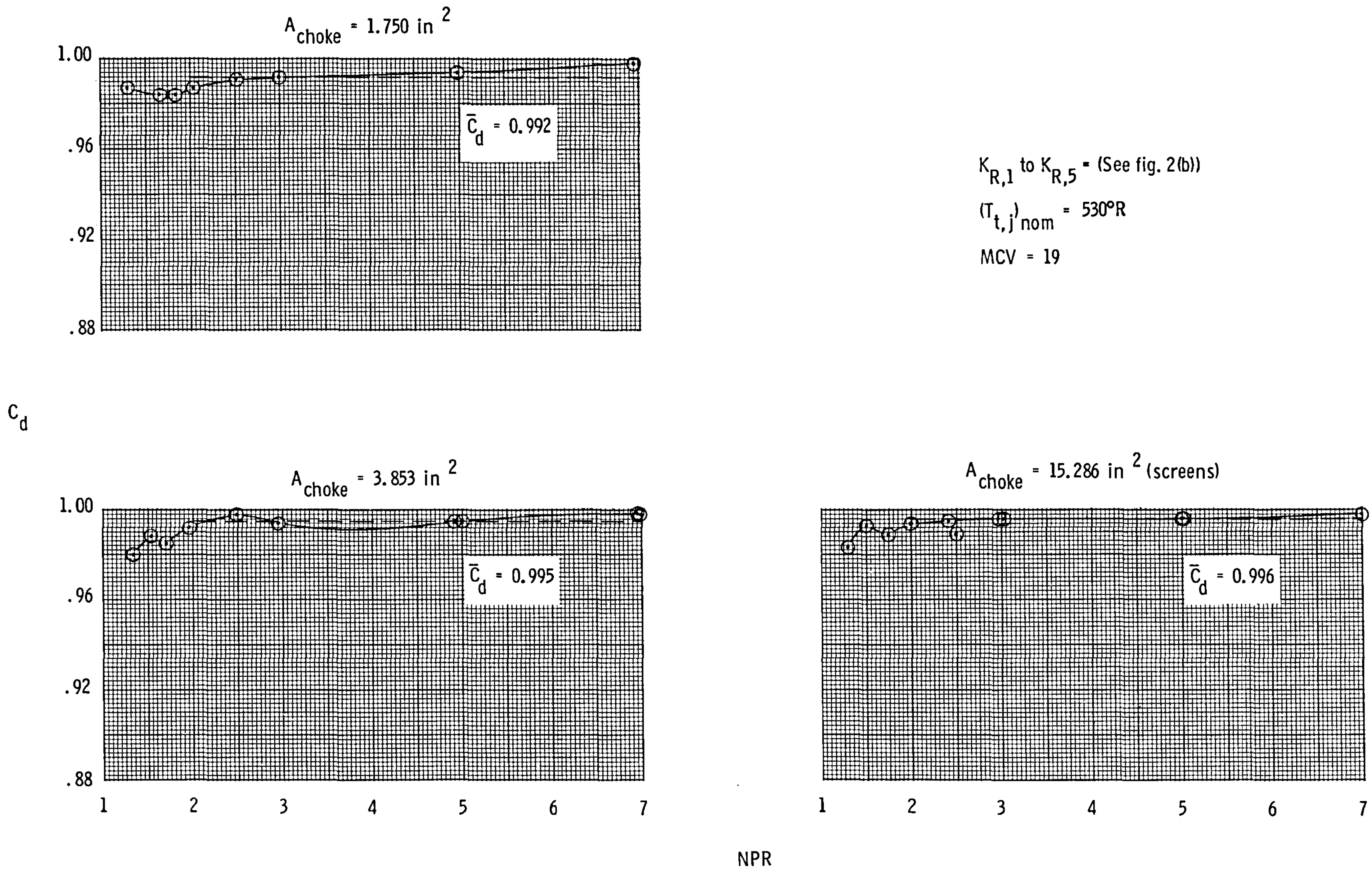

(a) $A_t = 0.999\ in^2$.

Figure 10.- Variation of standard-nozzle discharge coefficient with nozzle pressure ratio for jet total pressure corrected with rake factors measured at throat.

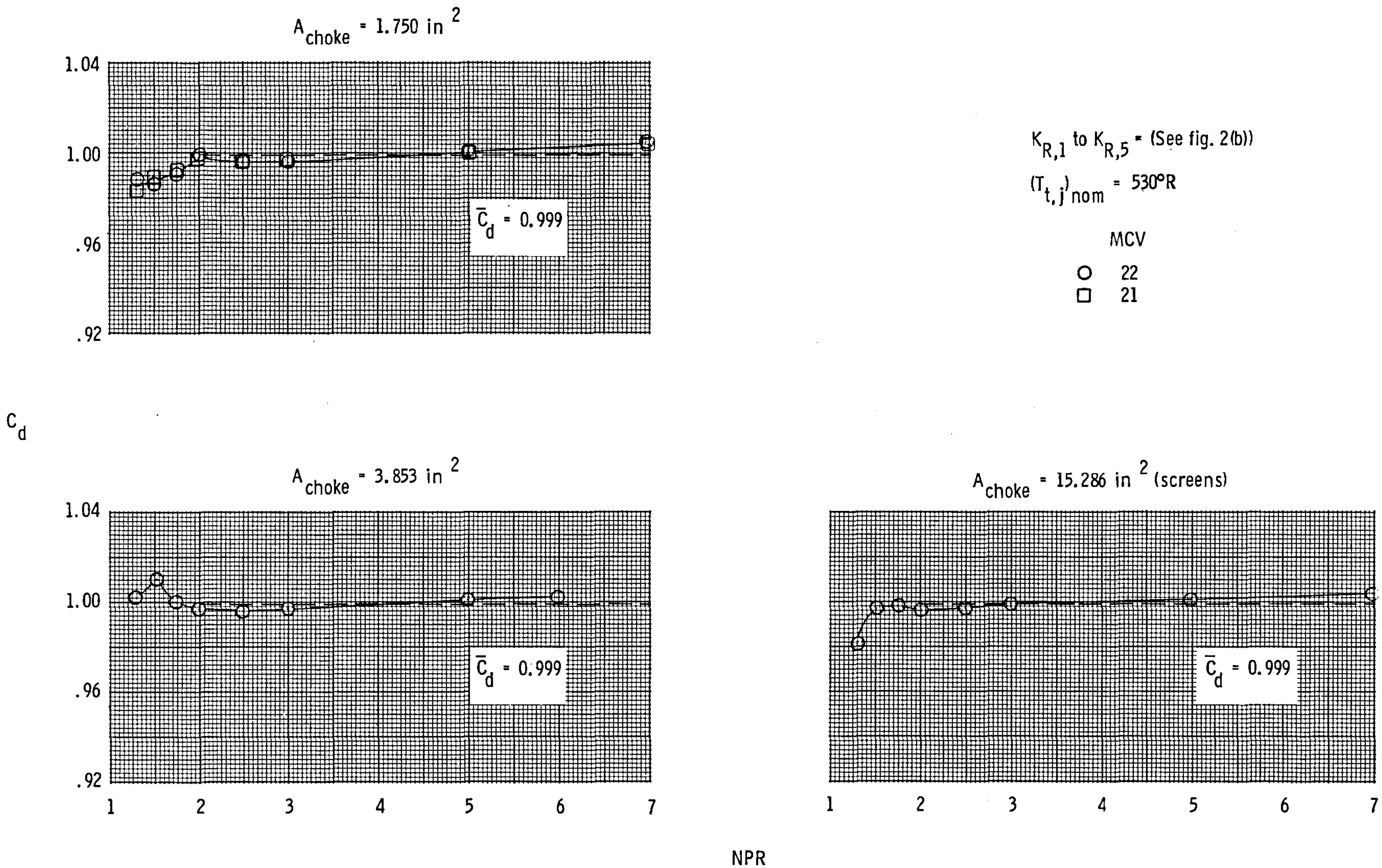

(b) $A_t = 1.933 \text{ in}^2$.

Figure 10.- Continued.

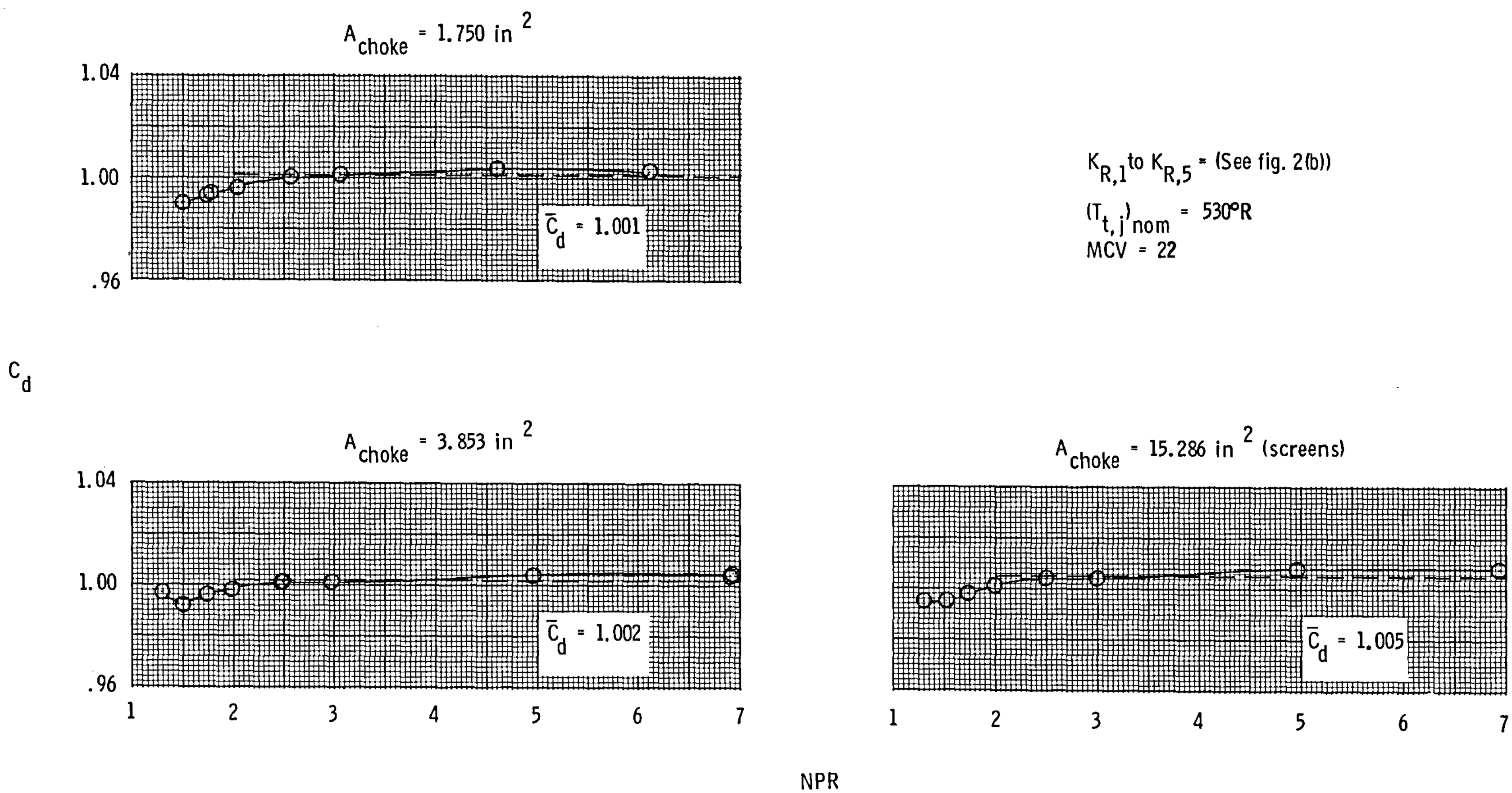

(c) $A_t = 3.002$ in^2.

Figure 10.- Continued.

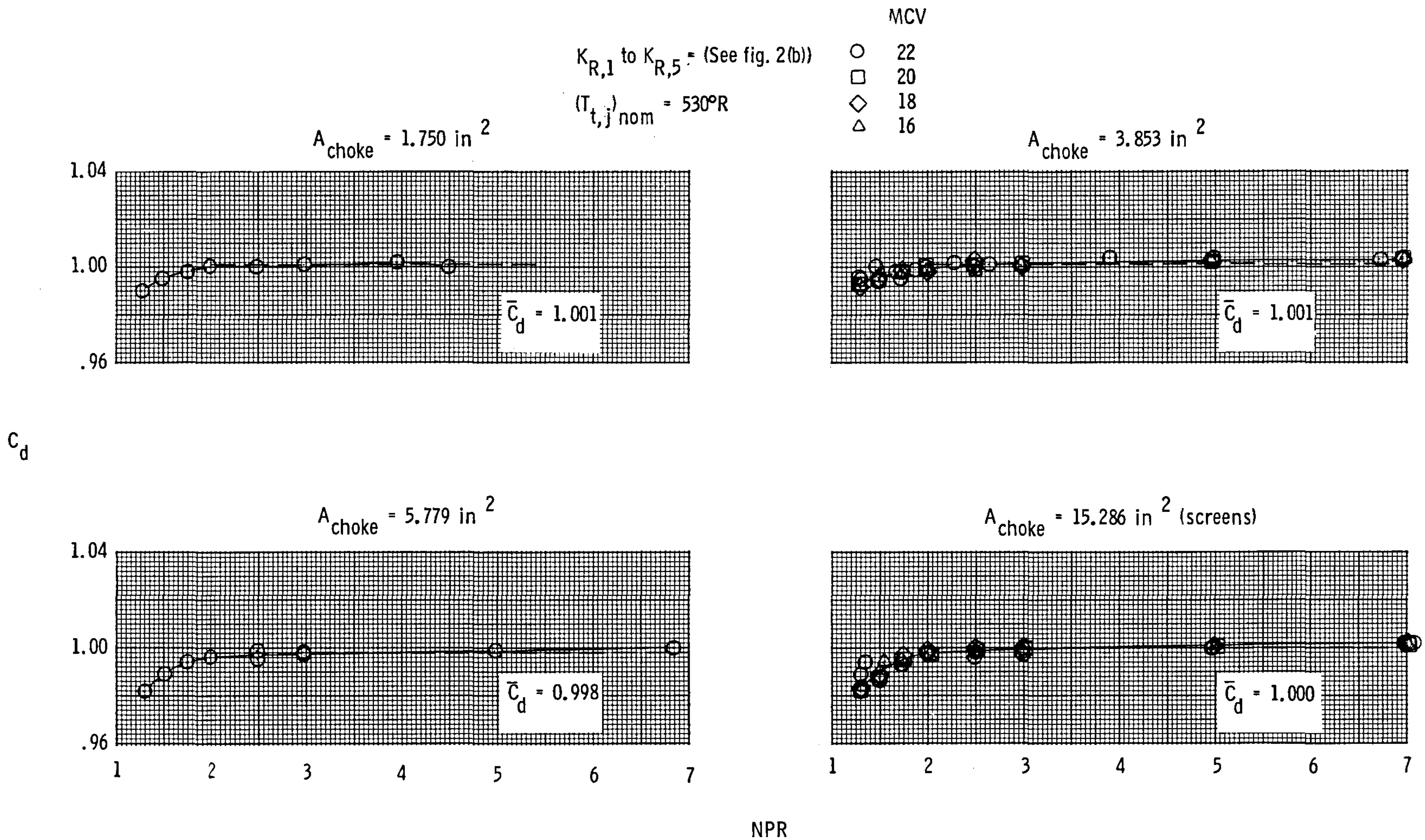

(d) $A_t = 3.992\ in^2$.

Figure 10.- Continued.

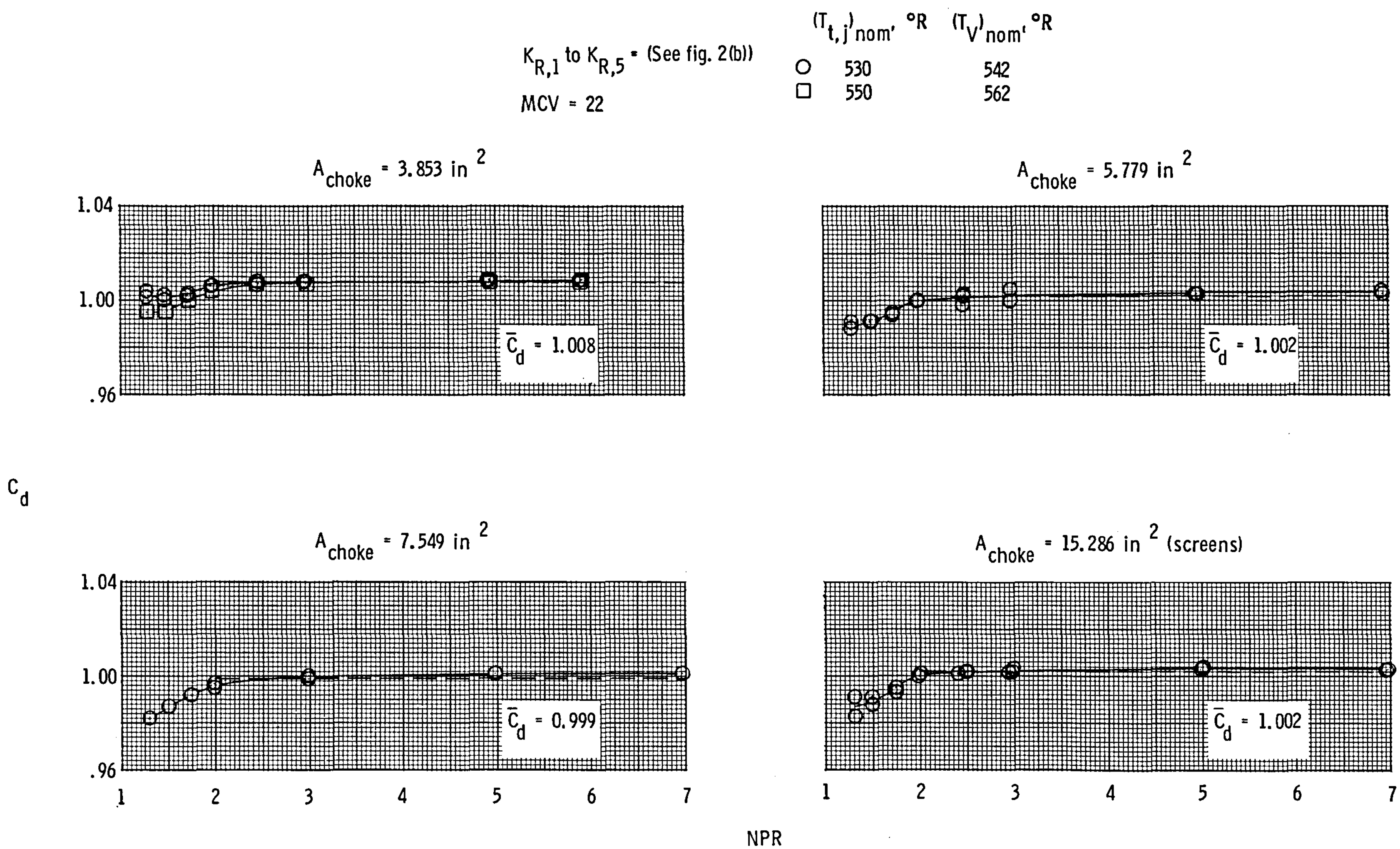

(e) $A_t = 5.711 \text{ in}^2$.

Figure 10.- Continued.

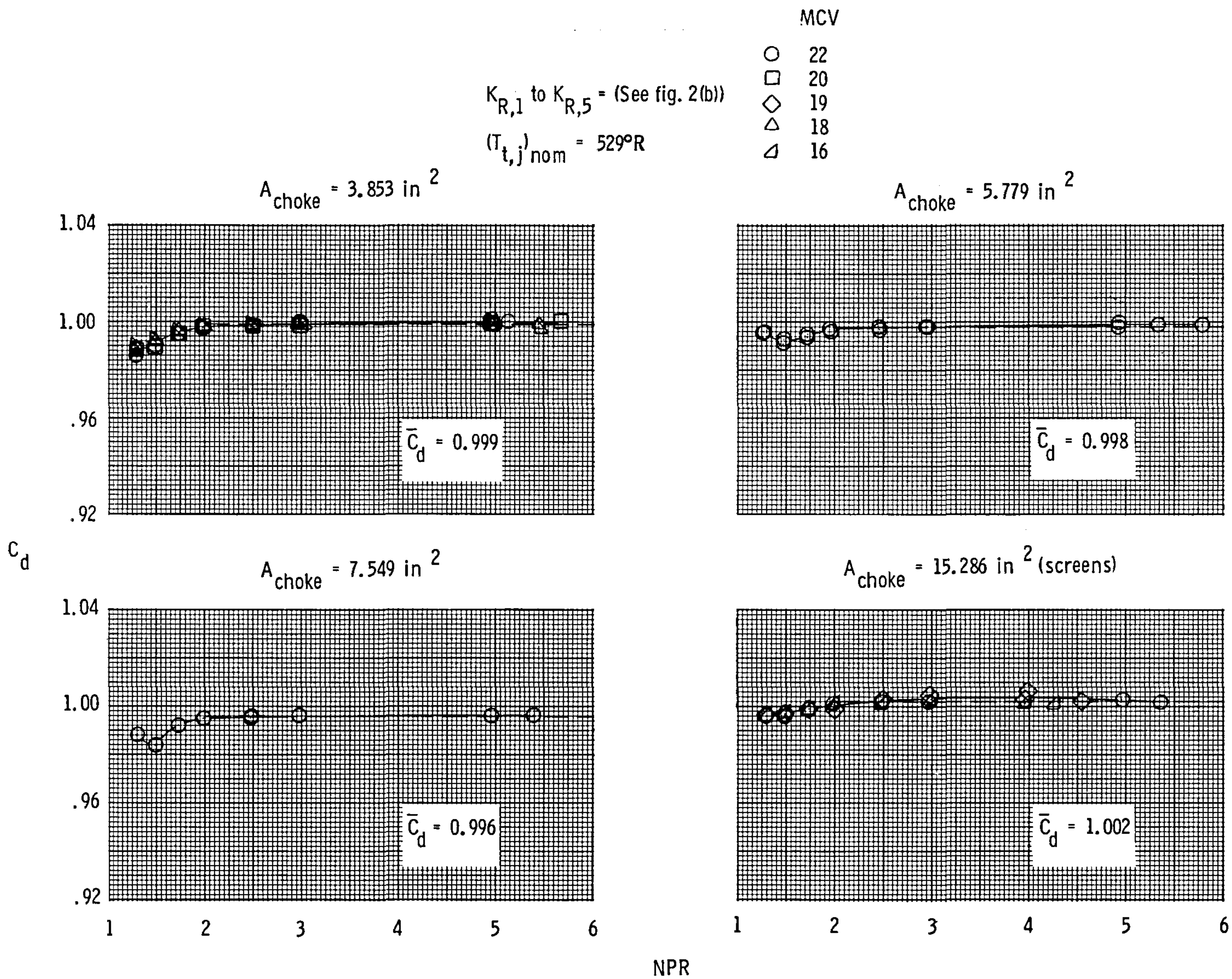

(f) A_t = 8.501 in^2.

Figure 10.- Continued.

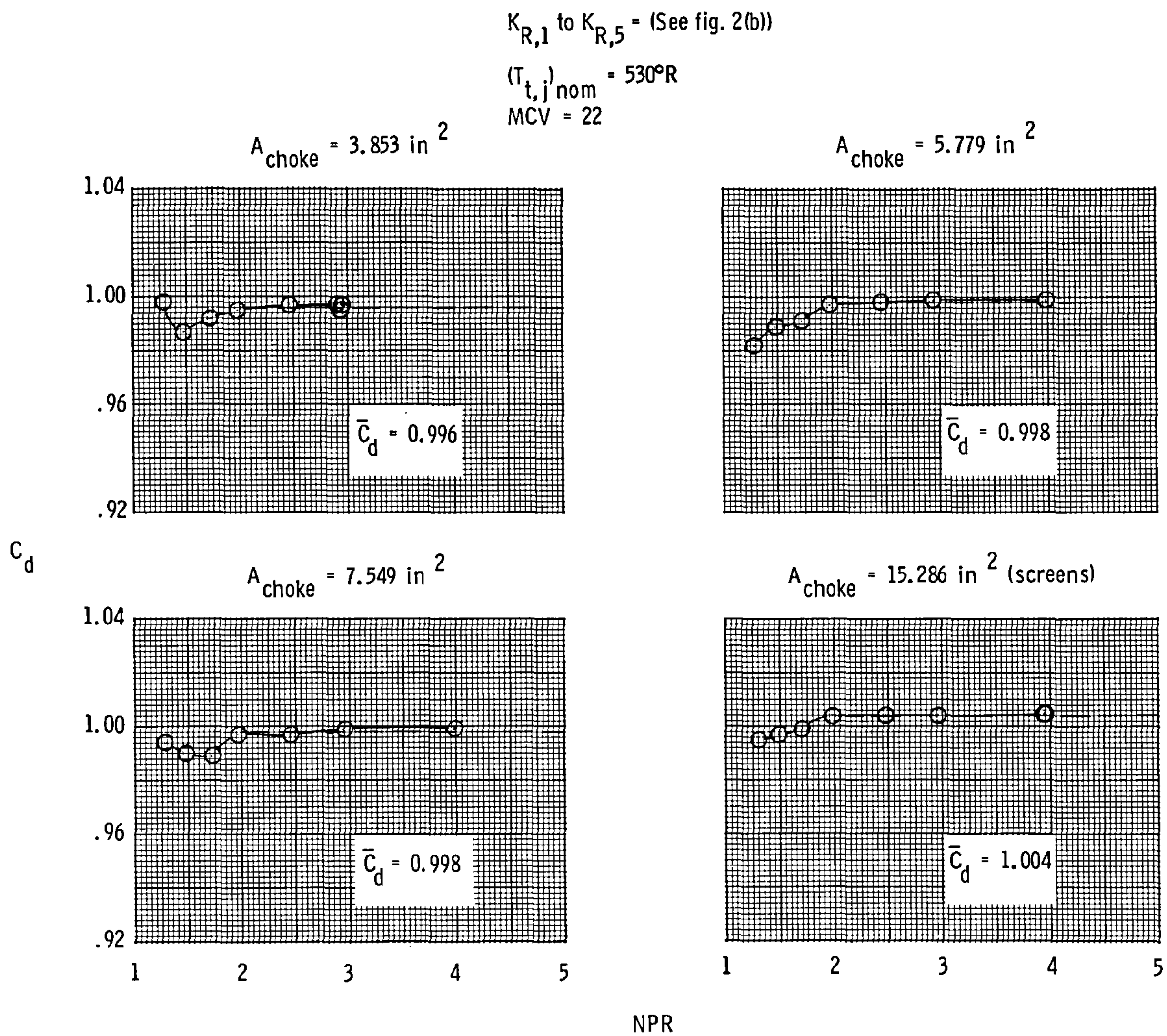

(g) $A_t = 11.352 \text{ in}^2$.

Figure 10.- Concluded.

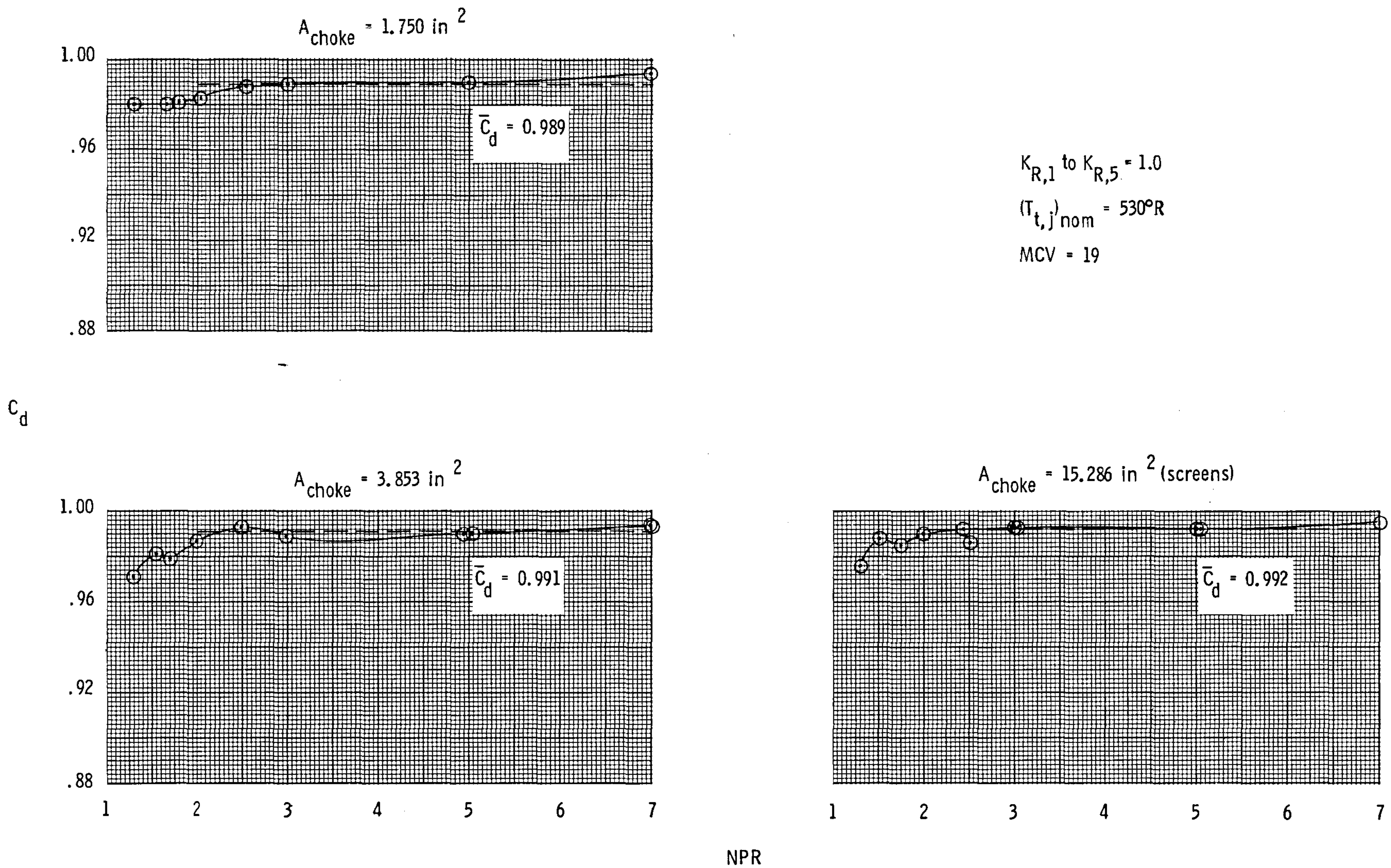

(a) $A_t = 0.999\ in^2$.

Figure 11.- Variation of standard-nozzle discharge coefficient with nozzle pressure ratio for average jet total pressure measured in instrumentation section.

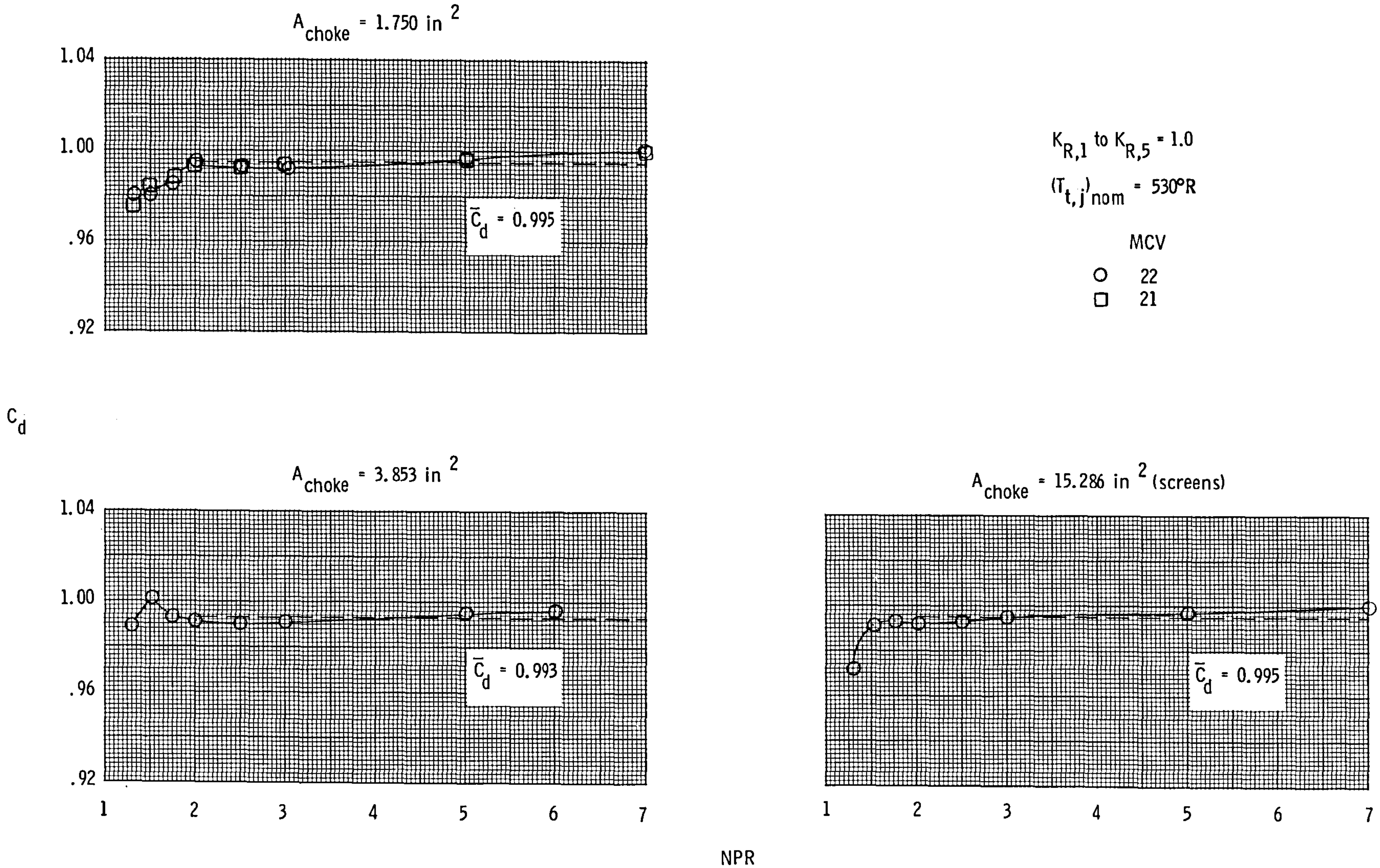

(b) $A_t = 1.933\ in^2$.

Figure 11.- Continued.

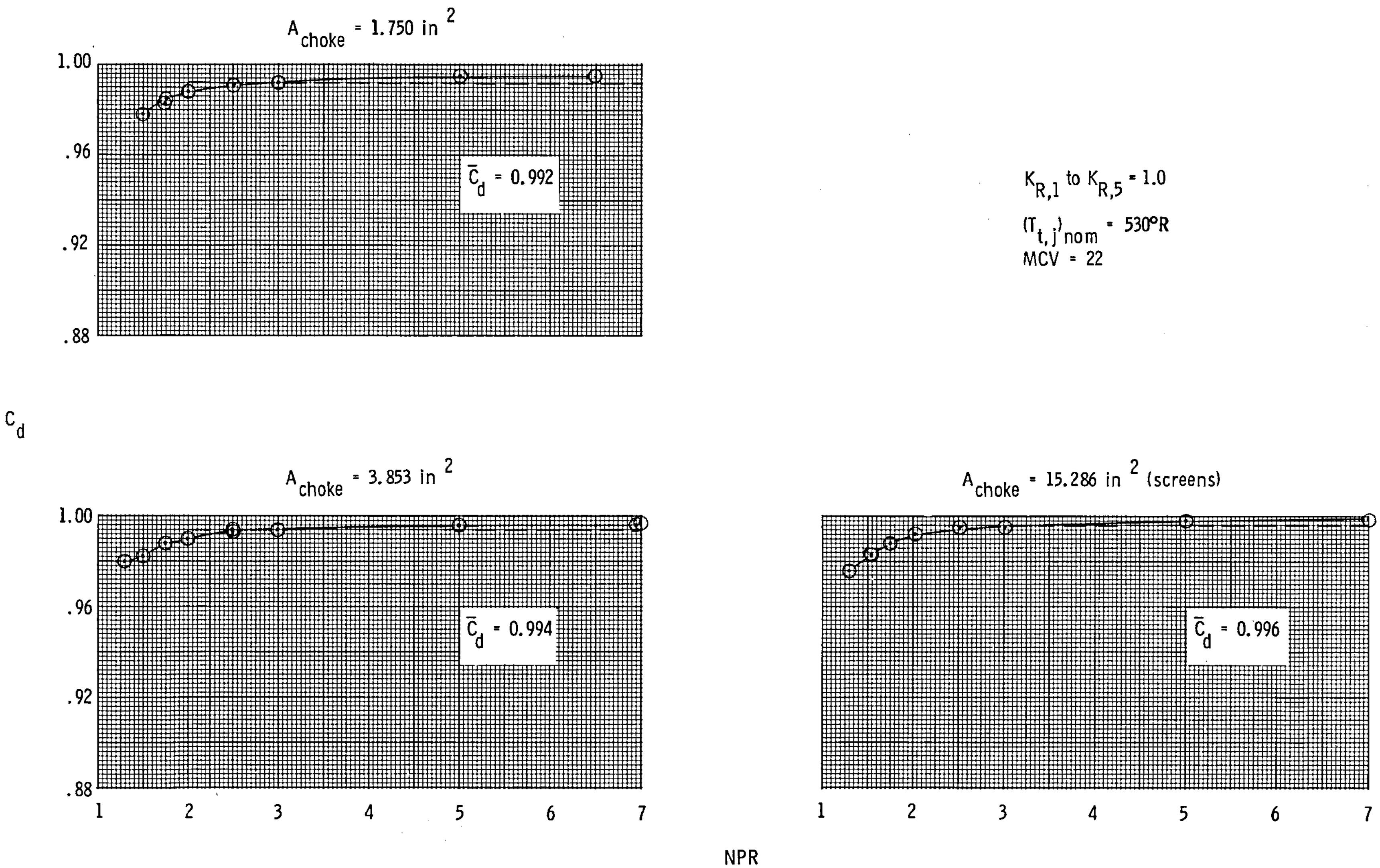

(c) $A_t = 3.002\ in^2$.

Figure 11.- Continued.

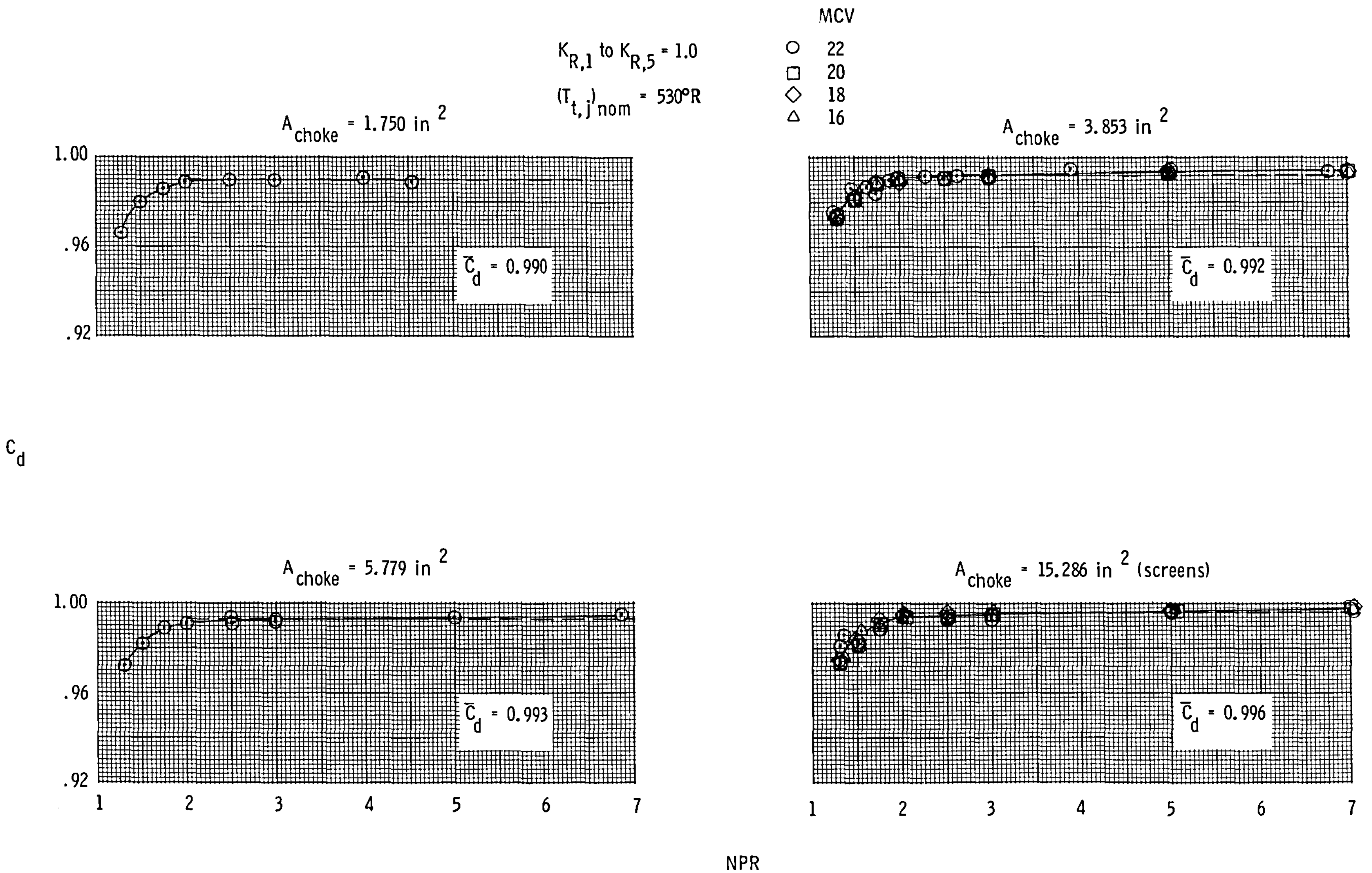

(d) $A_t = 3.992\ in^2$.

Figure 11.- Continued.

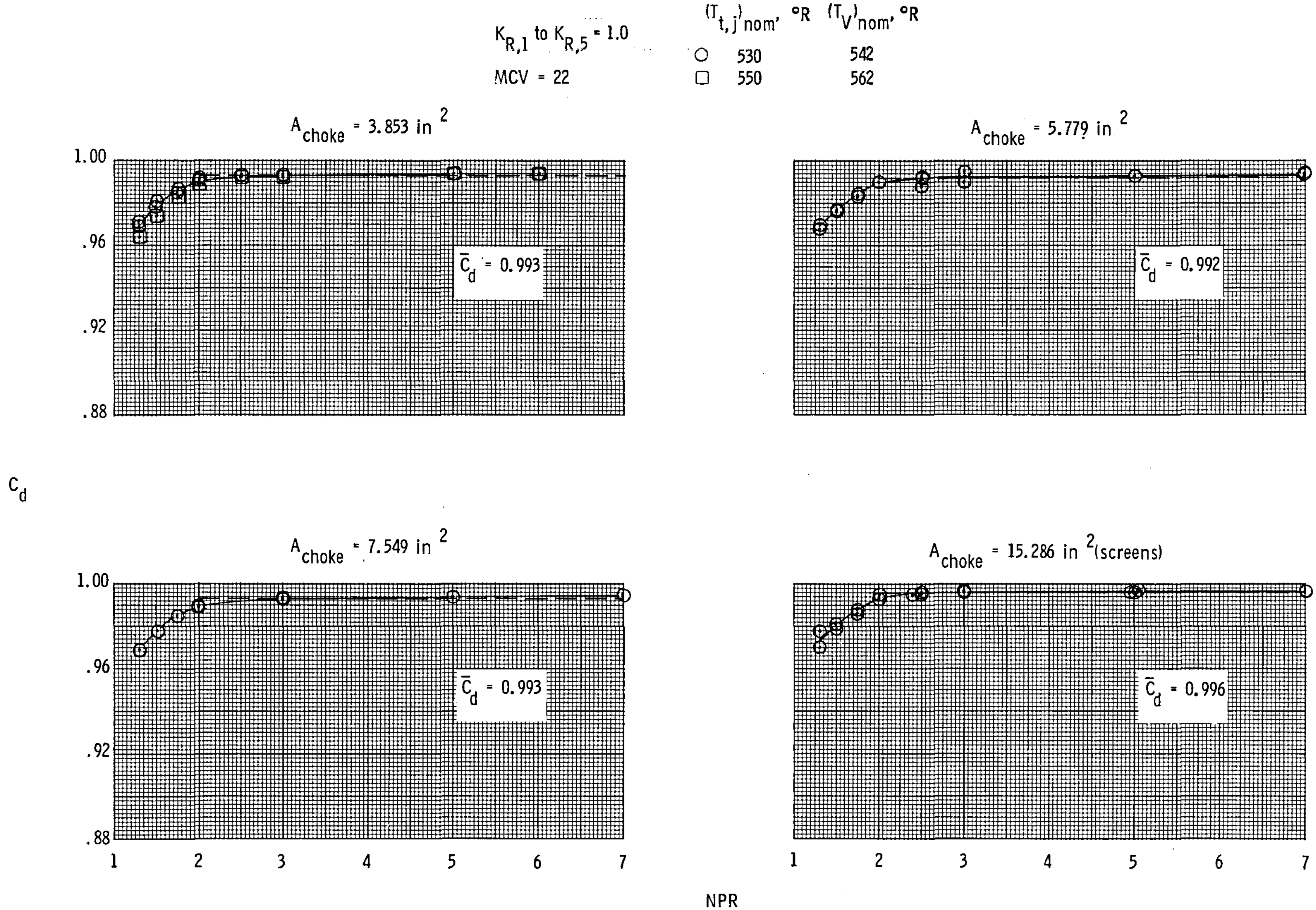

(e) $A_t = 5.711\ in^2$.

Figure 11.- Continued.

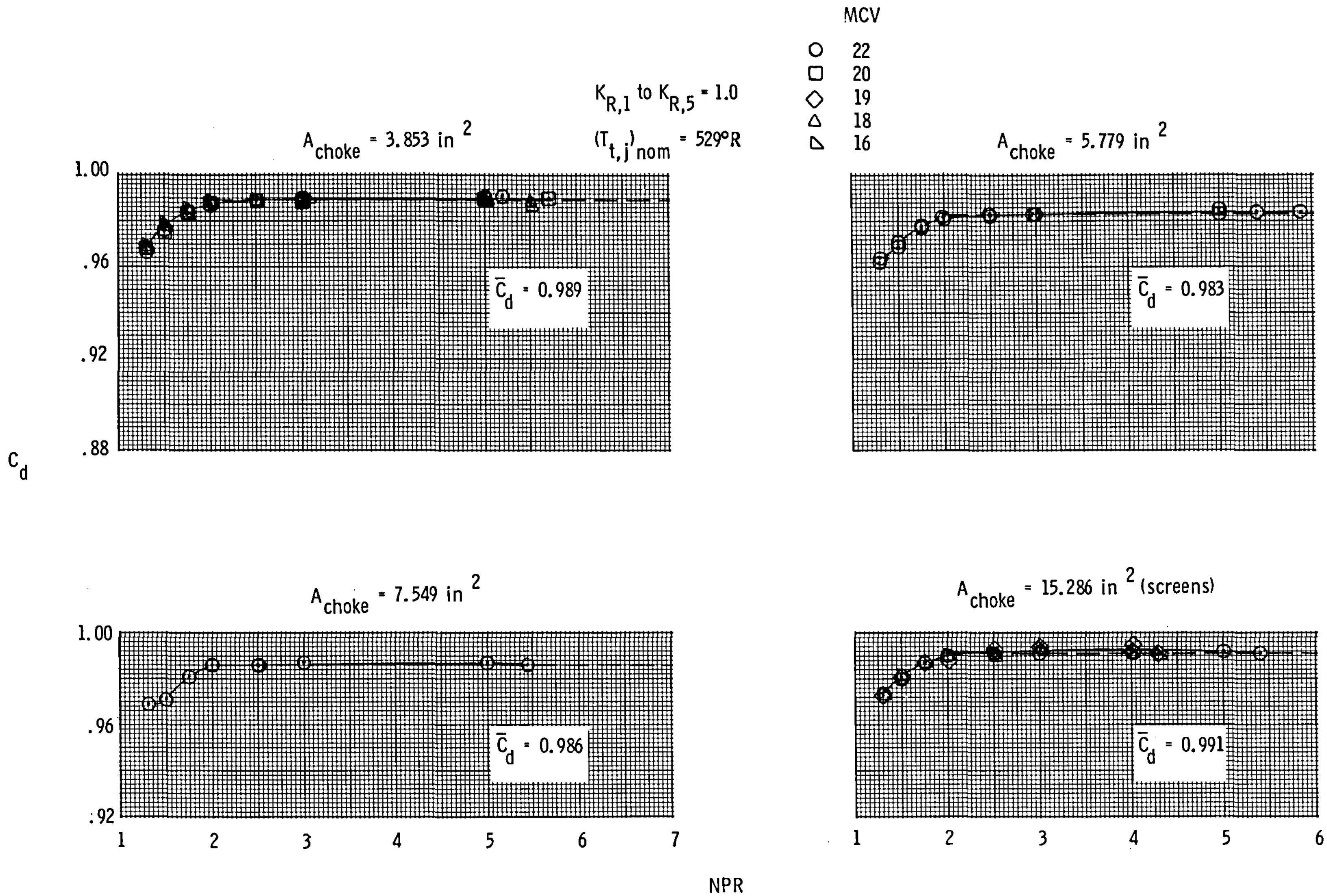

(f) $A_t = 8.501$ in^2.

Figure 11.- Continued.

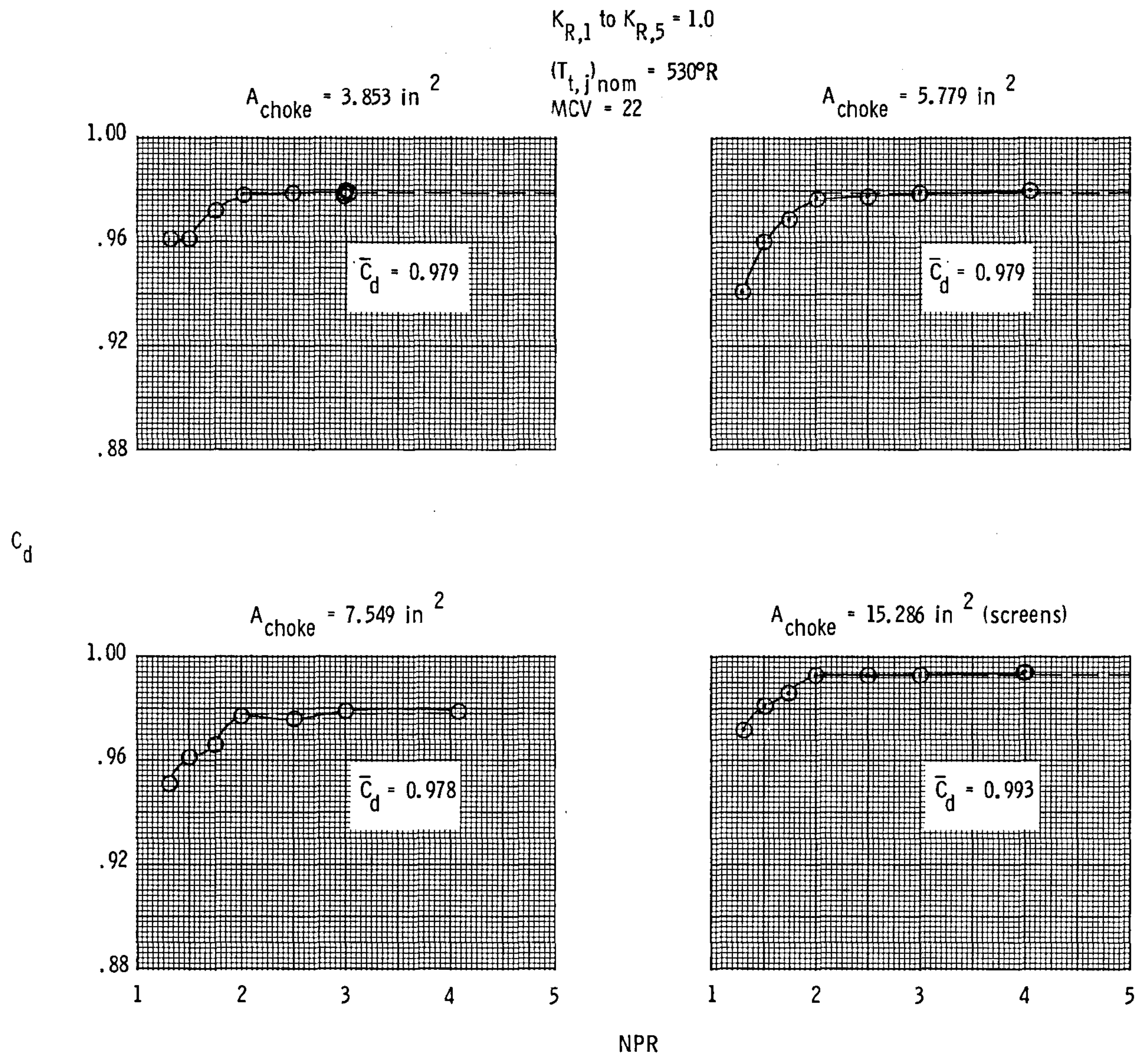

(g) $A_t = 11.352$ in^2.

Figure 11.- Concluded.

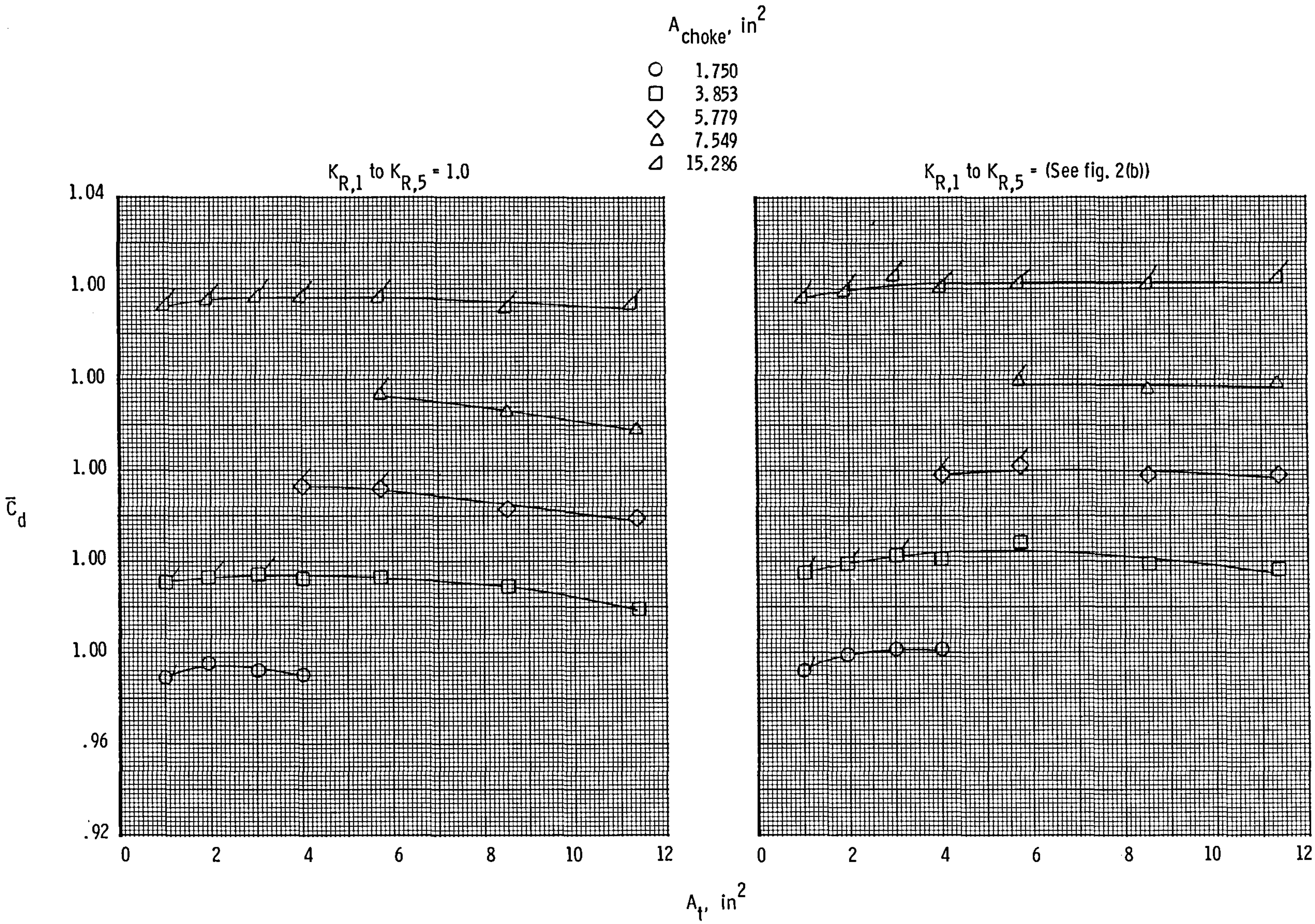

Figure 12.- Effect of nozzle-throat area on discharge coefficient. Flagged symbols indicate $A_{choke} > A_t$.

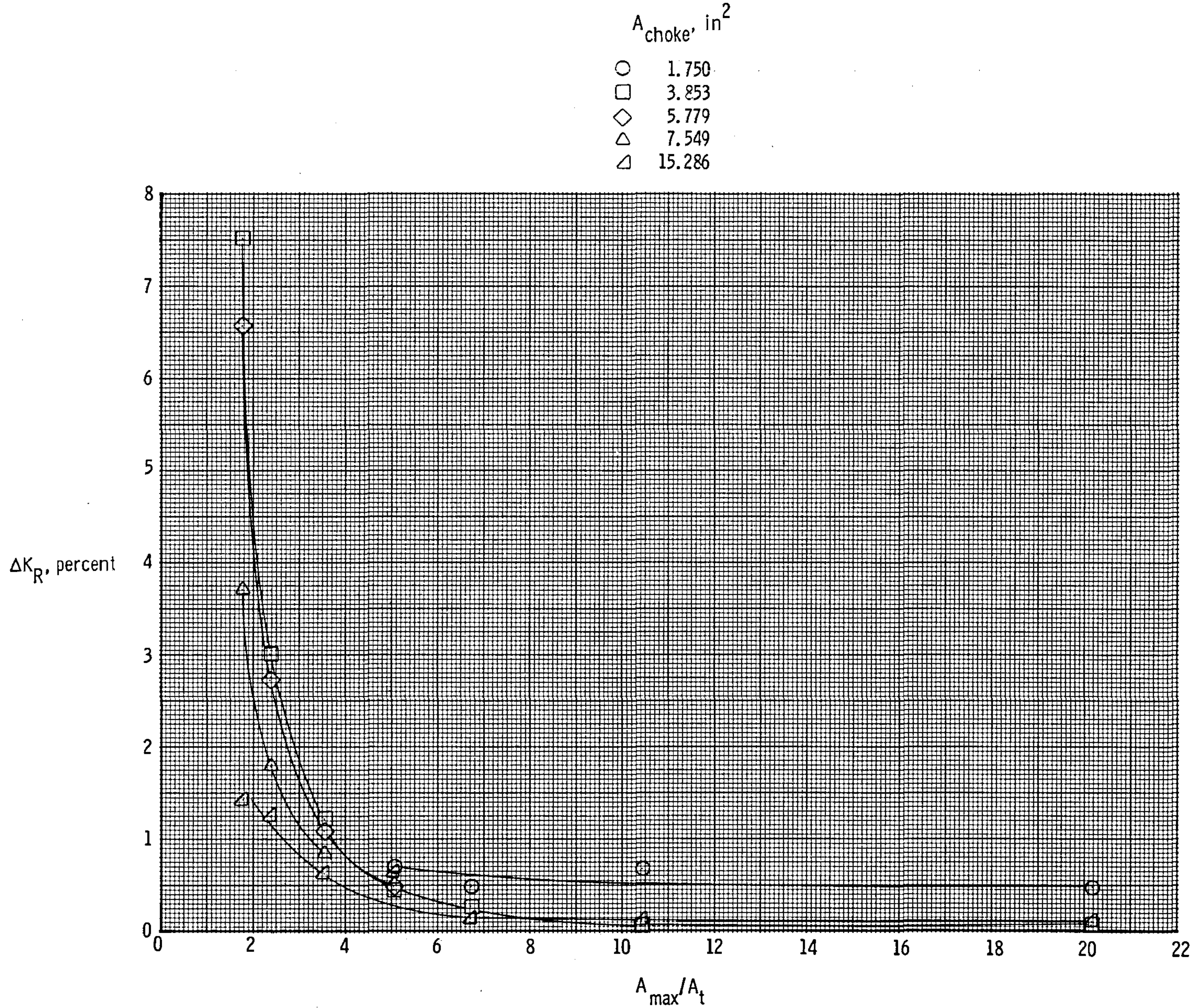

Figure 13.- Effect of contraction ratio and choke-plate open area on total-pressure distortion parameter.

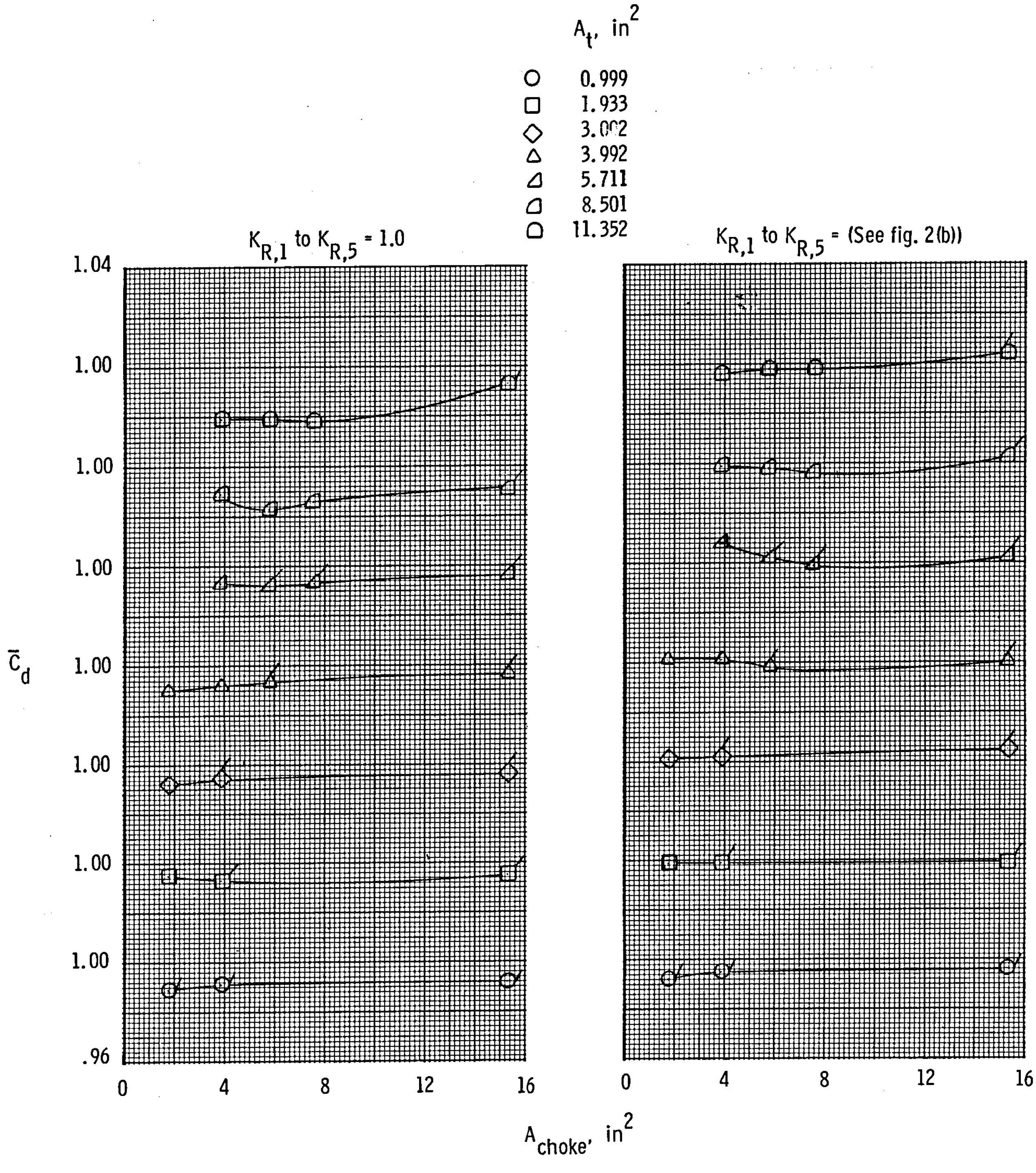

Figure 14.- Effect of choke-plate open area on discharge coefficient. Flagged symbols indicate $A_{choke} > A_t$.

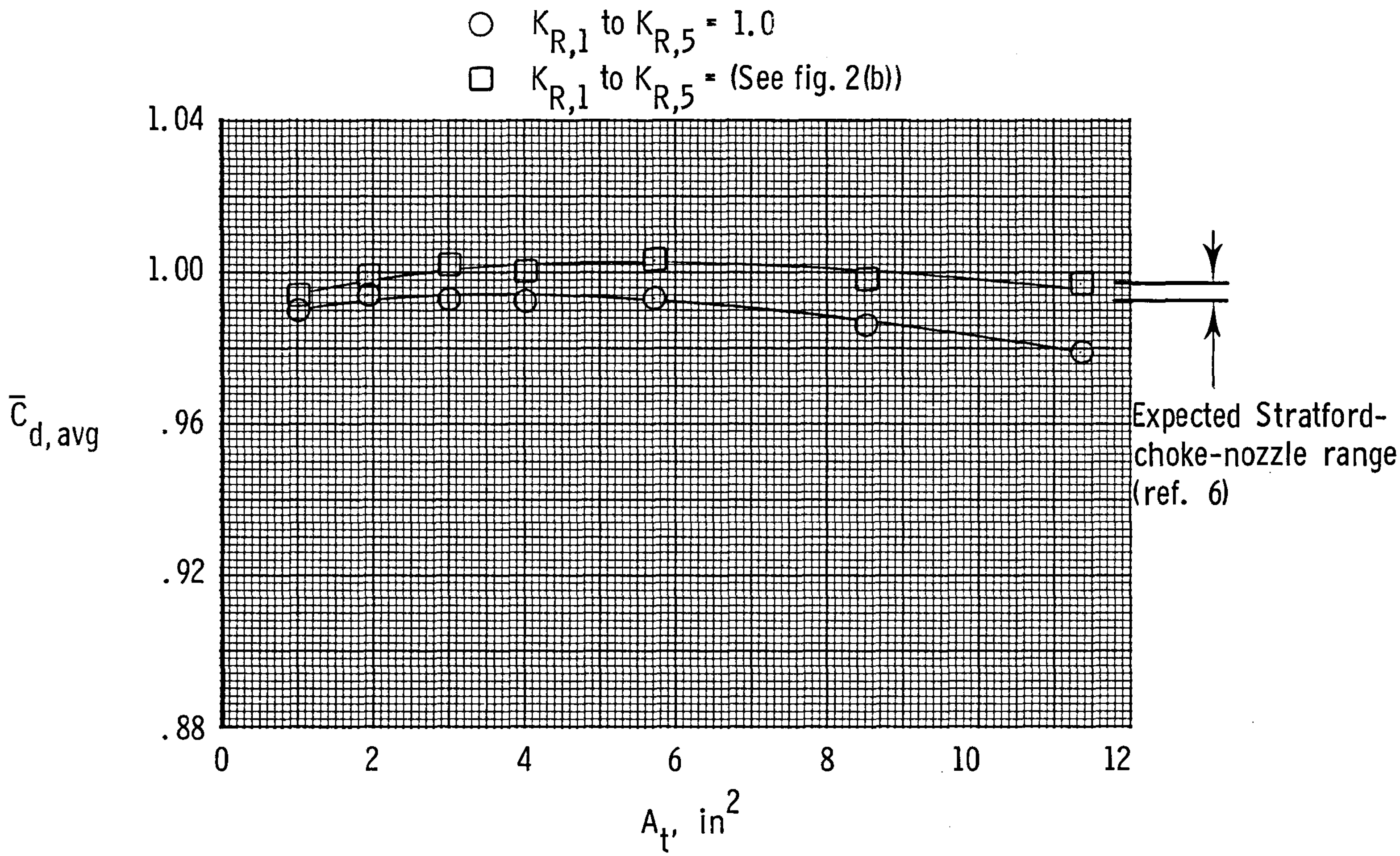

Figure 15.- Variation of average of $\bar{C}_d$ for all A_{choke} except screens with nozzle-throat area for choked-nozzle flow operation. Choke-plate flow straightener installed; NPR > 1.89.

1. Report No.	2. Government Accession No.	3. Recipient's Catalog No.
NASA TM-86405		

4. Title and Subtitle	5. Report Date
Operating Characteristics of the Multiple Critical Venturi System and Secondary Calibration Nozzles Used for Weight-Flow Measurements in the Langley 16-Foot Transonic Tunnel	September 1985
	6. Performing Organization Code 505-40-90-01
7. Author(s) Bobby L. Berrier, Laurence D. Leavitt, and Linda S. Bangert	8. Performing Organization Report No. L-15960
9. Performing Organization Name and Address NASA Langley Research Center Hampton, VA 23665-5225	10. Work Unit No.
	11. Contract or Grant No.
12. Sponsoring Agency Name and Address National Aeronautics and Space Administration Washington, DC 20546-0001	13. Type of Report and Period Covered Technical Memorandum
	14. Sponsoring Agency Code

15. Supplementary Notes

16. Abstract

An investigation has been conducted in the Langley 16-Foot Transonic Tunnel to determine the weight-flow measurement characteristics of a multiple critical venturi system and the nozzle discharge coefficient characteristics of a series of convergent calibration nozzles. The effects on model discharge coefficient of nozzle-throat area, model choke-plate open area, nozzle pressure ratio, jet total temperature, and number and combination of operating venturis were investigated. Tests were conducted at static conditions (tunnel wind off) at nozzle pressure ratios from 1.3 to 7.0.

17. Key Words (Suggested by Author(s))	18. Distribution Statement
Venturi Measurements Weight flow Mass flow Stratford nozzles	Unclassified - Unlimited Subject Category 02

19. Security Classif. (of this report)	20. Security Classif. (of this page)	21. No. of Pages	22. Price
Unclassified	Unclassified	72	A04

NASA-Langley, 1985

End of Document